The Dissertation Committee for Che-Yun Lin

certifies that this is the approved version of the following dissertation:

Silicon Integrated Nanophotonic Devices for on-Chip Optical Interconnects

Committee:

Ray T. Chen, Supervisor

C. Grant Willson

Jack Lee

Seth R. Bank

Andrea Alu

Alan X. Wang

Silicon Integrated Nanophotonic Devices for on-Chip Optical Interconnects

by

Che-Yun Lin, B.S., M.S.E.

Dissertation

Presented to the Faculty of the Graduate School of

the University of Texas at Austin

in Partial Fulfillment

of the Requirements

for the Degree of

Doctor of Philosophy

The University of Texas at Austin

May 2012

Dedicated to my wife and parents

Acknowledgements

I would like to thank the faculty and staff of the Microelectronics Research Center and the Department of Electrical and Computer Engineering at The University of Texas at Austin for providing me with such an intellectually stimulating environment to conduct my research and pursue my graduate education. I greatly appreciate my advisor, Dr. Ray T. Chen, for his support and guidance in my research work. Many thanks also go to my committee members, Dr. Jack C. Lee, Dr. Grant Willson, Dr. Seth Bank, Dr. Andrea Alu, and Dr. Alan X. Wang, for their insightful advices on my dissertation.

I would like to acknowledge the productive collaborations with Dr. Beomsuk Lee, a former student in the Optical Interconnect Group and now a research staff at Samsung Electronics. I also want to thank Dr. Alan X. Wang, Dr. Swapnajit Chakravarty, Dr. Amir Hosseini, Dr. Harish Subbaraman and other group members for their help over the years.

Finally, I would like to express my gratitude to my wife, Peiyu for her love and support during my Ph.D. program.

Silicon Integrated Nanophotonic Devices for on-Chip Optical Interconnects

Che-Yun Lin, Ph.D.
The University of Texas at Austin, 2012

Supervisor: Ray T. Chen

Silicon is the dominant material in Microelectronics. Building photonic devices out of silicon can leverage the mature processing technologies developed in silicon CMOS. Silicon is also a very good waveguide material. It is highly transparent at 1550nm, and it has very high refractive index of 3.46. High refractive index enables building high index contrast waveguides with dimensions close to the diffraction limit. This provides the opportunity to build highly integrated photonic integrated circuit that can perform multiple functions on the same silicon chip, an optical parallel of the electronic integrated circuit. However, silicon does not have some of the necessary properties to build active optical devices such as lasers and modulators. For Example, silicon is an indirect band gap material that can't be used to make lasers. The centro-symmetric crystal structure in silicon presents no electro-optic effect. By contrast, electro-optic polymer can be engineered to show very strong electro-optic effect up to 300pm/V. In this research we

have demonstrated highly compact and efficient devices that utilize the strong optical confinement ability in silicon and strong electro-optic effect in polymer. We have performed detailed investigations on the optical coupling to a slow light waveguide and developed solutions to improve the coupling efficiency to a slow light photonic crystal waveguides (PCW). These studies have lead to the demonstration of the most hybrid silicon modulator demonstrate to date and a compact chip scale true time delay module that can be implemented in future phased array antenna systems. In the future, people may be able to realize a photonic integrated circuit for optical communication or sensor systems using the devices we developed in our research.

TABLE OF CONTENTS

TABLE OF FIGURES

Chapter 1 Introduction on photonic crystal

1.1 Introduction

Photonic crystals are periodic dielectric structures that can prevent light propagation in certain frequency range. This phenomenon is analogous to the energy band gap for electron that exists in semiconductors. Because this band gap behavior is for photons instead of electrons, it is called a photonic band gap[1,2]. Photons with an energy that meets the criteria of the allowed states can propagate through the photonic band gap structure. Conversely, photons with energy that falls in the disallowed states (photonic band gap) will be reflected. When defects are introduced into a photonic crystal, they induce strong localization of light in the defect area, which can be useful in a number of applications[3]. An example of this line defect waveguide can be formed by etching an array of air holes on a silicon nanomembrane on a silicon-on-insulator (SOI) wafer, which is shown in Figure 1 - 1.

The wave-guiding mechanism for a photonic crystal waveguide is different from conventional waveguides. For conventional waveguides, the guiding is based on the refractive index difference between the core and the cladding materials, in which light is confined by total internal reflection. For a slab-type photonic crystal waveguide, a guided mode is confined by both index guiding in vertical direction and coherent back scattering in horizontal direction.

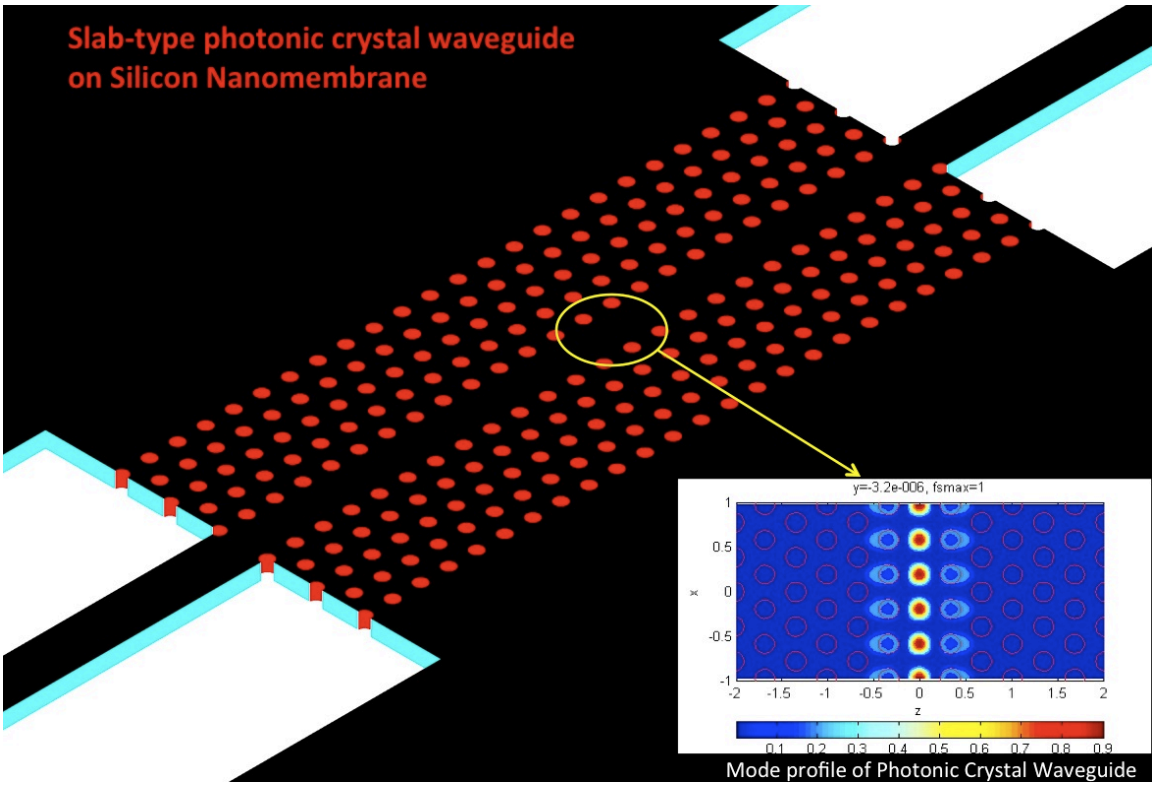

Figure 1 - 1. Two-dimensional photonic crystal waveguide on silicon nanomembrane

A unique feature in a photonic crystal waveguide is that it supports "slow light" at the band edge of the defect induced guided mode[4]. Slow light in photonic crystal waveguide is the combined effect of coherent backscattering and omni-directional reflection from the photonic band gap. In a photonic crystal waveguide, light is back scattered at every unit cell. When the forward propagating and the back scattering components agree in phase and amplitude, they form a standing wave at the boundary of Brillouin zone. This can be viewed as light propagates with zero group velocity. If we move away from the edge of the Brillouin zone, the forward and back-scattering wave begin to move out of phase and form a slowly propagating interference pattern—the "slow light mode". The

left side of Figure 1 - 1 uses three arrows forward and two arrows backwards to represent that the wave is slowly traveling in the photonic crystal waveguide as if it is moving three steps forward and two steps backward. Lateral confinement of light is created by omni-directional backscattering from the periodic structure. Unlike conventional index-guided waveguides, which have a critical angle, light propagation is reflected by photonic band gap in the lateral direction at any angle except for the direction of waveguide. As a result, this mode travels slowly along the waveguide.

1.2 **Slow light enhanced light-matter interaction**

In an electro-optic switching device such a Mach-Zehnder modulator[5], the phase change is proportional to the slow down factor S, which is defined as the ration of the phase velocity over the group velocity:

$$S = \frac{v_\phi}{v_g} = \frac{n_\phi}{n_g} \qquad \text{Equation 1}$$

The phase change in the interaction region is expressed as $\Delta k \cdot L$. The required phase change for Mach-Zehnder interferometer to complete full on/off operation is $\Delta k \cdot L = \Delta n k_0 \cdot L = \pi$, where Δn is the index change in the nonlinear material caused by applied voltage and k_0 is the wave vector in vacuum. It appears that slow light effect does not enter into this equation. However, the switching device operates with guided modes, so the Δn should be the change in effective mode index instead of the change in material index. In a slow light photonic crystal waveguide, the index change in material

Δn_{mat} gives rise to a change in resonance frequency $\Delta\omega$, and the corresponding change in resonant frequency is proportional to the index change $\Delta\omega/\omega \approx \Delta n/n$. However, from the dispersion relation in the photonic crystal waveguide, a small amount material index change (Δn_{mat}) can give rise to large phase change. This effect is illustrated in Krauss, et al[3].

Since Δk scales with the slope of the dispersion curve, it also scales with slow down factor S. As a result, the condition for switching can be re-written as

$$\Delta k \cdot L = \pi = \Delta n k_0 S \cdot L \qquad \text{Equation 2}$$

, which now includes the slow down factor. As a result, although the index change is limited by the electro-optic effect of the material, the phase difference can be significantly enhanced by the strong dispersion in the slow light region.

Throughout this work, we have successfully demonstrated devices and modules based on slow light silicon photonics, which will be described in the following chapters.

1.3 **References**

[1] Eli Yablonovitch, "*Inhibited Spontaneous Emission in Solid-State Physics and Electronics*," Phys. Rev. Lett. **58** (20), 2059 (1987).

[2] Sajeev John, "*Strong localization of photons in certain disordered dielectric superlattices*," Phys. Rev. Lett. **58** (23), 2486 (1987).

[3] Thomas F. Krauss, "*Slow light in photonic crystal waveguides*," J. Phys. D: Appl.

Phys. **40**, 2666-2670 (2007).

[4] Masaya Notomi, K Yamada, A Shinya, J Takahashi, C Takahashi, and I Yokohama, "*Extremely Large Group-Velocity Dispersion of Line-Defect Waveguides in Photonic Crystal Slabs*," Phys. Rev. Lett. **87** (25), 253902 (2001).

[5] Marin Soljačić and John. D. Joannopoulos, "*Enhancement of nonlinear effects using photonic crystals*," Nat Mater **3** (4), 211-219 (2004).

Chapter 2 Wideband and Group Velocity Independent Coupling into Slow Light Silicon Photonic Crystal Waveguide

2.1 Introduction

Slow light in photonic crystal waveguides can significantly enhance light-matter interactions[1-3] and therefore is a promising approach toward realizing advanced photonic devices such as tunable delay lines[4], ultra-compact optical switches[5], and highly-efficient modulators[6-11]. To fully utilize the benefits of the slow light effect, it is crucial to efficiently couple in and out of photonic crystal waveguides from external optical devices. However, coupling between a strip waveguide and a slow light photonic crystal waveguide is challenging. In a conventional silicon strip waveguide, the group index (n_g) is around 3.5, whereas n_g can be as high as 400[12] in a photonic crystal waveguide operating in slow light region. This apparent mismatch in group index can cause strong reflection at the photonic crystal-strip waveguide interface. Without addressing the group velocity mismatch issue, coupling efficiency can become unacceptably low in the slow light region, which significantly limits the usefulness of slow light in practical applications.

Numerous efforts have been made to address this issue predominantly using numerical simulation with a few experimental demonstrations. Here we review several representative cases.

It has been shown theoretically that a quarter-wave transformer concept developed in thin film optics can be utilized to improve strip-photonic crystal waveguide coupling. By designing the photonic crystal waveguide between the strip waveguide and slow light photonic crystal waveguide as a quarter wave transformer[13], simulations have shown very low reflectance around v_g=0.01c, where v_g is the group velocity of the guided mode in photonic crystal waveguide and c is the speed of light in vacuum. However, the narrow band nature of the transformer limits its usage in practical applications. Alternatively, photonic crystal hetero structure injectors can provide efficient coupling for group indices up to 400 with very compact coupling structures[14], but no experimental evidence has been reported to support the feasibility of this approach.

It was also shown experimentally that hetero group velocity photonic crystal waveguides can improve coupling efficiency with improved bandwidth[15]. However, the best experiment result only show 3dB improvement in slow light region and the coupling efficiency at the normal group velocity region even becomes 2dB lower than the control group. Contrast in transmission between the defect guided mode and the photonic bandgap is also limited to less than 10dB. A more convincing experimental work suggests that exact termination of the photonic crystal lattice at the coupling interface can significantly improve the coupling efficiency[16]. The difference in transmission between the defect mode and the photonic bandgap also shows a very good contrast of 30dB. However, this approach cannot maintain the same high coupling efficiency for slow modes near the band-edge[16,17].

By contrast, several theoretical and experimental studies have shown that an adiabatic transition in a pillar-type photonic crystal waveguide can enable efficient coupling into photonic crystal waveguides[18,19]. Recently, theoretical study on photonic crystal waveguide formed by etching air holes on silicon, which should be further studied experimentally for developing compact and efficient coupling structures.

In this work, we present the design and experimental demonstration of efficient and wavelength-independent coupling into a slow light photonic crystal waveguide using two parabolic photonic crystal tapers with gradually changing air hole diameters. Based on the design of reducing the group velocity mismatch between the strip waveguide and the photonic crystal waveguide, our coupling structure requires only eight periods of photonic crystals, a length of 3.24μm, to achieve efficient coupling over the entire spectrum of the guided mode.

2.2 **Design of Photonic Crystal Group Velocity Taper**

A schematic of the slow light photonic crystal waveguide (highlighted in blue) with the photonic crystal taper (highlighted in green) is shown in Figure 2 - 1 (a), which comprises a standard W1 line-defect-induced photonic crystal waveguide with a unified lattice constant of a=405nm and two photonic crystal tapers (symmetric) with gradually changing air hole size. The control group, which has identical slow light waveguide (blue) but without the photonic crystal taper, is shown in Figure 2 - 1 (b). Both waveguides have the same number of periods. The silicon slab thickness and the air hole

diameters are chosen to be h=230nm and d=180nm, respectively, such that the W1 photonic crystal waveguide supports single mode operation.

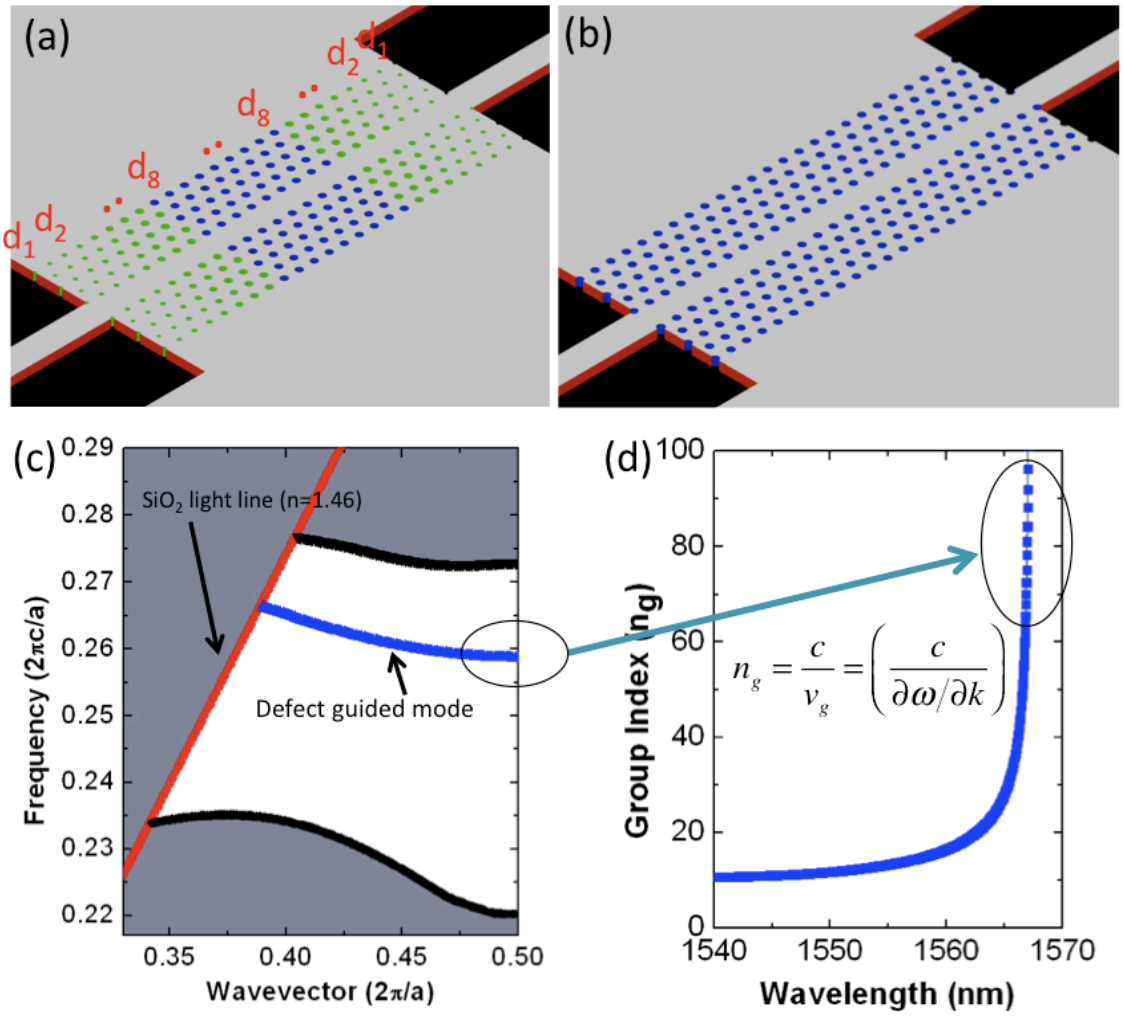

Figure 2 - 1. Schematic of the device structure which shows input and output strip waveguides (red), photonic crystal taper with gradually changing hole sizes (green, not to scale), and the slow light photonic crystal waveguide (blue) (b) Control group: same slow light photonic crystal waveguide as in (a) with same total periods but without group index taper. (c) Dispersion relation of the defect-guided mode in the slow light photonic crystal waveguide, as highlighted in blue in (a) and (b) (d) Group index of each periods of the photonic crystal waveguide shown in (a).

The dispersion relation (photonic band diagram) and group index (n_g) versus wavelength relation of the defect-guided mode were calculated using a three-dimensional (3D) plane-wave expansion (PWE) method as shown in Figure 2 - 1 (c) and (d). The simulated band diagram shows a guided mode from 1522nm to 1567nm, which falls inside our experiment observation window.

The choice of air hole diameters (d_n, n=1,2,…8) to create the photonic crystal tapers is based on an empirical equation $d_n = 144.15 + 8.19n - 0.46n^2$, which can create a smooth group velocity taper. The choice of air hole diameters in the taper region is plotted in Figure 2 - 2 (a). To have a better understanding on the effect of group index taper, we calculate the group index (n_g) of each period of the taper as a function of wavelength using a 3D PWE method as shown in Figure 2 - 2 (b). One can see from the group index dispersion relation in Figure 2 - 2 (b) that this gradual increment of hole size results in a gradual increase of group index for the guided mode. Compared to butt coupling, the guided mode sees a smoother transition in group index as it enters the photonic crystal waveguide. As a result, the guided mode coupled from the strip waveguide can slow down gradually over the eight periods of taper region as it enters the slow light waveguide. Coupling out of the slow light photonic crystal waveguide to a strip waveguide is simply the reverse process. Under this design, the group velocity mismatch between a strip waveguide and a slow light photonic crystal waveguide is significantly reduced, which should lead to significant improvement of coupling efficiency.

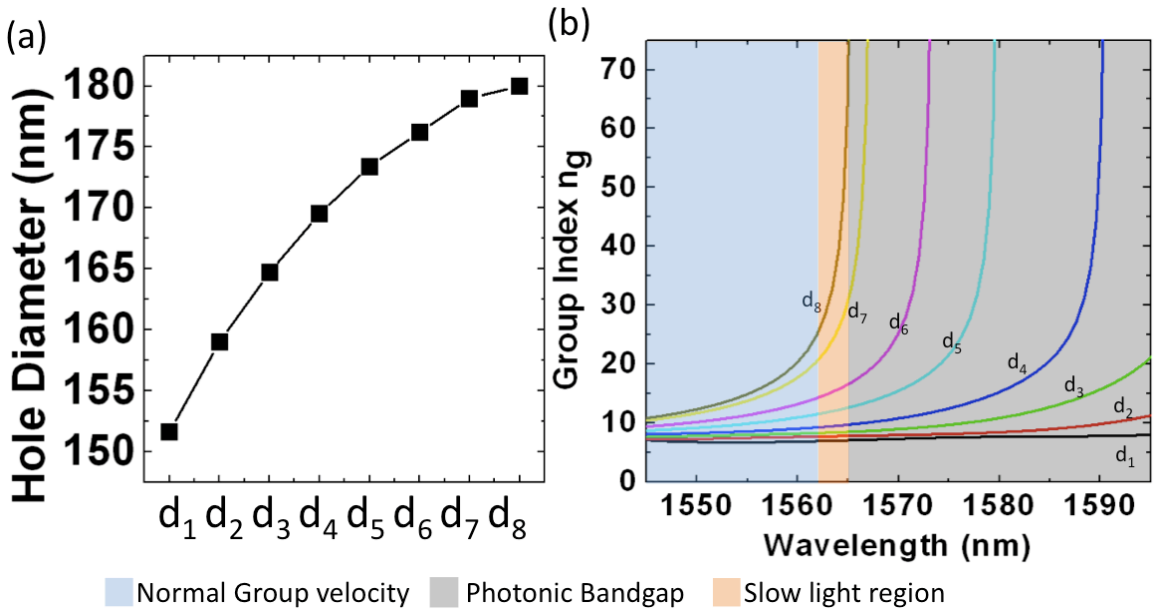

Figure 2 - 2. (a) The hole diameters of d_1, d_2,…d_8. (b) Group index (n_g) versus wavelength relation for different hole diameters in (a).

Transmission through the photonic crystal waveguide devices was simulated by 2D FDTD and the result is shown in Figure 2 - 3. Although the group index taper is only eight periods (3.24μm long) of the photonic crystal waveguide, this coupling structure has a dramatic impact on coupling efficiency into a slow light mode. For a photonic crystal waveguide without any taper, coupling efficiency starts to drop well before the band edge. By contrast, when photonic crystal taper is included in the photonic crystal waveguide, coupling efficiency remains nearly the same as its peak value even in the slow light region. Additionally, this coupling structure reduces the fluctuation of coupling efficiency due to reduced Fabry-Perot reflections.

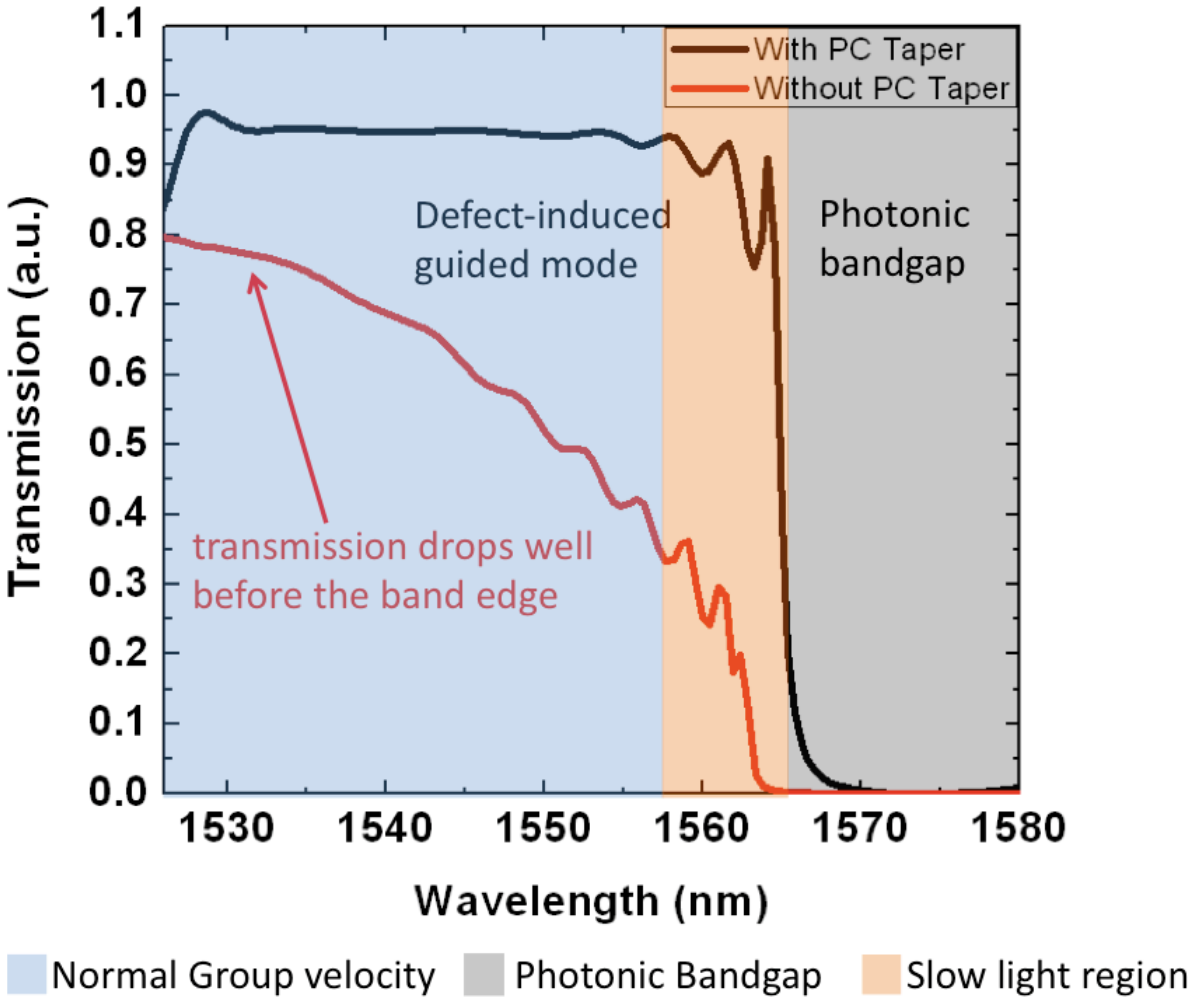

Figure 2 - 3. Simulated transmission spectrum using 2D FDTD analysis, comparing the coupling performance of W1 photonic crystal waveguides with (black curve) and without (red curve) group index tapers.

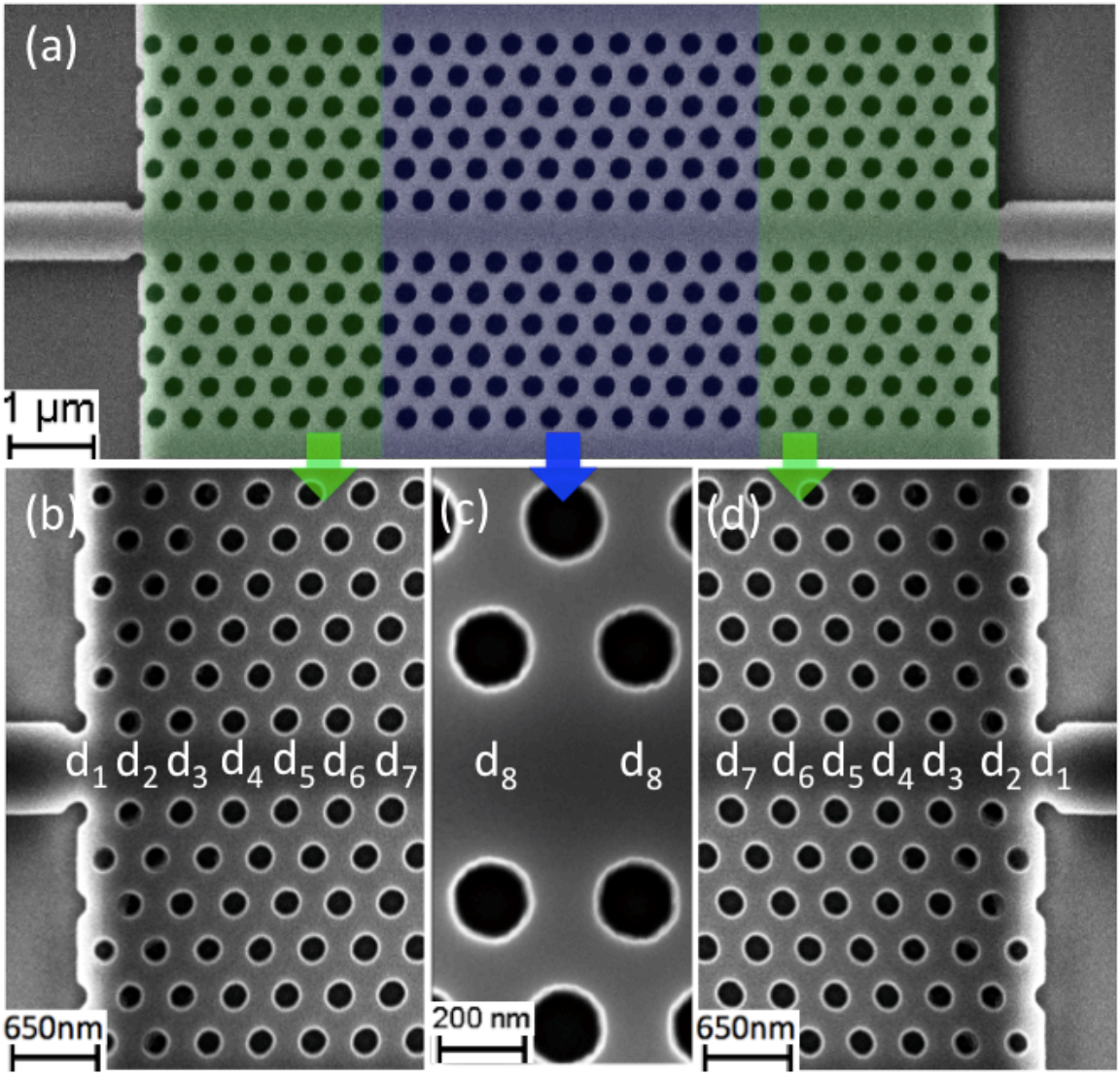

Figure 2 - 4. Scanning electron micrograph (SEM) of the fabricated photonic crystal waveguide structure. (a) Global look of the photonic crystal waveguide device, which includes a strip waveguide, a group index taper (green), and a slow light photonic crystal waveguide (blue). (b), (d) Enlarged view of the eight periods of group index taper. (c) Enlarged view of the slow light photonic crystal waveguide region.

2.3 Fabrication of Photonic Crystal Taper and Slow Light Waveguides

Photonic crystal waveguide devices were fabricated on a Unibond silicon-on-insulator (SOI) wafer with a 230nm top silicon layer and a 3μm buried oxide (BOX) layer. 45nm of thermal oxide was thermally grown as an etching mask for pattern transfer. Photonic crystal waveguides, photonic crystal tapers, and strip waveguides are patterned in one step with a JEOL JBX-6000FS electron-beam lithography system followed by reactive ion etching. Photonic crystal waveguide devices were formed in a non-membrane configuration with the patterned silicon photonic crystal waveguide core supported by the 3μm BOX as bottom cladding layer. The hole dimension and the width of photonic crystal waveguides can be precisely controlled with errors less than 2nm and sidewall roughness ~5nm estimated by scanning electron microscope (SEM) inspection. Photonic crystal waveguide devices with and without a group index taper were fabricated on the same chip with an identical fabrication process. SEM images of the fabricated structure are shown in Figure 2 - 4.

2.4 Device Testing: Transmission Spectrum Measurement

To characterize the coupling performance, photonic crystal waveguide devices were tested on a Newport six-axis auto-aligning station. Testing setup is shown in Figure 2 - 5. Input light from a broadband ASE source (Thorlab ASE-FL7002) covering the 1520nm~1620nm wavelength range was TE-polarized with a 23dB TE/TM rejection ratio and butt-coupled to / from the device with a polarization maintaining single mode tapered lensed fiber with a mode field diameter of 3μm. Transmitted light was analyzed with an

optical spectrum analyzer (ANDO AQ6317B) with 0.04nm resolution. The transmission spectra of photonic crystal waveguides with and without group index tapers were normalized to the transmission spectrum without the device as shown in Figure 2 - 6.

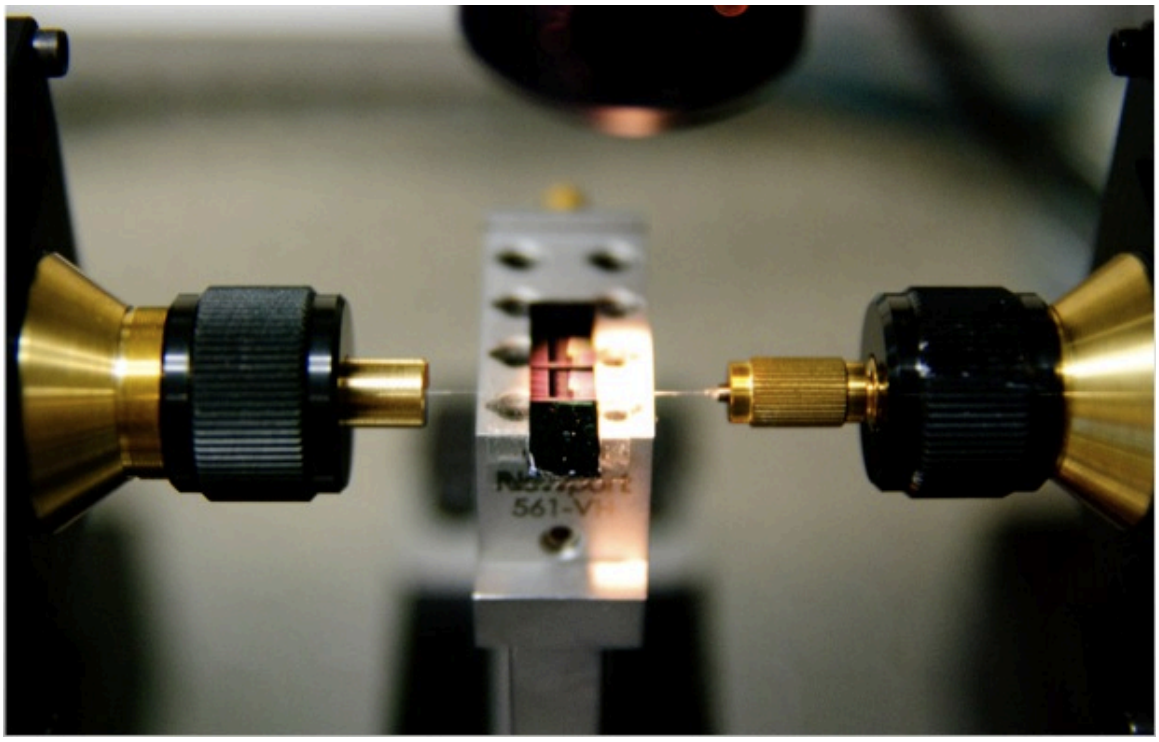

Figure 2 - 5. Testing setup for the photonic crystal waveguide devices.

2.5 **Experiment Result and Discussion**

In Figure 2 - 6, the transmission spectra show that the photonic crystal waveguide devices support defect-guided modes from 1523nm to 1568nm, which agrees well with both PWE and FDTD simulation. Compared with direct coupling from a strip waveguide, the W1 photonic crystal waveguide with group index taper shows several distinct improvements in the coupling efficiency. First, one can see significantly less Fabry-Perot

noise when the group index tapers are added. The transmission fluctuation caused by the Fabry-Perot effect is suppressed by 5dB throughout the defect mode. As a result, photonic crystal waveguide with group index taper shows a nearly flat transmission. Secondly, the transmission is improved by more than 20dB over the entire guided mode bandwidth of 45nm. Third, the coupling efficiency remains very close to its peak value until 2 nm away from the photonic bandgap cut-off at 1568nm, meaning slow light modes near the band edge with very high group index can be coupled into the photonic crystal waveguide as low group index mode. Fourth, the group index taper offers even better coupling enhancement for the slow light mode near the bandedge. For the photonic crystal waveguide with group index taper, the normalized transmission at 1566 nm (2nm from the photonic bandgap) only drops 2dB from its peak transmission, whereas it drops 10dB without the group index taper. Under 20dB of baseline enhancement, this translates into 28dB improvement for the band edge slow light mode.

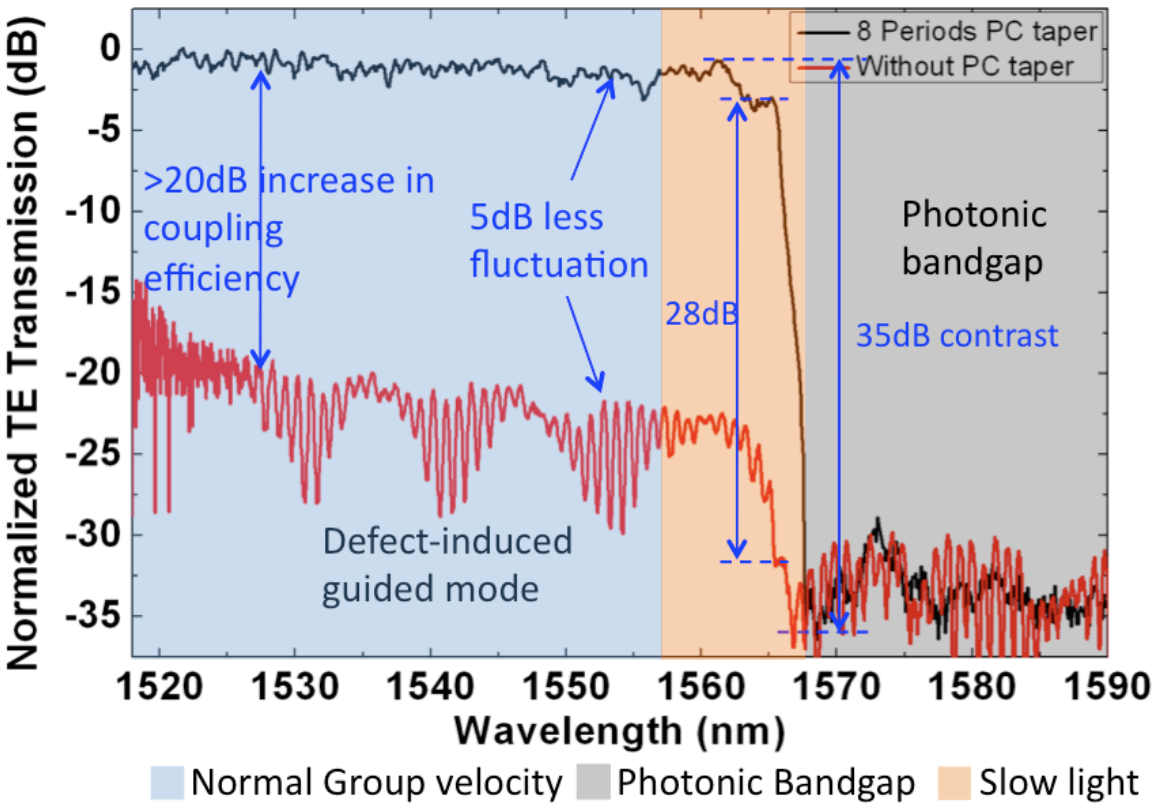

Figure 2 - 6. Transmission spectrum comparison for photonic crystal waveguide with group index tapers (black curve) and the control group without taper (red curve).

2.6 **Limitation of The Group Index Taper**

The limitation of this coupling approach can also be observed from the band edge cut off behavior. One may notice that the slope of the transmission drop between 1566nm and 1568nm has two distinct regions. The first region from 1566nm to 1567.5nm shows a 25dB drop in transmission within 2.5nm, indicating this coupling mechanism starts to reach its limitation when group velocity slows rapidly as a function of wavelength. The second region from 1566.5nm to 1567nm shows a 10dB drop in transmission in just

0.5nm, which is likely due to the very high propagation loss associated with extremely high group index.

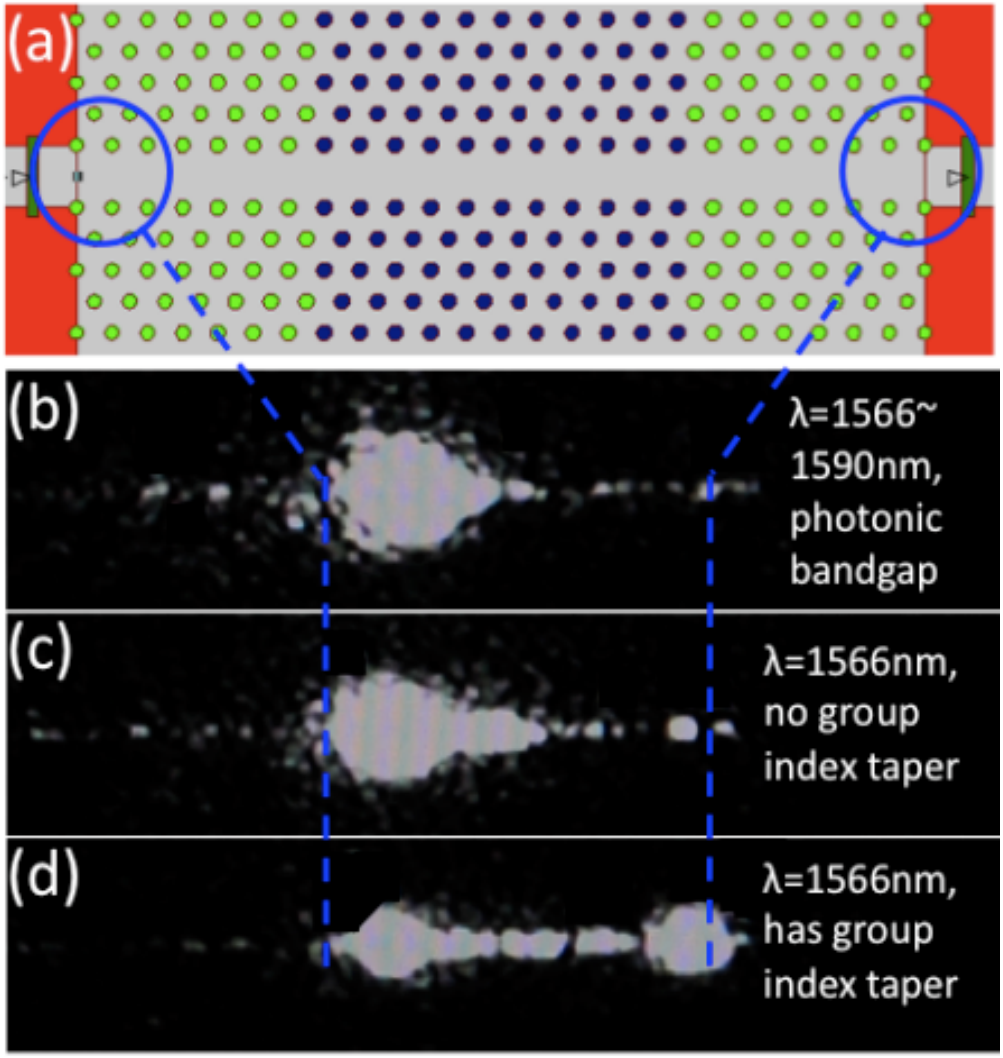

Figure 2 - 7. (a) Schematic of the photonic crystal waveguide device. (b) IR image taken at the wavelength of the photonic bandgap. (c) IR image for the control group without group index taper. (d) IR image for the photonic crystal waveguide with group index taper.

2.7 Visualization of Photonic Bandgap Effect and Coupling

To visualize the effect of the group velocity taper, we observe the light transmission behavior with infrared (IR) microscope above the photonic crystal waveguide. The waveguide testing setup is identical to the device characterization section, except we replace the broadband light source with a tunable laser (Santec ECL-2000) for input source. The IR images are shown in Fig. 8. At the wavelength of the photonic bandgap (1568nm and longer), the input light from the strip waveguide is completely blocked by the photonic bandgap effect and no light is observed at the output of the photonic crystal waveguide as shown in Figure 2 - 7 (b). Figure 2 - 7 (c) and (d) show the transmission behavior at the slow light wavelength (1565nm) of defect mode for photonic crystal devices without and with group index taper. One can see in Figure 2 - 7 (d) that the input light from strip waveguide is better transmitted when the group index taper is present, whereas it is mostly reflected for the control group without taper as shown in Figure 2 - 7 (c).

2.8 Conclusion

In conclusion, we show the design and experimental results of efficient coupling into a photonic crystal waveguide using group index tapers based on matching the group velocity between a conventional strip waveguide and a slow light photonic crystal waveguide. Experiments show good coupling efficiency can be maintained to the photonic crystal band edge regardless of the group velocity of the guided mode by using only eight periods of group index taper. The measurement results also shows excellent

agreement with plane wave expansion (BandSOLVE) and fininte-difference time domain (FDTD) simulation with discrepancy less than 2nm. Compared to a photonic crystal waveguide without a group index taper, measurements show a 20dB baseline improvement in coupling efficiency, 5dB less fluctuation, and a 28dB enhancement for the slow light mode using only 3.24μm long of group index taper. The experimental result also shows that less than 10μm of photonic crystal waveguide is needed to create a 35dB contrast in transmission. Such a photonic crystal waveguide structure could serve as the stepping-stone toward building ultra-compact photonic devices for on-chip optical interconnects.

2.9 **Acknowledgement**

The authors would like to acknowledge the Air Force Office of Scientific Research (AFOSR) for supporting this work under the AFOSR Multidisciplinary University Research Initiative (MURI) grant (Grant No. FA 9550-08-1-0394) monitored by Dr. Gernot Pomrenke and the Small Business Technology Transfer Research (STTR) program (Grant No. FA 9550-09-C-0086) monitored by Dr. Charles Y-C. Lee.

2.10 References

[1] Thomas F. Krauss, "*Slow light in photonic crystal waveguides*," J. Phys. D: Appl. Phys. **40**, 2666-2670 (2007).

[2] Toshihiko Baba, "*Slow light in photonic crystals*," Nature Photonics **2** (8), 465-473 (2008).

[3] B. Corcoran, C. Monat, C. Grillet, D. J. Moss, B. J. Eggleton, T. P. White, O'FaolainL, and T. F. Krauss, "*Green light emission in silicon through slow-light enhanced third-harmonic generation in photonic-crystal waveguides*," Nat Photon **3** (4), 206-210 (2009).

[4] M. Povinelli, Steven Johnson, and J. Joannopoulos, "*Slow-light, band-edge waveguides for tunable time delays*," Opt. Express **13** (18), 7145-7159 (2005).

[5] Daryl M. Beggs, Thomas P. White, Liam O'Faolain, and Thomas F. Krauss, "*Ultracompact and low-power optical switch based on silicon photonic crystals*," Opt. Lett. **33** (2), 147-149 (2008).

[6] Che-Yun Lin, Xiaolong Wang, Swapnajit Chakravarty, Beom Suk Lee, Weicheng Lai, Jingdong Luo, Alex K.-Y. Jen, and Ray T. Chen, "*Electro-optic polymer infiltrated silicon photonic crystal slot waveguide modulator with 23 dB slow light enhancement*," Appl. Phys. Lett. **97** (9), 093304 (2010).

[7] Xiaolong Wang, Swapnajit Chakravarty, Boem Suk Lee, Che-Yun Lin, and Ray T. Chen, "*Ultraefficient control of light transmission through photonic potential barrier modulation*," Opt. Lett. **34** (20), 3202-3204 (2009).

[8] Jan-Michael Brosi, Christian Koos, Lucio C. Andreani, Michael Waldow, Juerg

Leuthold, and Wolfgang Freude, "*High-speed low-voltage electro-optic modulator with a polymer-infiltrated silicon photonic crystal waveguide*," Optics Express **16** (6), 4177-4191 (2008).

[9] Lanlan Gu, Wei Jiang, Xiaonan Chen, Li Wang, and Ray T. Chen, "*High speed silicon photonic crystal waveguide modulator for low voltage operation*," Appl. Phys. Lett. **90** (7), 071105 (2007).

[10] Lanlan Gu, Wei Jiang, Xiaonan Chen, and Ray T. Chen, "*Thermooptically Tuned Photonic Crystal Waveguide Silicon-on-Insulator Mach-Zehnder Interferometers*," Photonics Technology Letters, IEEE **19** (5), 342-344 (2007).

[11] Yongqiang Jiang, Wei Jiang, Lanlan Gu, Xiaonan Chen, and Ray T. Chen, "*80-micron interaction length silicon photonic crystal waveguide modulator*," Appl. Phys. Lett. **87** (22), 221105-221103 (2005).

[12] Yurii A. Vlasov, Martin O'Boyle, Hendrik F. Hamann, and Sharee J. McNab, "*Active control of slow light on a chip with photonic crystal waveguides*," Nature (London) **438** (7064), 65-69 (2005).

[13] C. Martijn de Sterke, J. Walker, Kokou B. Dossou, and Lindsay C. Botten, "*Efficient slow light coupling into photonic crystals*," Opt. Express **15** (17), 10984-10990 (2007).

[14] J. P. Hugonin, P. Lalanne, T. P. White, and Thomas. F. Krauss, "*Coupling into slow-mode photonic crystal waveguides*," Opt. Lett. **32** (18), 2638-2640 (2007).

[15] Nobuhiko Ozaki, Yoshinori Kitagawa, Yoshiaki Takata, Naoki Ikeda, Yoshinori Watanabe, Akio Mizutani, Yoshimasa Sugimoto, and Kiyoshi Asakawa, "*High transmission recovery of slow light in a photonic crystal waveguide using a hetero*

groupvelocity waveguide," Opt. Express **15** (13), 7974-7983 (2007).

[16] Yurii A. Vlasov and Sharee J. McNab, "*Coupling into the slow light mode in slab-type photonic crystal waveguides*," Opt. Lett. **31** (1), 50-52 (2006).

[17] Masaya Notomi, K Yamada, A Shinya, J Takahashi, C Takahashi, and I Yokohama, "*Extremely Large Group-Velocity Dispersion of Line-Defect Waveguides in Photonic Crystal Slabs*," Phys. Rev. Lett. **87** (25), 253902 (2001).

[18] Solomon Assefa, Peter T. Rakich, Peter Bienstman, Steven G. Johnson, Gale S. Petrich, John D. Joannopoulos, Leslie A. Kolodziejski, Erich P. Ippen, and Henry I. Smith, "*Guiding 1.5 mu m light in photonic crystals based on dielectric rods*," Appl. Phys. Lett. **85** (25), 6110-6112 (2004).

[19] Steven G. Johnson, Peter Bienstman, M. A. Skorobogatiy, Mihai Ibanescu, Elefterios Lidorikis, and J. D. Joannopoulos, "*Adiabatic theorem and continuous coupled-mode theory for efficient taper transitions in photonic crystals*," Phys. Rev. E **66** (6), 066608 (2002).

Chapter 3 Coupling Loss Minimization of Slow Light Slotted Photonic Crystal Waveguides Using Mode Matching with Continuous Group Index Perturbation

3.1 Abstract

We experimentally demonstrate highly efficient coupling into a slow light slotted photonic crystal waveguide. With optical mode converters and group index tapers that provide good optical mode matching and impedance matching, a nearly flat transmission over the entire guided mode spectrum of 68.8nm range with 2.4dB minimum insertion loss is demonstrated. Measurements also show up to 20dB baseline enhancement and 30dB enhancement in the slow light region, indicating that it is possible to design highly efficient and compact devices that benefit from the slow light enhancement without increasing the coupling loss.

3.2 Introduction

Slotted photonic crystal waveguides (Slotted PCWs) offer a unique platform that merges the best properties of slot waveguides and photonic crystal waveguides (PCW): strong optical confinement in slot waveguides[1-4] and slow light enhanced light-matter interaction in PCWs[5-7]. In a W1 PCW, the optical mode profile spreads deeper into the photonic lattice with reduced group velocity[5,8]. This lateral spread reduces optical confinement and increases propagation loss for slow light modes, which can weaken some of the benefits

derived from the slow light effect. By contrast, in slotted PCW, optical confinement does not decrease with increased group index, as a result of the high index contrast in silicon platform. In a high index contrast interface, a transverse electric guided mode is required to have much higher intensity in the low index region. Consequently, when approaching the edge of the photonic band gap, the percentage of energy concentration in the low index slot will increase rather than decrease[9]. The increasing optical confinement with slower group velocity is a very advantageous property for compact optical communication devices[9-19] and on-chip sensors[20,21]. Despite these benefits, optical coupling between a strip waveguide and a slotted PCW is more challenging than conventional PCW due to the exotic mode profile and slow group velocity in the slotted PCW. Without a properly designed coupling interface, strongly confined guided mode profile with minimal overlap and large group index mismatch result in negligible coupling[22]. Efforts to improve the coupling efficiency include using a multi-mode interference (MMI) coupler[22], changing the termination of the slot[23], and resonant coupling[24]. However, MMI coupler only provides efficient coupling with limited bandwidth. Changing the slot termination position improves bandwidth[23], but with low overall transmission. Resonant coupler approach shows better coupling efficiency, but could not avoid a strong transmission dip ~-10dB in the slow light region. By contrast, a theoretical study suggests that good coupling is achievable with good mode profile and group index matching[16]. Based on similar concept, we present a simpler design and experimentally demonstrate highly efficient coupling into slow light slotted PCW. We

also study the effect of mode matching and group index matching experimentally, which offers more insights on the strip-slotted PCW coupling process.

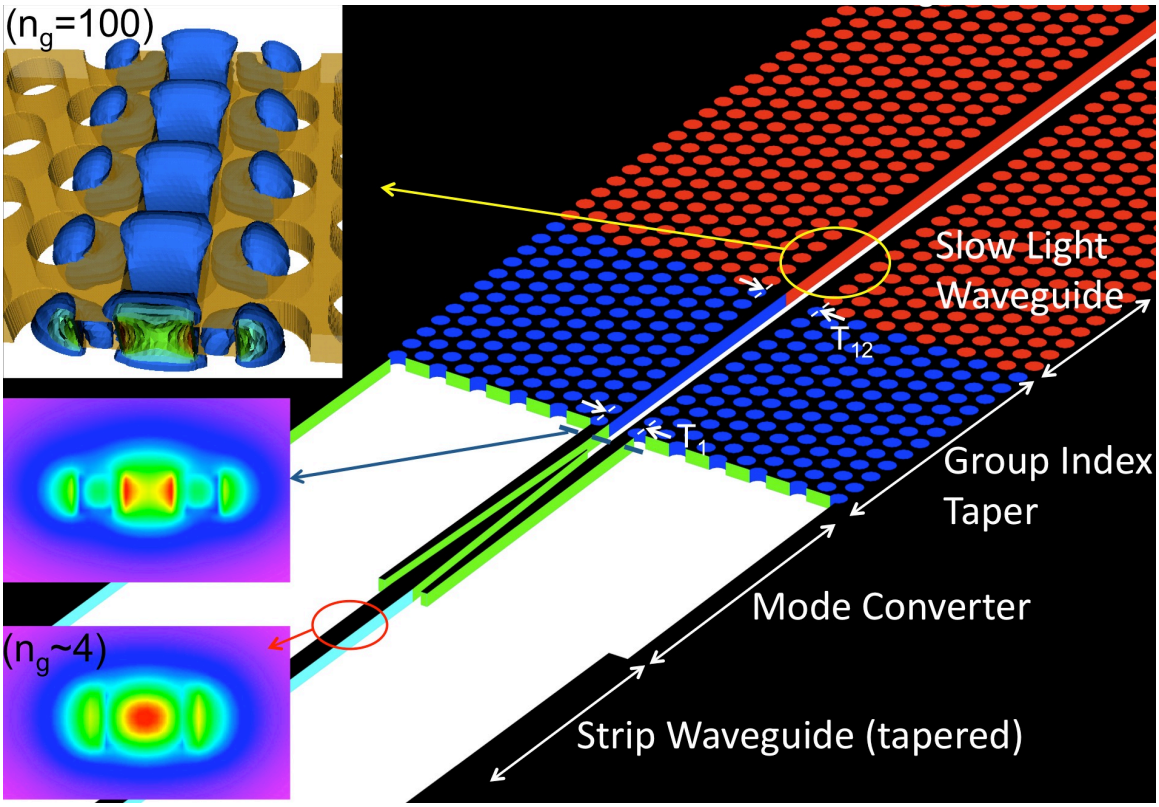

Figure 3 - 1. Schematic of the slow light slotted PCW, group index taper, mode converter, and strip waveguide (tapered). The insets show the mode profiles of a strip waveguide and a slow light slotted PCW at high group index (n_g=100).

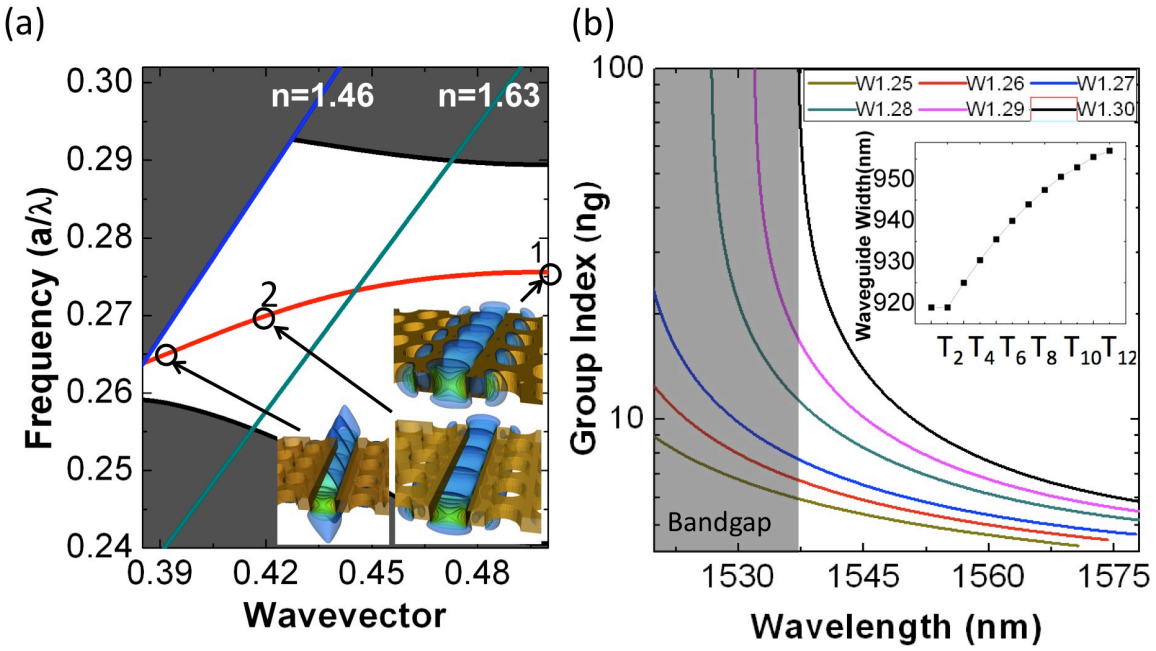

Figure 3 - 2. (a) Photonic band diagram. (b) Group index versus wavelength. The inset shows the waveguide width in the group index taper region.

3.3 **Design of The Group Index Taper**

The schematic of the slotted PCW is shown in Figure 3 - 1. The slotted PCW devices are formed by etching air holes and slots on a 230nm crystalline silicon nanomembrane sandwiched between a 3μm thick silicon dioxide layer (n=1.46) and a 2μm thick polymer layer (n=1.63), which serves as the bottom and top cladding layers, respectively. Air holes and slots are filled with the same material as the top cladding, which also prevents undesirable oxidation of the silicon layer. The lattice constant (a), air hole diameter (d), slot width (sw), silicon thickness (h) and line defect waveguide width (T_{12}) for the slow light waveguide are chosen to be a=425nm, d=297nm, sw=320nm, h=230nm, and T_{12}= $1.3\sqrt{3}a$ so that this waveguide supports a defect-guided mode that falls inside our

experiment observation window of 1520~1610nm. The photonic band diagram for the slow light waveguide is shown in Figure 3 - 2 (a). The in-plane electric field distributions of the guided mode at wave vectors below and above polymer light line are also shown in the inset of Figure 3 - 2 (a). The radiation loss above polymer light line is small for the length of our devices. Therefore it is possible to have transmission between polymer light line (n=1.63) and oxide light line (n=1.46). This phenomenon was also verified experimentally as shown in Figure 3 - 4. To minimize the modal mismatch, we use an optical mode converter that can convert a strip waveguide mode into a conventional slot waveguide mode[25], which has a mode profile similar to that of a slotted PCW[1,2,22]. To further improve mode profile matching with a strip waveguide, a wide slot width of 320nm is intentionally chosen, a maximum width that supports a mode size similar to that of a 340nm wide silicon strip waveguide. For a photonic crystal modulator operating in the slow light region, the increased slow light mode coupling efficiency and relaxed fabrication requirements compensate for the loss in optical confinement, leading to better overall performance with a wider slot[9,10]. The group index mismatch can be adiabatically tuned by using a photonic crystal group index taper[26,27] that provides a smooth transition in group index[26] as shown in Figure 3 - 2 (b). The taper is formed by parabolically reducing the width of a line defect waveguide from ($T_{12}=1.3\sqrt{3}a$) towards the coupling interface ($T_1=1.25\sqrt{3}a$) as shown schematically in Figure 3 - 1. The parabolic photonic crystal taper is designed by choosing a line defect waveguide width (T_1) that has lower group index than the slow light waveguide (T_{12}) over the entire guided mode spectrum followed by parabolic fitting to determine the waveguide widths (T_2~T_{11}) between them.

The taper design uses unified hole size, which is much easier to realize than the taper in[16]. It is worth nothing that these design principles based on mode profile matching and parabolic group index taper should work for narrower slots as well. However, narrower slots are more sensitive to sidewall roughness due to higher field intensity

3.4 **Fabrication of Four Test Structures**

Slotted PCW devices were fabricated on a silicon-on-insulator wafer with 230nm top silicon layer and 3μm buried oxide. Details on the fabrication and characterization methods were described elsewhere[9,10,27]. Four different designs were fabricated to experimentally study the effect of mode matching and group index matching in a strip waveguide-slotted PCW coupling. Scanning electron microscopy (SEM) pictures of the fabricated devices are shown in Figure 3 - 4.

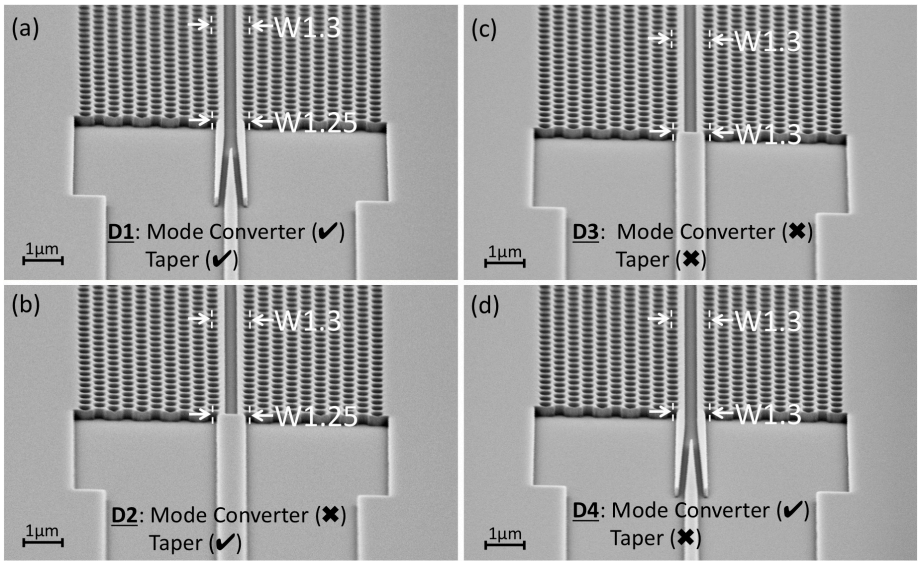

Figure 3 - 3. Scanning electron microscope (SEM) pictures of the fabricated slotted PCW devices.

3.5 **Transmission Spectra Measurements**

Figure 3 - 4 shows the comparison of transmission spectra measured from the four different devices (D1-D4) in Figure 3 - 3 and experimental n_g value calculated from the fringes in D4 using the method described in[28]. These results highlight the importance of mode matching and impedance matching for achieving wide bandwidth, low loss, and group velocity independent coupling. Several distinct differences are observed in the transmission spectra. First, the transmission spectrum of D1 shows the best coupling efficiency, featuring minimum insertion loss of 2.4dB around 1546.5nm in reference to a strip waveguide of equal length on the same chip. Second, low frequency fringes due to Fabry-Perot reflections at the strip-Slotted PCW interface are suppressed. This results in a nearly flat and high transmission throughout the entire defect-guided mode spectrum. Third, comparing D1 to D4 demonstrates a 7 dB loss in coupling efficiency if group index matching is not achieved. Fourth, the comparison between D1 and D3 shows the loss in transmission can be as high as 13dB if both mode matching and group index matching are not attempted. Fifth, the transmission cut-off wavelengths of slotted PCW devices without mode converters (D2 and D3) happen at 1538.8nm and 1538.4nm, as opposed to 1537.3nm and 1537.4nm for devices that have mode converters (D1 and D4). It is known that cut-off wavelength is a unique property of the guiding region, which is identical for D1~D4. This result illustrates that the coupling loss for slow light can be very high for non-optimized structures. To make sure that this difference in cut off wavelengths is not a result of fabrication error, careful SEM inspection was performed on three sets of samples to confirm that all devices are identical in the slow light waveguide

region. The same measurement was also repeated multiple times on each set of samples. All measurements show identical trends with minor variations. Finally, D2 shows the lowest coupling efficiency despite having the group index taper design. This is mainly due to the gradually decreasing waveguide width in the photonic crystal taper region. Without a mode converter to achieve mode matching, the narrower width of slotted PCW at the taper region can deteriorate the modal mismatch and cause low coupling efficiency when compared with the scenario shown in D3.

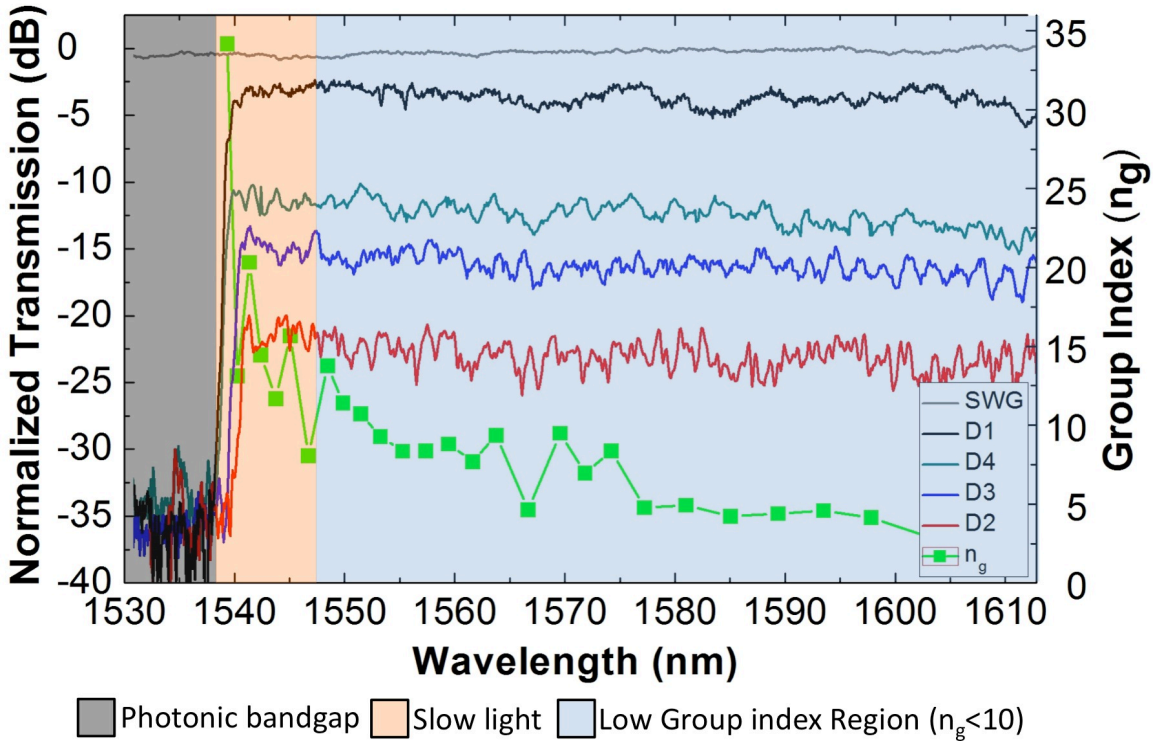

Figure 3 - 4. Transmission spectra of D1, D2, D3, and D4. SWG represents strip waveguide

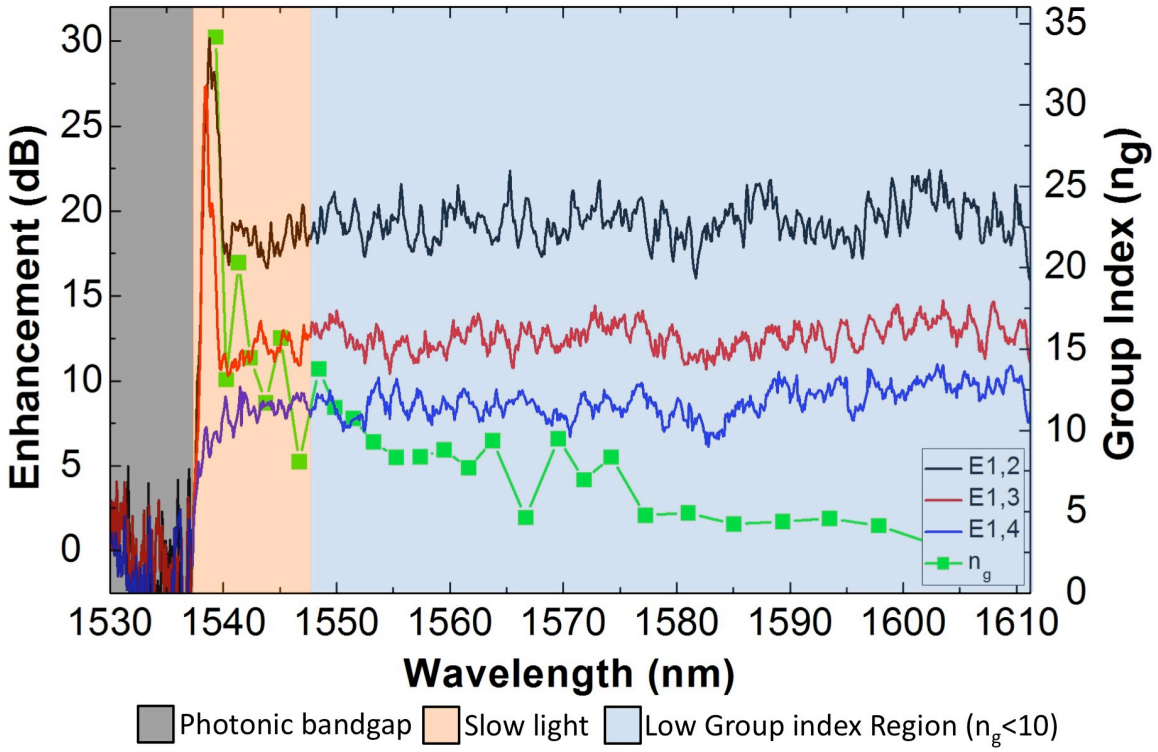

Figure 3 - 5. Enhancement spectrum defined as the transmission difference between device D1 and other devices.

In order to accurately depict the enhancement of coupling efficiency in the slow light region, we also show the difference in transmission between the best case of D1 and others (D2, D3, and D4) together with group index. From Figure 3 - 5, one can see that the baseline in D1 is more than 17dB (E1,2 curve), 10dB (E1,3 curve), and 7dB (E1,4 curve) higher than D2, D3, and D4. The transmission enhancement in the high group index region around 1537nm~1541nm is even more significant. Curves E1,2 and E1,3 show strong enhancements of 30dB and 27dB within a 3nm and a 2nm spectrum next to the photonic bandgap. These results highlight the coupling efficiency enhancement in the most important region for the operation of slow light devices.

3.6 **Conclusion**

In conclusion, the experimental demonstration of efficient coupling into a slow light slotted photonic crystal waveguide is reported. Measurement results show up to 20dB enhancement in overall coupling efficiency and up to 30dB enhancement in the high group index region near the band edge. Suppression of low frequency fringes confirms that Fabry-Perot reflection at a strip-slotted PCW interface is minimized. A flat-top transmission spectrum and a 2.4dB insertion loss for a 34μm long slotted PCW represents the possibility to design devices that benefit from slow light enhancement without the classically high coupling loss associated with group index or modal mismatch.

3.7 **Acknowledgement**

The authors would like to acknowledge the Air Force Office of Scientific Research (AFOSR) for supporting this work under the AFOSR Multidisciplinary University Research Initiative (MURI) grant (Grant No. FA 9550-08-1- 0394) monitored by Dr. Gernot Pomrenke and the Small Business Technology Transfer Research (STTR) program (Grant No. FA 9550-09-C-0086) monitored by Dr. Charles Y.-C. Lee.

3.8 **References**

[1] Vilson R. Almeida, Qianfan Xu, Carlos A. Barrios, and Michal Lipson, "*Guiding and confining light in void nanostructure*," Opt. Lett. **29** (11), 1209-1211 (2004).

[2] Qianfan Xu, Vilson R. Almeida, Roberto R. Panepucci, and Michal Lipson, "*Experimental demonstration of guiding and confining light in nanometer-sizelow-refractive-index material*," Opt. Lett. **29** (14), 1626-1628 (2004).

[3] Xu Qianfan, R. Almeida Vilson, A. Barrios Carlos, R. Panepucci Roberto, and Lipson Michal, "*Silicon void nano-waveguides for guiding and confining light***"**, presented at the Conference on Lasers and Electro-Optics/International Quantum Electronics Conference and Photonic Applications Systems Technologies, (2004).

[4] P. Andrew Anderson, Bradley S. Schmidt, and Michal Lipson, "*High confinement in silicon slot waveguides with sharp bends*," Opt. Express **14** (20), 9197-9202 (2006).

[5] Thomas F. Krauss, "*Slow light in photonic crystal waveguides*," J. Phys. D: Appl. Phys. **40**, 2666-2670 (2007).

[6] Toshihiko Baba, "*Slow light in photonic crystals*," Nature Photonics **2** (8), 465-473 (2008).

[7] Thomas F. Krauss, "*Why do we need slow light?*," Nat Photon **2** (8), 448-450 (2008).

[8] M. R. Patterson, S. Hughes, S. Schulz, D. M. Beggs, T. P. White, L. O'Faolain, and Thomas. F. Krauss, "*Disorder-induced incoherent scattering losses in photonic crystal waveguides: Bloch mode reshaping, multiple scattering, and breakdown of the Beer-Lambert law*," Phys. Rev. B **80** (19), 195305 (2009).

[9] Che-Yun Lin, Xiaolong Wang, Swapnajit Chakravarty, Beom Suk Lee, Weicheng Lai, Jingdong Luo, Alex K.-Y. Jen, and Ray T. Chen, "*Electro-optic polymer infiltrated silicon photonic crystal slot waveguide modulator with 23 dB slow light enhancement*," Appl. Phys. Lett. **97** (9), 093304 (2010).

[10] Xiaolong Wang, Che-Yun Lin, Swapnajit Chakravarty, Jingdong Luo, Alex K. Y. Jen, and Ray T. Chen, "*Effective in-device r33 of 735pm/V on electro-optic polymer infiltrated silicon photonic crystal slot waveguides*," Opt. Lett. **36** (6), 882-884 (2011).

[11] Hong C. Nguyen, Yuya Sakai, Mizuki Shinkawa, Norihiro Ishikura, and Toshihiko Baba, "*10 Gb/s operation of photonic crystal silicon optical modulators*," Opt. Express **19** (14), 13000-13007 (2011).

[12] Xiaolong Wang, Swapnajit Chakravarty, Boem Suk Lee, **Che-Yun Lin**, and Ray T. Chen, "*Ultraefficient control of light transmission through photonic potential barrier modulation*," Opt. Lett. **34** (20), 3202-3204 (2009).

[13] Xiaonan Chen, Alan X. Wang, Swapnajit Chakravarty, and Ray T. Chen, "*Electrooptically-Active Slow-Light-Enhanced Silicon Slot Photonic Crystal Waveguides*," IEEE J. Sel. Top. Quantum Electron. **15** (5), 1506-1509 (2009).

[14] Xiaonan Chen, Yun-Sheng Chen, Yang Zhao, Wei Jiang, and Ray T. Chen, "*Capacitor-embedded 0.54 pJ/bit silicon-slot photonic crystal waveguide modulator*," Opt. Lett. **34** (5), 602-604 (2009).

[15] Gu Lanlan, Jiang Wei, Chen Xiaonan, and R. T. Chen, "*Physical Mechanism of p-i-n-Diode-Based Photonic Crystal Silicon Electrooptic Modulators for Gigahertz Operation*," Selected Topics in Quantum Electronics, IEEE Journal of **14** (4), 1132-1139 (2008).

[16] Jan-Michael Brosi, Christian Koos, Lucio C. Andreani, Michael Waldow, Juerg Leuthold, and Wolfgang Freude, "*High-speed low-voltage electro-optic modulator with a polymer-infiltrated silicon photonic crystal waveguide*," Optics Express **16** (6), 4177-4191 (2008).

[17] Lanlan Gu, Wei Jiang, Xiaonan Chen, Li Wang, and Ray T. Chen, "*High speed silicon photonic crystal waveguide modulator for low voltage operation*," Appl. Phys. Lett. **90** (7), 071105 (2007).

[18] Lanlan Gu, Wei Jiang, Xiaonan Chen, and Ray T. Chen, "*Thermooptically Tuned Photonic Crystal Waveguide Silicon-on-Insulator Mach-Zehnder Interferometers*," Photonics Technology Letters, IEEE **19** (5), 342-344 (2007).

[19] Yurii A. Vlasov, Martin O'Boyle, Hendrik F. Hamann, and Sharee J. McNab, "*Active control of slow light on a chip with photonic crystal waveguides*," Nature (London) **438** (7064), 65-69 (2005).

[20] Wei-Cheng Lai, Swapnajit Chakravarty, Xiaolong Wang, Cheyun Lin, and Ray T. Chen, "*On-chip methane sensing by near-IR absorption signatures in a photonic crystal slot waveguide*," Opt. Lett. **36** (6), 984-986 (2011).

[21] Wei-Cheng Lai, Swapnajit Chakravarty, Xiaolong Wang, Cheyun Lin, and Ray T. Chen, "*Photonic crystal slot waveguide absorption spectrometer for on-chip near-infrared spectroscopy of xylene in water*," Appl. Phys. Lett. **98** (2), 023304 (2011).

[22] Xiaonan Chen, Wei Jiang, Jiaqi Chen, Lanlan Gu, and Ray T. Chen, "*20 dB-enhanced coupling to slot photonic crystal waveguide using multimode interference coupler*," Appl. Phys. Lett. **91** (9), 091111 (2007).

[23] Andrea Di Falco, L OíFaolain, and Thomas F. Krauss, "*Dispersion control and slow light in slotted photonic crystal waveguides*," Appl. Phys. Lett. **92**, 083501 (2008).

[24] M. G. Scullion, T. F. Krauss, and A. Di Falco, "*High Efficiency Interface for Coupling Into Slotted Photonic Crystal Waveguides*," Photonics Journal, IEEE **3** (2), 203-208 (2011).

[25] Zhechao Wang, Ning Zhu, Yongbo Tang, Lech Wosinski, Daoxin Dai, and Sailing He, "*Ultracompact low-loss coupler between strip and slot waveguides*," Opt. Lett. **34** (10), 1498-1500 (2009).

[26] Pierre Pottier, Marco Gnan, and Richard M. De La Rue, "*Efficient coupling into slow-light photonic crystal channel guides using photonic crystal tapers*," Opt. Express **15** (11), 6569-6575 (2007).

[27] Che-Yun Lin, Xiaolong Wang, Swapnajit Chakravarty, Beom Suk Lee, Wei-Cheng Lai, and Ray T. Chen, "*Wideband group velocity independent coupling into slow light silicon photonic crystal waveguide*," Appl. Phys. Lett. **97** (18), 183302 (2010).

[28] Yurii A. Vlasov and Sharee J. McNab, "*Coupling into the slow light mode in slab-type photonic crystal waveguides*," Opt. Lett. **31** (1), 50-52 (2006).

Chapter 4 Ultra-Efficient EO Polymer Infiltrated Slotted Photonic Crystal Waveguide Modulator

4.1 Introduction

Silicon has long been the optimal material for microelectronics. Building photonic devices in silicon carries the advantage of being compatible to complementary metal-oxide-semiconductor (CMOS) fabrication technology, which can lead to monolithic integration of microelectronic and photonic devices on a single silicon chip. However, due to its centro-symmetric crystal structure, silicon shows no Pockels Effect. Electrically driven optical modulation in silicon photonic devices typically relies on free carrier injection[1] or depletion[2] where the achievable modulation bandwidth is limited by time constants related to removing or injecting free carriers to the modulation arm.

By contrast, electro-optic (EO) polymers offer very high Pockels coefficient (r_{33}>300pm/V)[3] with extremely fast response speed in the terahertz range[4]. Ultra-high bandwidth[5] and sub-volt half-wave driving voltage (V_π)[6,7] have been demonstrated in EO polymer modulators. However, the size of these devices is limited by conventional waveguide structures with millimeter to center meter interaction length. Compared to conventional waveguides, silicon photonic crystal waveguide offers slow light-enhanced light-matter interaction[8-13], which can shrink the interaction length down to 80μm[14] and a reduced index change of 4.2×10^{-3} to achieve switching in a silicon-based structure[15]. Photonic devices based on silicon / EO polymer hybrid material system combine strong

optical confinement abilities of silicon with superior EO modulation efficiency of polymers[16-20]. Compared with conventional EO polymer photonic devices, this hybrid approach requires no cladding polymer layers, which should lead to higher poling efficiency and lower driving voltage with fabrication simplicity[16,18]. Slot waveguide infiltrated with EO polymers in Mach-Zehnder modulators (MZM) have reported half wave voltage of 0.25V, and $V_\pi \cdot L$ of 5V·mm[18]. A more advanced design using silicon photonic crystal slot waveguide can exploit slow light effect from the defect mode close to the photonic band edge[21], thus even lower $V_\pi \cdot L$ can be expected. Compared with photonic crystal devices without slot[14,15], integrating EO polymer in slot photonic crystal waveguide utilizes faster modulation mechanism[19], which offers better potential for high speed operation[5]. In this letter, we present the design and experimental demonstration of a MZM based on EO polymer infiltrated silicon photonic crystal slot waveguide with slow light enhanced EO modulation.

4.2 **Design of Slotted Photonic Crystal Waveguide**

Figure 4 - 1 shows the schematic of the photonic crystal slot waveguide. Input and output waveguides are conventional silicon strip waveguide, which connect to photonic crystal slot waveguide with optical mode converter[22] for better mode-matching. The photonic crystal waveguide is a W1 waveguide formed by replacing a row of air holes by a narrow slot of width w=75nm, which provides good optical confinement and modulation efficiency without compromising the feasibility of EO polymer infiltration. The modulation region with slot nanostructures, is formed in a hexagonal lattice photonic

crystal slab with lattice constant *a*=385nm and hole diameter *d*=217nm, which has a total length of 308μm. Silicon photonic crystal regions including air holes and slot are fully infiltrated by EO polymer with strong EO coefficient (AJ-CKL1/APC)[23]. Refractive index of infiltrated polymer is 1.63 at 1.55μm. Dispersion diagram of the guided mode is shown in Figure 4 - 2 (a), which is calculated by 3D plane wave expansion (PWE) method. The group refractive index n_g of the guided mode as a function of wavelength is shown in Fig. 2(b), which shows that n_g can exceed 100 when the wavelength is tuned close to the band edge of 1569nm. The optical intensity profile ($|E|^2$) of the guided mode at n_g=100 is shown in inset of Figure 4 - 2 (b). Figure 4 - 2 (b) also shows in-slot optical power weight (Γ) in the total guided mode power. It should be noted that integration of 75nm slot waveguide into photonic crystal waveguide causes light with low group velocity within the defect mode spectrum remain concentrated in the slot, which will otherwise penetrate to second or third row of holes without the presence of slot[24]. With lightly doped silicon functioning as electrode, huge electric field can be induced with small driving voltage. This design enables ultra-efficient electro-optic interaction within EO polymer infiltrated slot. To effectively couple light into slow light region, a photonic crystal taper from W1.08 to W1.0 is designed to minimize the group index mismatch between strip waveguide and slow light photonic crystal waveguide[25], as shown in Figure 4 - 1.

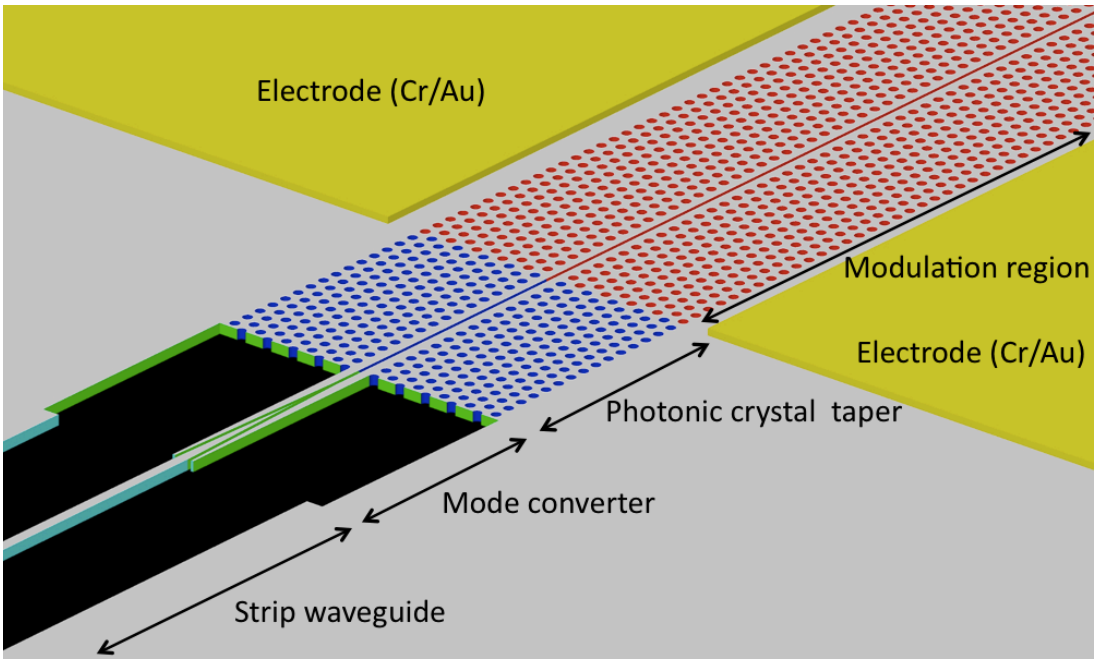

Figure 4 - 1. Schematic of the input strip waveguide, optical mode converter, photonic crystal taper, and modulation region.

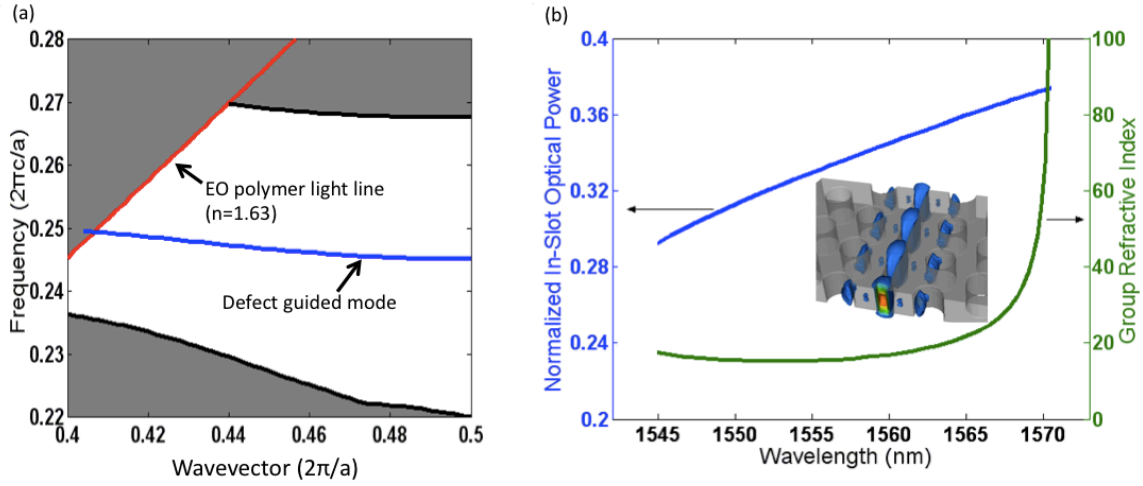

Figure 4 - 2. (a) Enlarged portion of the dispersion diagram for the guided mode. (b) Group index (n_g) and normalized in-slot optical power of the guided mode as a function of the optical wavelength. Optical mode profile at n_g=100 is shown in inset.

4.3 **Fabrication of Slotted Photonic Crystal Waveguide Modulator**

The hybrid nano-photonic modulator is fabricated on a silicon-on-insulator (SOI) wafer with 230nm lightly doped top silicon and 3μm buried oxide (BOX). Details of fabrication are described in previous chapter. Figure 4 - 3 (a) shows the fabricated MZI structure with gold electrodes. Figure 4 - 3 (b) shows scanning electronic microscopy (SEM) image of the silicon photonic crystal slot waveguide. The EO polymer was processed using standard methods[26] and poled with high electric field of 200V/μm. Figure 4 - 3 (c) shows cross sectional view of the 75nm slot infiltrated with EO polymer. Compared to other devices with slot width over 120nm[18,27], our narrower slot will provide higher modulation efficiency at same driving voltage.

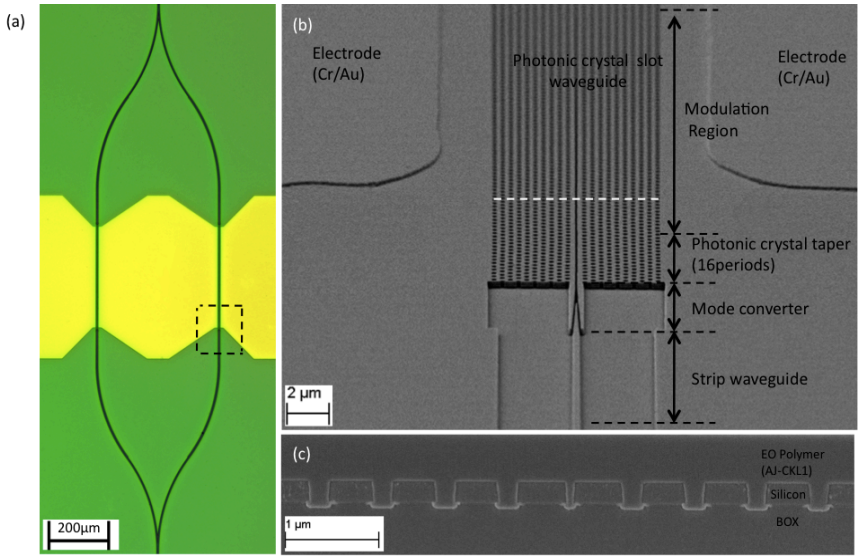

Figure 4 - 3. (a) Optical microscope picture of the fabricated MZM structure. (b) Scanning electron microscopy (SEM) picture showing the enlarged view of the dotted square area in (a). (c) Cross-sectional SEM picture take across the dotted line in (b) after covering the entire structure in (a) with AJ-CKL1/APC. Complete infiltration of EO polymer into the 217nm air holes and 75nm slot is confirmed.

4.4 Transmission Spectrum Testing & Modulation Testing

To characterize the modulator performance, transverse electric (TE) light from a broadband source was butt coupled into the modulator with a polarization maintaining tapered lensed fiber. Transmitted light was collected by a single mode lensed fiber and analyzed with an optical spectrum analyzer. We observe a 5nm deviation in the photonic band edge at 1569nm compared to plane wave expansion simulation results, which is attributed to fabrication errors. A laser source was tuned to 1564.5nm, corresponding to the slow light region, where maximum modulation response is achieved. The modulator was set at 3-dB point and driven by a 50KHz triangular wave. Modulated optical signal was converted to electrical signal through a gain-switchable photo detector.

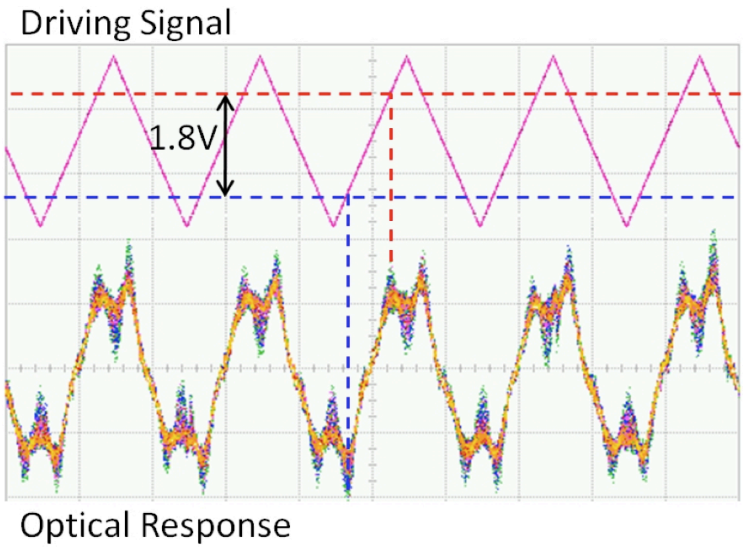

Figure 4 - 4. Low frequency modulation transfer-function measurement at 1564.5nm wavelength: Upper, applied voltage; lower, optical output signal. The half-wave voltage V_π is determined by finding the difference between the applied voltage at which the optical output is at a maximum and the voltage at which the optical output is at the next minimum

Figure 4 - 4 shows that the EO polymer nano-photonic modulator has a V_π of 1.8V. The effective EO coefficient is defined as

$$\gamma_{33} = \frac{\lambda w}{n^3 V_\pi \Gamma L} = \frac{1565nm \times 75nm}{1.63^3 \times 1.8V \times 0.37 \times 308\mu m} = 132\,pm/V \qquad \text{Equation 3}$$

, where Γ is the fraction of the total power in the slot. The value of Γ =0.37 is given by simulation results in Figure 4 - 4 (b). The device also achieves very high modulation efficiency: $V_\pi \cdot L = 1.8V \times 308\mu m = 0.56V \cdot mm$ Equation 4

This result is nearly one order of magnitude lower than that reported by Caltech group[18].

high E-O modulation (orange); Photonic band gap and beyond with minimized modulation (gray).

4.5 **Slow Light Enhanced Modulation**

To confirm the dramatic EO modulation enhancement out of slow light effect, all testing conditions were fixed and wavelength tuned from 1535nm to 1575nm. The wavelength dependence of normalized modulated signal under 1V of driving voltage is plotted in Figure 4 - 5, together with normalized optical transmission spectrum of the EO polymer nano-photonic modulator. The defect-guided mode of photonic crystal slot waveguide occurs from 1538nm to 1567nm. Although optical transmission reaches maximum at ~1550nm, the normalized modulated signal is only about -45dB. As we tune to longer wavelength (*Transitional region* in Figure 4 - 5), intensity of the modulated signal increases dramatically due to slow light enhancement. The maximum modulated signal around 1565nm is 23dB higher than in transitional region, where the photo-detector starts

to measure sensible modulation response. Above 1566nm, modulated signal decreases sharply due to transmission cut-off by photonic bandgap. The modulated signal shows strong wavelength dependence and peak enhancement of 23dB near the band edge of defect mode, which confirms the signature of the slow light effect.

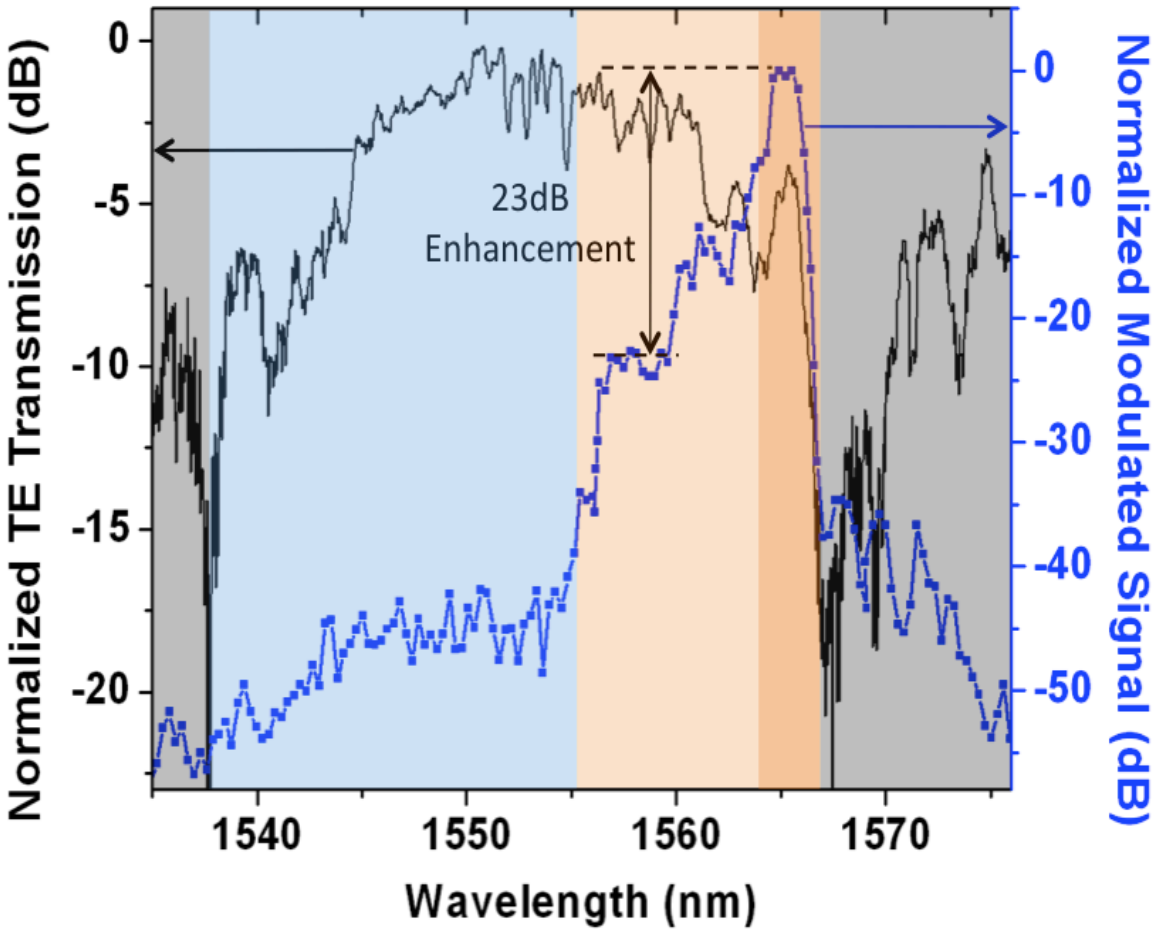

Figure 4 - 5. Normalized optical transmission (black) and normalized modulated signal (blue) as a function of optical wavelength. Four distinct regions are shown in this figure: Normal group velocity region with high optical transmission and low modulated signal (blue); Transitional region with gradually decreased optical transmission and rapidly increased modulated signal (light orange); Slow light region with relatively low optical transmission but extremely

4.6 **Conclusion**

In summary, we achieved 23dB modulation enhancement of EO polymer nano-photonic modulator from slow light effect. The low $V_\pi \cdot L$ of 0.56V·mm represents the best figure of merit achieved for EO polymer modulator. Such compact and highly efficient nano-photonic modulator is an ideal candidate for on-chip optical interconnects. It should be noted that efficiency from poled EO polymer materials in silicon nano-slot is still lower compared to the best results obtained from poling of thin films. Solving issues related to high electric field poling of EO polymer in silicon could lead to ultra-compact devices with extremely low power operation for applications in dense wavelength-division multiplexing (DWDM), phased array antennas (PAA), and photonic analog-to-digital converters.

4.7 **Acknowledgement**

This work was supported by AFOSR STTR program (Grant No. FA9550-09-C-0086), monitored by Dr. Charles Y-C. Lee.

4.8 **References**

[1] Qianfan Xu, Bradley Schmidt, Sameer Pradhan, and Michal Lipson, "*Micrometre-scale silicon electro-optic modulator*," Nature (London) **435** (7040), 325-327 (2005).

[2] Ansheng Liu, Richard Jones, Ling Liao, Dean Samara-Rubio, Doron Rubin, Oded Cohen, Remus Nicolaescu, and Mario Paniccia, "*A high-speed silicon optical modulator based on a metal-oxide-semiconductor capacitor*," Nature (London) **427**

(6975), 615-618 (2004).

[3] Tomoko Gray, Tae-Dong Kim, Daniel B. Knorr, Jingdong Luo, Alex K. Y. Jen, and Rene M. Overney, "*Mesoscale Dynamics and Cooperativity of Networking Dendronized Nonlinear Optical Molecular Glasses*," Nano Lett. **8** (2), 754-759 (2008).

[4] Mark Lee, Howard E. Katz, Christoph Erben, Douglas M. Gill, Padma Gopalan, Joerg D. Heber, and David J. McGee, "*Broadband Modulation of Light by Using an Electro-Optic Polymer*," Science **298** (5597), 1401-1403 (2002).

[5] Datong Chen, Harold R. Fetterman, Antao Chen, William H. Steier, Larry R. Dalton, Wenshen Wang, and Yongqiang Shi, "*Demonstration of 110 GHz electro-optic polymer modulators*," Appl. Phys. Lett. **70** (25), 3335-3337 (1997).

[6] Yasufumi Enami, C. T. Derose, D. Mathine, C. Loychik, C. Greenlee, R. A. Norwood, T. D. Kim, Jingdong Luo, Y. Tian, Alex. K. Y. Jen, and Naser Peyghambarian, "*Hybrid polymer/sol-gel waveguide modulators with exceptionally large electro-optic coefficients*," Nature Photonics **1** (3), 180-185 (2007).

[7] Y. Enami, D. Mathine, C. T. DeRose, R. A. Norwood, J. Luo, A. K. Y. Jen, and N. Peyghambarian, "*Hybrid cross-linkable polymer/sol-gel waveguide modulators with 0.65 V half wave voltage at 1550 nm*," Appl. Phys. Lett. **91** (9), 093505-093503 (2007).

[8] Thomas F. Krauss, "*Why do we need slow light?*," Nat Photon **2** (8), 448-450 (2008).

[9] Toshihiko Baba, "*Slow light in photonic crystals*," Nature Photonics **2** (8), 465-473 (2008).

[10] Thomas F. Krauss, "*Slow light in photonic crystal waveguides*," J. Phys. D: Appl. Phys. **40**, 2666-2670 (2007).

[11] Yurii A. Vlasov, Martin O'Boyle, Hendrik F. Hamann, and Sharee J. McNab, "*Active control of slow light on a chip with photonic crystal waveguides*," Nature (London) **438** (7064), 65-69 (2005).

[12] Marin Soljačić and John. D. Joannopoulos, "*Enhancement of nonlinear effects using photonic crystals*," Nat Mater **3** (4), 211-219 (2004).

[13] Marin Soljačić, Steven G. Johnson, Shanhui Fan, Mihai Ibanescu, Erich Ippen, and J. D. Joannopoulos, "*Photonic-crystal slow-light enhancement of nonlinear phase sensitivity*," J. Opt. Soc. Am. B **19** (9), 2052-2059 (2002).

[14] Yongqiang Jiang, Wei Jiang, Lanlan Gu, Xiaonan Chen, and Ray T. Chen, "*80-micron interaction length silicon photonic crystal waveguide modulator*," Appl. Phys. Lett. **87** (22), 221105-221103 (2005).

[15] Daryl M. Beggs, Thomas P. White, Liam O'Faolain, and Thomas F. Krauss, "*Ultracompact and low-power optical switch based on silicon photonic crystals*," Opt. Lett. **33** (2), 147-149 (2008).

[16] Ding Ran, T. Baehr-Jones, Kim Woo-Joong, A. Spott, M. Fournier, J. M. Fedeli, Huang Su, Luo Jingdong, A. K. Y. Jen, L. Dalton, and M. Hochberg, "*Sub-Volt Silicon-Organic Electro-optic Modulator With 500 MHz Bandwidth*," Lightwave Technology, Journal of **29** (8), 1112-1117 (2011).

[17] C Koos, P Vorreau, T Vallaitis, P Dumon, W Bogaerts, R Baets, B Esembeson, I Biaggio, T Michinobu, and F Diederich, "*All-optical high-speed signal processing*

with silicon/organic hybrid slot waveguides," Nature Photonics (2009).

[18] Tom Baehr-Jones, Boyan Penkov, Jingqing Huang, Phil Sullivan, Joshua Davies, Jocelyn Takayesu, Jingdong Luo, Tae-Dong Kim, Larry Dalton, Alex Jen, Michael Hochberg, and Axel Scherer, "*Nonlinear polymer-clad silicon slot waveguide modulator with a half wave voltage of 0.25 V*," Appl. Phys. Lett. **92** (16), 163303 (2008).

[19] Michael Hochberg, Tom Baehr-Jones, Guangxi Wang, Michael Shearn, Katherine Harvard, Jingdong Luo, Baoquan Chen, Zhengwei Shi, Rhys Lawson, Phil Sullivan, Alex K. Y. Jen, Larry Dalton, and Axel Scherer, "*Terahertz all-optical modulation in a silicon-polymer hybrid system*," Nature Materials **5** (9), 703-709 (2006).

[20] T. Baehr-Jones, M. Hochberg, Guangxi Wang, R. Lawson, Y. Liao, P. Sullivan, L. Dalton, A. Jen, and A. Scherer, "*Optical modulation and detection in slotted Silicon waveguides*," Opt. Express **13** (14), 5216-5226 (2005).

[21] Xiaonan Chen, Alan X. Wang, Swapnajit Chakravarty, and Ray T. Chen, "*Electrooptically-Active Slow-Light-Enhanced Silicon Slot Photonic Crystal Waveguides*," IEEE J. Sel. Top. Quantum Electron. **15** (5), 1506-1509 (2009).

[22] Zhechao Wang, Ning Zhu, Yongbo Tang, Lech Wosinski, Daoxin Dai, and Sailing He, "*Ultracompact low-loss coupler between strip and slot waveguides*," Opt. Lett. **34** (10), 1498-1500 (2009).

[23] H. Chen, B. Chen, D. Huang, D. Jin, Jingdong Luo, Alex. K. Y. Jen, and Raluca. Dinu, "*Broadband electro-optic polymer modulators with high electro-optic activity and low poling induced optical loss*," Appl. Phys. Lett. **93** (4), 043507-043503 (2008).

[24] M. R. Patterson, S. Hughes, S. Schulz, D. M. Beggs, T. P. White, L. O'Faolain, and Thomas. F. Krauss, "*Disorder-induced incoherent scattering losses in photonic crystal waveguides: Bloch mode reshaping, multiple scattering, and breakdown of the Beer-Lambert law*," Phys. Rev. B **80** (19), 195305 (2009).

[25] Pierre Pottier, Marco Gnan, and Richard M. De La Rue, "*Efficient coupling into slow-light photonic crystal channel guides using photonic crystal tapers*," Opt. Express **15** (11), 6569-6575 (2007).

[26] Che-Yun Lin, Beomsuk Lee, Alan X. Wang, Wei-Cheng Lai, Swapnajit Chakravarty, Yazhao Liu, David Kwong, Ray T. Chen, Jingdong Luo, and Alex K. Y. Jen, "*Ultra-compact silicon nanophotonic modulator based on electro-optic polymer infiltrated slot photonic crystal waveguide***"**, presented at the Proc. SPIE, San Francisco, (2010).

[27] Jan Hendrik Wulbern, Jan Hampe, Alexander Petrov, Manfred Eich, Jingdong Luo, Alex K. Y. Jen, Andrea Di Falco, Thomas F. Krauss, and Jurgen Bruns, "*Electro-optic modulation in slotted resonant photonic crystal heterostructures*," Appl. Phys. Lett. **94** (24), 241107-241103 (2009).

Chapter 5 Effective in-Device r_{33} of 735 pm/V on Electro-Optic Polymer Infiltrated Silicon Photonic Crystal Slot Waveguides

5.1 Introduction

We design and fabricate a 320nm slot for E-O polymer infiltrated silicon photonic crystal waveguide. Due to the large slot width, the poling efficiency of the infiltrated E-O polymer (AJCKL1/APC) is significantly improved. When coupled with slow light effect from the silicon photonic crystal waveguide, a record-high effective in-device r_{33} of 735pm/V is demonstrated, which is ten times higher than the E-O coefficient achieved in thin film material. Because of this ultra high E-O efficiency, the $V_\pi L$ of the device is only 0.44Vmm, which is the best result of all E-O polymer modulators.

Electro-Optic (E-O) polymer modulators have demonstrated exceptional performances for ultra-high bandwidth[1] and sub-volt half-wave driving voltage (V_π)[2-5]. However, the improvement of E-O polymer photonic devices is limited by conventional waveguide structures with micrometer feature size. The flourish of silicon nano-photonics, especially silicon slot waveguide[6] and photonic crystal waveguides[7-10], provides a platform for E-O polymer integration into nano-meter scale waveguide, for instance, E-O polymer infiltrated slot waveguides[2,11-14]. Nevertheless, the in-slot E-O efficiency is relatively low comparing with the r_{33} value provided by the E-O polymer. In most cases, the in-slot r_{33} can only achieve 10~30% of the thin film value. The mechanism that hinders the E-O poling efficiency in narrow slot waveguide is not fully understood yet. Recent research

has shown that large leakage current during the poling process can degrades the poling efficiency[15]. Using TiO_2 modified electrodes[15] or new E-O polymer materials (such as 15% wt AJLZ53/PMMA) with lower conductivity will significantly reduce the leakage current, and it can increase the thin film poling efficiency by more than 40%. Recently, we demonstrated an E-O polymer infiltrated silicon photonic crystal slot waveguide modulator using Mach-Zehnder interferometer (MZI) structure. The device showed the lowest $V_\pi L$ of 0.56Vmm and an effective in-device r_{33} of 132pm/V in the 75nm slot waveguide[11]. These improvements are attributed to the advanced design using silicon photonic crystal waveguide, which exploits the slow light effect from the defect mode close to the photonic band edge[16]. Although a high effective E-O coefficient is achieved under strong slow light enhancement[11], a relatively low modulation response at normal light region without slow light enhancement indicates poor E-O poling efficiency. Additionally, the fabrication procedures of 75nm E-O polymer infiltrated slot waveguide can be challenging both in e-beam lithography and reactive ion etching. It requires tremendous efforts to ensure precise control over the designed features and seamless infiltration into the sub-100nm slot.

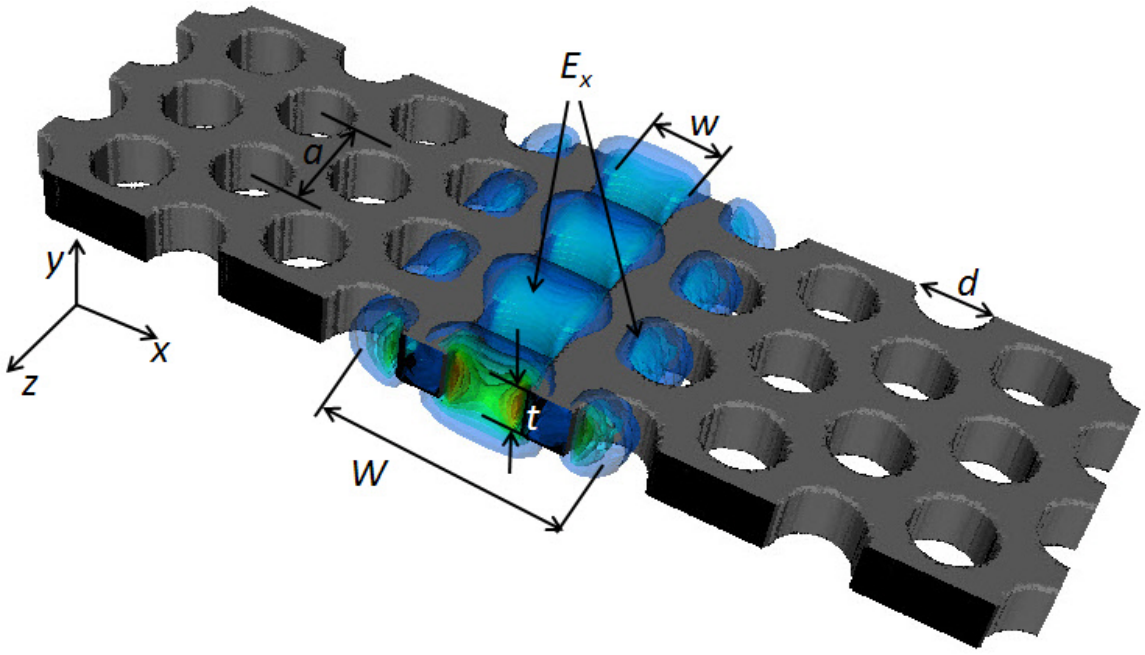

Figure 5 - 1. Schematic of the photonic crystal waveguide with 320nm slot and the simulated optical mode profile of the guided mode at the photonic band edge

5.2 Design and Optimization of Wide Slot Photonic Crystal Waveguide Modulator

In this paper, we present the physical insight into the increased poling efficiency achieved by wide photonic crystal slot waveguide, and experimentally verify the concept by using an MZI structure. The design principle is based on the fact that wider slot waveguide will significantly suppress the leakage current, and thus can increase the poling efficiency. Plus, wider slot will greatly relieve the stringent requirements on device fabrication. The basic photonic crystal slot waveguide structure is schematically shown in Figure 5 - 1. The hexagonal lattice photonic crystal slab waveguide with thickness of t=230nm has a lattice constant of a=425nm and hole diameter of d=297nm. To

accommodate the wide slot of w=320nm, a W1.3 waveguide (the air hole spacing outside of the slot is $W=1.3\sqrt{3}\,a$) is chosen. The total length of the photonic crystal slot waveguide is 340μm. The silicon photonic crystal regions including air holes and the slot are fully covered by polymer materials consisting of a guest host system of 25% weight chromophore AJCKL1 into amorphous polycarbonate (APC). The refractive index of the infiltrated polymer is n=1.63 at 1.55μm wavelength. The optical intensity profiles ($|E_x|^2$) of the guided mode at the band edge (wave vector of π/a) are simulated by three-dimensional planar wave expansion (3-D PWE) method and are also shown in Figure 5 - 1. The optical power concentrated in the 320nm slot is around 30% of the total optical power, which is very similar to the case of 75nm slot waveguide. Because the guided mode penetrates into air holes in slow light regime[17], air hole diameter strongly controls the dispersion curve of conventional silicon photonic crystal waveguides. For photonic crystal slot waveguide, however, slot width w plays a much more important role, because the optical power is tightly concentrated in the slot, especially in slow light region. In this paper, we investigate the effect of slot width for silicon photonic crystal waveguide. Figure 5 - 2 shows the simulated band diagrams of photonic crystal slot waveguides with different slot widths in conjunction with 2-D cross sectional views of the optical intensity profiles of the guided modes at the photonic band edges. Although wider slot is good for suppressing the leakage current, the slot cannot be arbitrarily wide. In Figure 5 - 2 (b), the slot mode profile becomes spindlier as the slot width increases, which means that the slot mode inclines to be decoupled into two separate waveguide modes. Additionally, large slot width is detrimental to E-O modulation since the electrodes separation is increased.

Therefore, we believe 300~350nm slot width with 30% in-slot power is the optimized design for E-O polymer infiltrated silicon photonic crystal modulator.

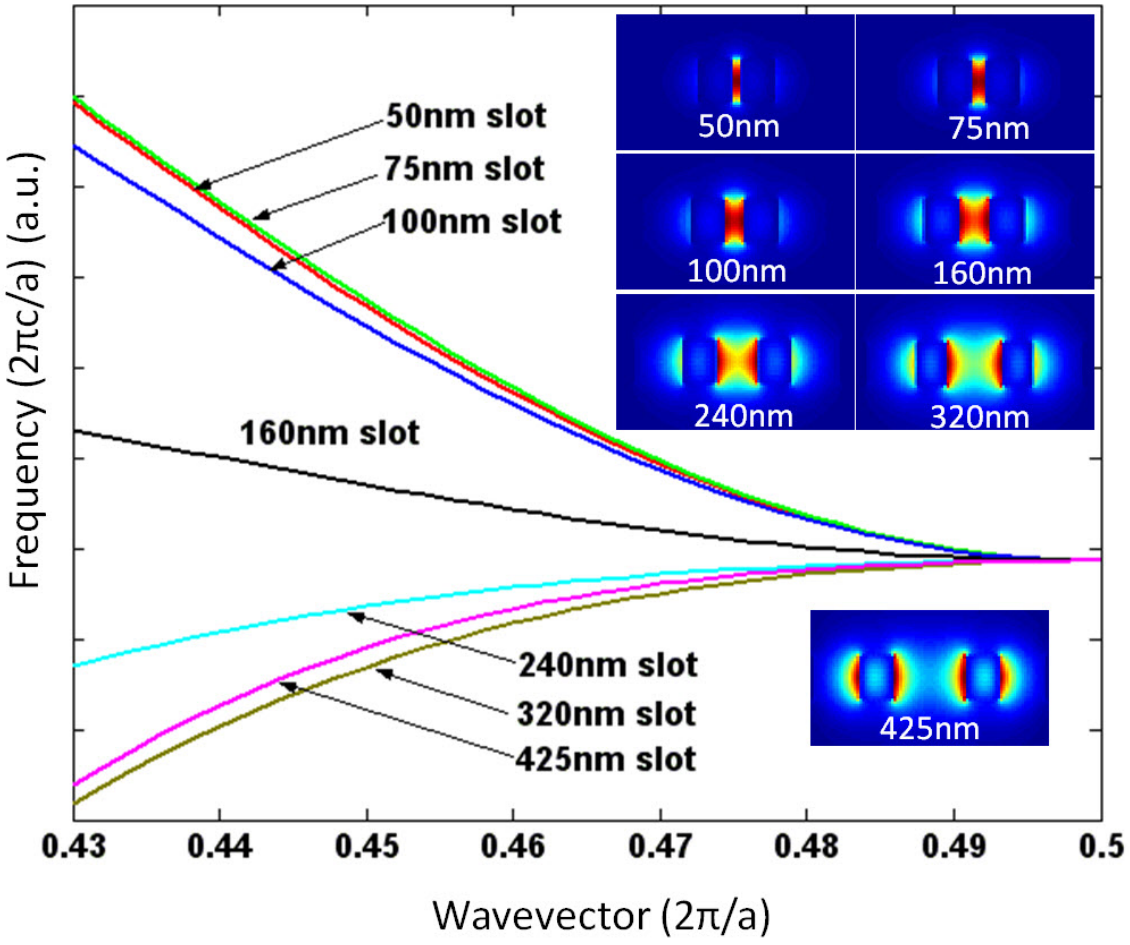

Figure 5 - 2. Photonic band diagrams and optical mode profiles of the photonic crystal slot waveguides with slot width from 50nm to 425nm

5.3 **Fabrication and Poling**

The fabrication procedures of the nano-photonic modulator are described in previous chapter. Figure 5 - 3 shows the scanning electronic microscopy (SEM) image of the

silicon photonic crystal slot waveguide. After infiltrating AJCKL1/APC, the sample is heated to the glass transition temperature (T_g=145°C) of the guest/host polymer while 86V/μm poling field is applied. The poling voltage is kept constant during the whole poling process. At the glass transition temperature, the chromophore molecules are free to move; therefore, it can be non-centro-symmetrically aligned with the poling field. Upon reaching the glass transition temperature, the sample is then cooled down to the room temperature, and the poling voltage is switched off, and thereby it freezes the aligned molecules of the chromophore. The leakage current as well as the heater temperature during the poling process is monitored in situ as shown in Figure 5 - 5 for the 75nm and 320nm photonic crystal slot waveguide. The peak current for the 75nm slot is 4.5×10^{-8}A, while it is only 6.2×10^{-10}A for the 320nm slot. If we assume the leakage current only goes through the slot waveguide, and with a cross sectional area of 340μm×0.23μm, the current density of the E-O poling process is 575A/m^2 and 7.9A/m^2 for the 75nm and the 320nm slot, respectively. Comparing with the typical 1~10A/m^2 leakage current of thin film AJCKL1/APC[15], the 320nm slot device shows comparable leakage current density. Therefore, poling efficiency similar to thin film is expected. This significant change of leakage currents as a function of the slot width deserves further investigation, in which the device dimension and the silicon/polymer interface are two of the key parameters in affecting the materials' conduction mechanism under the poling condition.

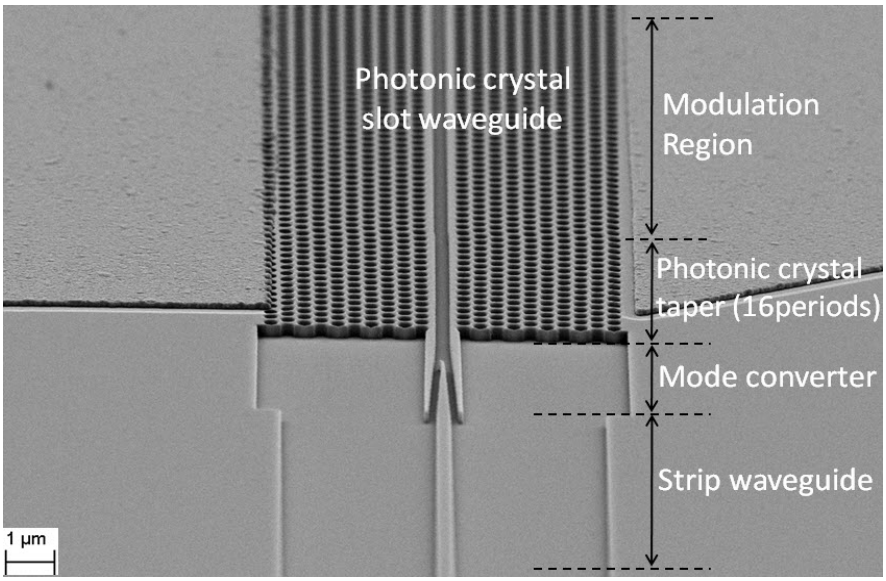

Figure 5 - 3. SEM picture of the 320nm wide silicon photonic crystal slot waveguide with input strip waveguide, optical mode converter and photonic impedance taper (b) Leakage current during the poling process for the 75nm and the 320nm photonic crystal slot waveguide infiltrated with AJCKL1/APC

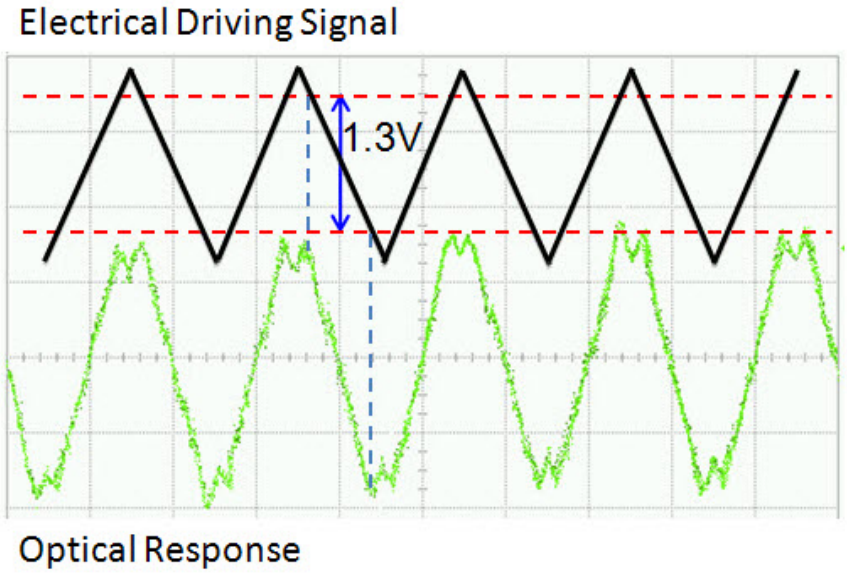

Figure 5 - 4. Low frequency modulation measurements showing a low V_π of 1.3V for the E-O polymer nano-photonic modulator with 340µm modulation arm

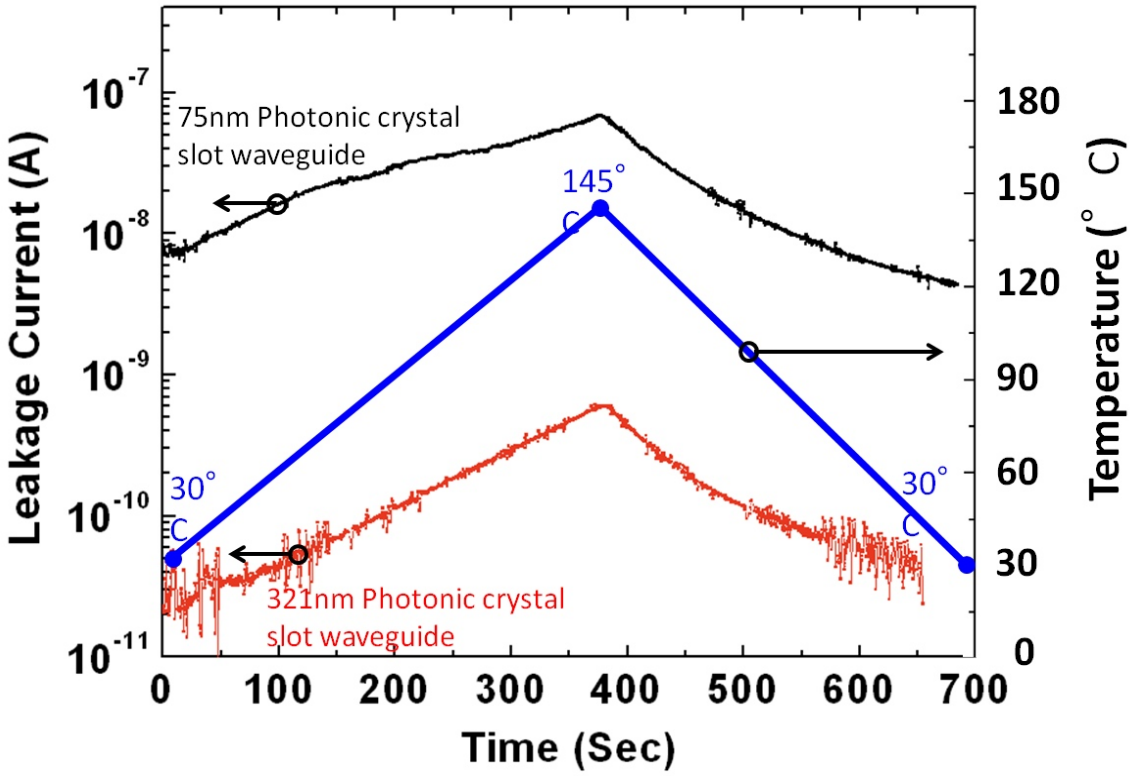

Figure 5 - 5. Leakage current during the poling process for the 75nm and the 320nm photonic crystal slot waveguide infiltrated with AJCKL1/APC

5.4 **Optical Testing, Results, and Discussion**

In the measurement, the output of the laser source is tuned to 1539nm wavelength, where maximum modulation response is achieved. The E-O polymer nano-photonic modulator was driven by a 100 KHz triangular wave with a peak-to-peak voltage V_{pp} of 1.7V. The total optical insertion loss (lensed fiber in, lensed fiber out) is 23dB, including 8dB/facet fiber-waveguide coupling loss. The waveform from a digital oscilloscope in Figure 5 - 4 shows that over modulation occurs at 1.3V, which is the V_{π} of the E-O polymer nano-photonic modulator. The effective in-device E-O coefficient is calculated as

$$\gamma_{33} = \frac{\lambda w}{n^3 V_\pi \Gamma L} = \frac{1540nm \times 320nm}{1.63^3 \times 1.3V \times 0.35 \times 340\mu m} = 735pm/V$$ Equation 5

In this equation, Γ is the ratio of the optical power that has interactions with the electric field. The value of Γ =0.35 is chosen after the consideration that the top cladding E-O polymer layer can also contribute to E-O modulation. The r_{33} value of the poled AJCKL1/APC films with 25wt% of chromophore loading is 90pm/V at 1.3μm, which is measured by Teng-Man reflection technique. This value corresponds to 70-75 pm/V at 1.55μm based on the two-level model approximation[18]. Comparing with the thin film r_{33} value, our effective in-device E-O efficiency is enhanced by almost ten times. Usually the in-device r_{33} of E-O polymer modulators is lower than that of the thin film material. This extraordinarily high r_{33} value proves the combined enhancement of slow light effect and an increased poling efficiency.

The nano-photonic modulator also achieves very high modulation efficiency with

$$V_\pi \cdot L = 1.3V \times 340\mu m = 0.44V \cdot mm$$ Equation 6

This $V_\pi L$ shows 22% improvement over the 0.56Vmm $V_\pi L$ as compared to the result achieve in 75nm slot photonic crystal waveguide, which is the best $V_\pi L$ that has ever been reported.

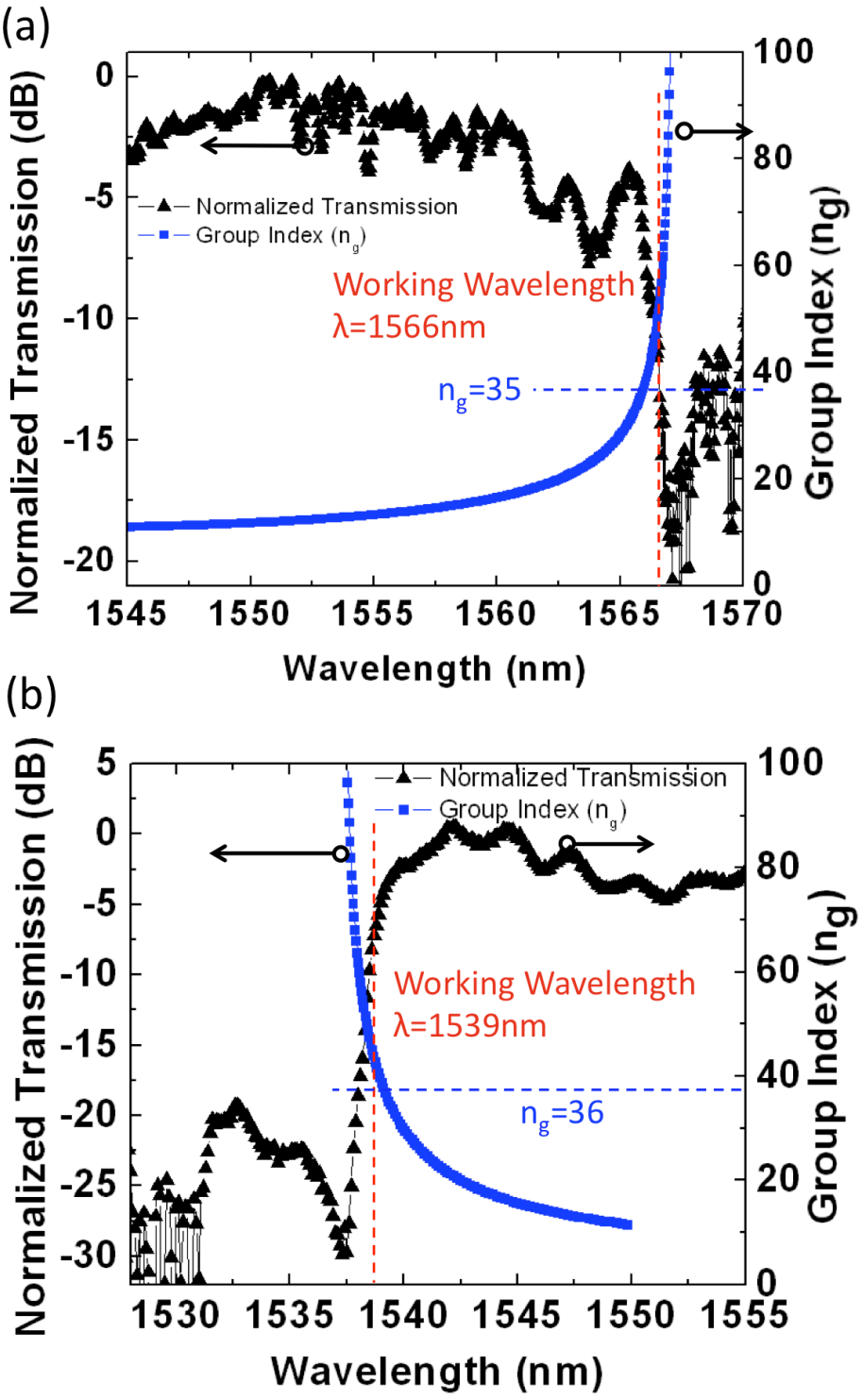

Figure 5 - 6. Group indices and optical transmission curves of the E-O polymer infiltrated silicon photonic crystal slot waveguide (a) 320nm slot and (b) 75nm slot

5.5 Comparison on Wide Slot and Narrow Slot: Poling Efficiency and Slow Light Enhancement

To effectively evaluate the poling efficiency of the E-O polymer inside the photonic crystal slot waveguide, we calculate the group indices of the 320nm and 75nm photonic crystal slot waveguide in Figure 5 - 6 (a) and (b). The experimentally measured optical transmission curves of these two devices are shown as well. At the working wavelengths of these two devices, the group indices are 36 and 35 in Figure 5 - 6 (a) and (b). The slow down factor S of the devices are given as[19]:

$$S = \frac{v_\phi}{v_g} = \frac{n_g}{n_\phi} \qquad \text{Equation 7}$$

While n_φ is the effective phase index of the waveguide. Considering the field distribution of 30% optical power in E-O polymer and 70% in silicon, n_φ is approximately 2.9 $(3.46 \times 70\% + 1.63 \times 30\% = 2.911)$. This gives the S of 320nm and 75nm photonic crystal slot waveguide around 12.4 and 12.1, respectively. Given the slow light enhanced effective r_{33} of 735pm/V and 132pm/V for the two devices, we can conclude that the material r_{33} from E-O poling is 59pm/V for 320nm slot, and 11pm/V for 75nm. The E-O poling efficiency is improved by five times due to the increased slot width.

5.6 **Summary**

In summary, we have achieved 735pm/V effective in-device r_{33} and 0.44Vmm $V_\pi L$, all of which are the best results that have ever been reported. These improvements are attributed to the increased poling efficiency of the E-O polymer inside the 320nm photonic crystal slot waveguide. The material r_{33} is calculated to be 59pm/V by excluding the slow light enhancement factor. As a comparison, the 75nm slot only achieves 11pm/V material r_{33}. This improvement is also confirmed by the reduced leakage current from 575A/m^2 to 7.9A/m^2 during the poling process. By further optimizing the silicon/organic interface and poling process with more efficient E-O polymer, we expect more significant improvement in device performance of the E-O polymer infiltrated silicon photonic crystal slot waveguide. It can ultimately lead to an ideal platform of ultra-compact and low driven voltage nano-photonic modulators for the emerging technology of on-chip optical interconnects.

5.7 **References**

[1] Datong Chen, Harold R. Fetterman, Antao Chen, William H. Steier, Larry R. Dalton, Wenshen Wang, and Yongqiang Shi, "*Demonstration of 110 GHz electro-optic polymer modulators*," Appl. Phys. Lett. **70** (25), 3335-3337 (1997).

[2] Tom Baehr-Jones, Boyan Penkov, Jingqing Huang, Phil Sullivan, Joshua Davies, Jocelyn Takayesu, Jingdong Luo, Tae-Dong Kim, Larry Dalton, Alex Jen, Michael Hochberg, and Axel Scherer, "*Nonlinear polymer-clad silicon slot waveguide modulator with a half wave voltage of 0.25 V*," Appl. Phys. Lett. **92** (16), 163303

(2008).

[3] Y. Enami, D. Mathine, C. T. DeRose, R. A. Norwood, J. Luo, A. K. Y. Jen, and N. Peyghambarian, "*Hybrid cross-linkable polymer/sol-gel waveguide modulators with 0.65 V half wave voltage at 1550 nm*," Appl. Phys. Lett. **91** (9), 093505-093503 (2007).

[4] Yasufumi Enami, C. T. Derose, D. Mathine, C. Loychik, C. Greenlee, R. A. Norwood, T. D. Kim, Jingdong Luo, Y. Tian, Alex. K. Y. Jen, and Naser Peyghambarian, "*Hybrid polymer/sol-gel waveguide modulators with exceptionally large electro-optic coefficients*," Nature Photonics **1** (3), 180-185 (2007).

[5] Yongqiang Shi, Cheng Zhang, Hua Zhang, James H. Bechtel, Larry R. Dalton, Bruce H. Robinson, and William H. Steier, "*Low (Sub-1-Volt) Halfwave Voltage Polymeric Electro-optic Modulators Achieved by Controlling Chromophore Shape*," Science **288** (5463), 119-122 (2000).

[6] Vilson R. Almeida, Qianfan Xu, Carlos A. Barrios, and Michal Lipson, "*Guiding and confining light in void nanostructure*," Opt. Lett. **29** (11), 1209-1211 (2004).

[7] D. M. Beggs, T. P. White, L. Cairns, L. O'Faolain, and T. F. Krauss, "*Ultrashort Photonic Crystal Optical Switch Actuated by a Microheater*," Photonics Technology Letters, IEEE **21** (1), 24-26 (2009).

[8] Masaya Notomi, Eiichi Kuramochi, and Takasumi Tanabe, "*Large-scale arrays of ultrahigh-Q coupled nanocavities*," Nat Photon **2** (12), 741-747 (2008).

[9] Daryl M. Beggs, Thomas P. White, Liam O'Faolain, and Thomas F. Krauss, "*Ultracompact and low-power optical switch based on silicon photonic crystals*," Opt.

Lett. **33** (2), 147-149 (2008).

[10] Yongqiang Jiang, Wei Jiang, Lanlan Gu, Xiaonan Chen, and Ray T. Chen, "*80-micron interaction length silicon photonic crystal waveguide modulator*," Appl. Phys. Lett. **87** (22), 221105-221103 (2005).

[11] Che-Yun Lin, Xiaolong Wang, Swapnajit Chakravarty, Beom Suk Lee, Weicheng Lai, Jingdong Luo, Alex K.-Y. Jen, and Ray T. Chen, "*Electro-optic polymer infiltrated silicon photonic crystal slot waveguide modulator with 23 dB slow light enhancement*," Appl. Phys. Lett. **97** (9), 093304 (2010).

[12] Jan H. Wulbern, Alexander Petrov, and Manfred Eich, "*Electro-optical modulator in a polymer-infiltrated silicon slotted photonic crystal waveguide heterostructure resonator*," Opt. Express **17** (1), 304-313 (2009).

[13] Jan Hendrik Wulbern, Jan Hampe, Alexander Petrov, Manfred Eich, Jingdong Luo, Alex K. Y. Jen, Andrea Di Falco, Thomas F. Krauss, and Jurgen Bruns, "*Electro-optic modulation in slotted resonant photonic crystal heterostructures*," Appl. Phys. Lett. **94** (24), 241107-241103 (2009).

[14] R. Ding, T. Baehr-Jones, Y. Liu, R. Bojko, J. Witzens, S. Huang, J. Luo, S. Benight, P. Sullivan, J. M. Fedeli, M. Fournier, L. Dalton, A. Jen, and M. Hochberg, "*Demonstration of a low VπL modulator with GHz bandwidth based on electro-optic polymer-clad silicon slot waveguides*," Opt. Express **18** (15), 15618-15623 (2010).

[15] Su Huang, Tae-Dong Kim, Jingdong Luo, Steven K. Hau, Zhengwei Shi, Xing-Hua Zhou, Hin-Lap Yip, and Alex K.-Y. Jen, "*Highly efficient electro-optic polymers through improved poling using a thin TiO_2-modified transparent electrode*," Appl.

Phys. Lett. **96** (24), 243311 (2010).

[16] Xiaonan Chen, Alan X. Wang, Swapnajit Chakravarty, and Ray T. Chen, "*Electrooptically-Active Slow-Light-Enhanced Silicon Slot Photonic Crystal Waveguides*," IEEE J. Sel. Top. Quantum Electron. **15** (5), 1506-1509 (2009).

[17] M. R. Patterson, S. Hughes, S. Schulz, D. M. Beggs, T. P. White, L. O'Faolain, and Thomas. F. Krauss, "*Disorder-induced incoherent scattering losses in photonic crystal waveguides: Bloch mode reshaping, multiple scattering, and breakdown of the Beer-Lambert law*," Phys. Rev. B **80** (19), 195305 (2009).

[18] Charles Greenlee, Anael Guilmo, Ayodeji Opadeyi, Roland Himmelhuber, Robert A. Norwood, Mahmoud Fallahi, Jingdong Luo, Su Huang, Xing-Hua Zhou, Alex K.-Y. Jen, and Nasser Peyghambarian, "*Mach--Zehnder interferometry method for decoupling electro-optic and piezoelectric effects in poled polymer films*," Appl. Phys. Lett. **97** (4), 041109 (2010).

[19] Thomas F. Krauss, "*Slow light in photonic crystal waveguides*," J. Phys. D: Appl. Phys. **40**, 2666-2670 (2007).

Chapter 6 Silicon Nanomembrane Based Photonic Crystal Waveguide Array for Wavelength-Tunable True-Time-Delay Lines

6.1 Abstract

We demonstrate a four-channel on-chip true-time-delay module based on a photonic crystal waveguide array. Using the photonic crystal taper to minimize the coupling loss, the delay lines with 1~3mm long photonic crystal waveguides can operate up to a group index n_g~23 without significant loss. The large group velocity dispersion enables continuous and wavelength-tunable time delays. Measurements show a highly linear phase-frequency relation, highest time delay up to 216.7ps, and large tuning ranges of 58ps, 116ps, and 194ps for 1~3mm delay lines. The chip-scale TTD module occupies only 0.18mm^2 area and can provide ±44.34° steering for an X-band phased-array-antenna (PAA).

6.2 Introduction

Photonic crystal waveguides (PCWs) offer strong optical confinement and slow light enhanced interactions, which enable realization of many miniaturized and highly efficient devices such as hybrid silicon modulators[1-9], electro-optic modulators based on carrier effect[10-18], thermo-optic modulators[19-21], optical switches[22], on-chip environmental sensors for underground water pollution detection[23], gas sensors for green house gas

detection[24], and bio-sensors[25]. It is possible to engineer the band structure of the PCWs in order to achieve high dispersion and high group index simultaneously[26]. Such high dispersion and slow-light PCWs will greatly benefit the development of lightweight and compact systems. Specifically, for applications requiring strict control on payload, such as phased array antenna (PAA) systems[27] in air-borne platforms, such miniaturized systems can enhance functionality while maintaining a minimum form factor. It is well known that photonic true-time-delay (TTD) systems enable broadband operation of PAA due to their inherent characteristic of providing a linear response of phase-frequency relationship across the entire operating bandwidth of the radio-frequency (RF) signal[28]. Furthermore, utilization of PCW TTDs can offer significant reduction in device footprint when operating in the high group index region. A TTD module based on PCW devices shall provide large bandwidth, small footprint, and tunable time delay.

In this paper, we explore the utilization of a slow-light PCW for application in an X-Band TTD module. In this application, where large delay time is highly desired, long PCWs with lengths in mm range are often required. However, the large insertion loss of PCWs can be a prohibitive factor for building such long-length TTD devices. While the propagation loss can be minimized with better etch processes and post-etching oxidation treatment[29], minimizing coupling loss requires a special design to achieve a better mode matching at the strip waveguide-PCW interface[30,31]. Previous demonstrations have achieved 80ps time delay with a 4mm long PCW when operated at group index n_g=12.5[32]. In the work reported herein, we use a photonic crystal waveguide taper[31] to minimize coupling loss, which allows the delay lines to operate at a much higher group

index n_g~23 that delivers much higher delay time with shorter physical length. Using the four-channel PCW array integrated with a 1x4 multimode interference (MMI) coupler, we experimentally demonstrate the first chip-scale integrated TTD module with three continuously tunable true time delays covering the ranges of (6.72,64.96), (10.56,126.31), and (22.54,216.66) ps.

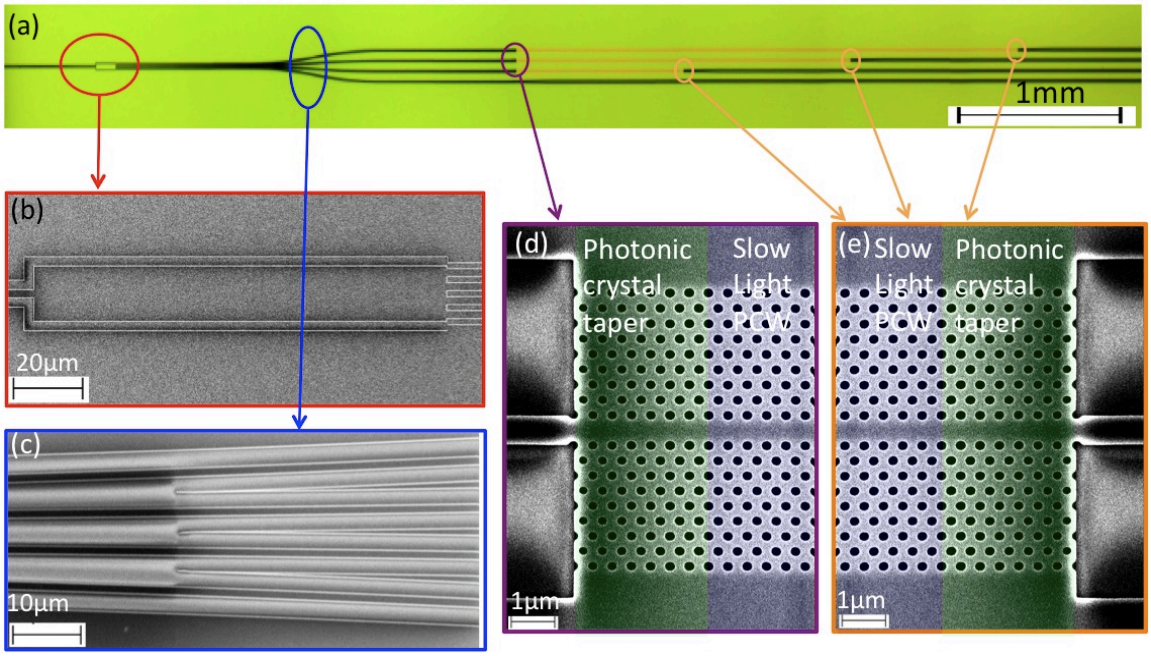

Figure 6 - 1. (a) Microscope picture of the TTD beamformer based on a 1*4 MMI and PCWs. (b) SEM picture of the enlarged view of the 1*4 MMI power splitter. (c) Enlarged view of the S-bends that increase the waveguide separations. (d) and (e) SEM pictures of the PCW region containing photonic crystal taper and slow light PCW region.

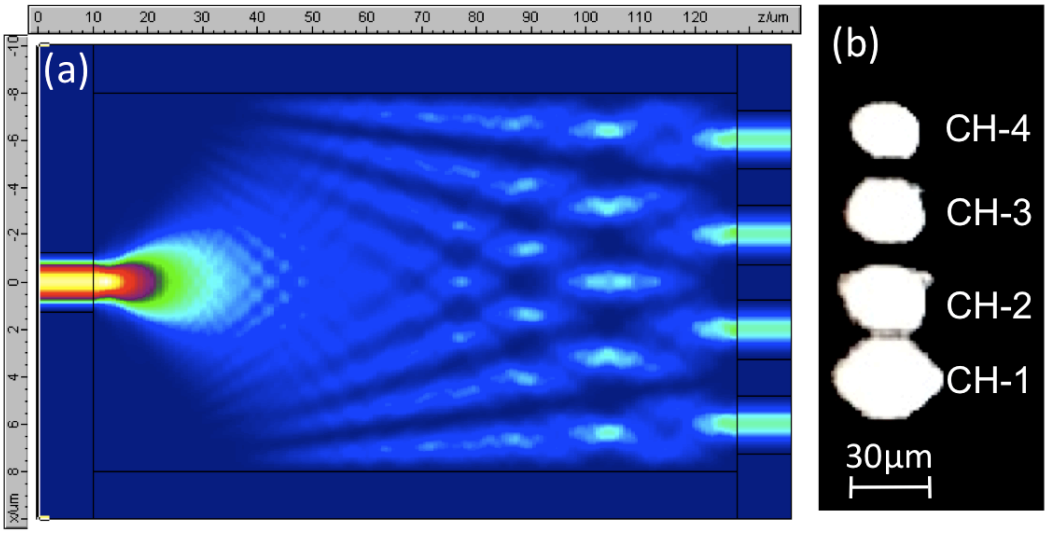

Figure 6 - 2. (a) Simulation of the field profile of a 1*4 MMI (b) MMI output at 1550nm imaged by top view IR camera.

6.3 **Design of A Chip Scale True-Time-Delay Module**

The micrograph of the PCW TTD module is shown in Figure 6 - 1 (a). The optical input power is uniformly divided into four channels using a 1x4 multimode interference (MMI) beam splitter, which has a width and length of 16µm and 117.7µm, respectively. The input and output access waveguides widths are 2.5µm on a 230 nm silicon nanomembrane on a silicon-on-insulator (SOI) wafer, which has been optimized for high MMI performance[33]. The FIMMPROP Eigenmode decomposition based simulation result of TE polarized light propagation inside the MMI at λ=1.55µm is shown in Figure 6 - 2 (a). Each channel consists of carefully chosen lengths of silicon strip waveguides and PCWs[31], such that at any given wavelength within the bandwidth of interest, a constant time delay difference is setup between adjacent channels. Channel-1 contains a 5mm-

long silicon strip waveguide and no PCW, and is chosen as a reference line. Channels-2, 3, and 4 contain 4mm, 3mm, and 2mm silicon strip waveguides and 1mm, 2mm, and 3mm-long PCWs, respectively, with identical PCW parameters. When the operating wavelength λ is tuned, this configuration creates proportional relative time delay 0, τ, 2τ, and 3τ in channels-1~4, respectively. Note that since a different τ_i time delay difference is achieved for different tuning wavelength λ_i, the time delay profiles can provide appropriate phase distribution at the output for operation in a PAA. Scanning electron micrographs of the 1x4 MMI and the waveguide splitting section for four channels are shown in Figure 6 - 1 (b) and (c), respectively. The enlarged view of the slow light PCWs and the PCW taper regions are shown in Figure 6 - 1 (d) and (e), respectively.

In our design, the lattice constant (a), hole diameter (d), and slab thickness (h) of the W1 PCWs are chosen as 405nm, 190nm, and 230nm, respectively so that the PCWs support a guided mode covering 1533~1573nm. Detailed design parameters are covered in our previous work[31]. To minimize the coupling loss into the slow light PCW, we utilize two photonic crystal tapers at the strip-PCW interfaces[31]. These structures significantly improve the matching of the two different waveguide modes and reduce coupling loss. Such a design enables operation in the high-group index region near the band-edge, which gives much larger delay time and faster tuning based on wavelength tuning.

6.4 Fabrication

The on-chip TTD module is fabricated on a Unibond SOI wafer with a 250 nm top silicon layer and a 3μm buried oxide (BOX) layer. First, a 45 nm of thermal oxide is thermally grown as an etching mask for pattern transfer. Then, MMI power splitter, PCWs, photonic crystal tapers, and strip waveguides are patterned in one step with a JEOL JBX-6000FS electron-beam lithography system followed by reactive ion etching.

6.5 Measurements on Transmission Spectra and Phase-Frequency Relations

The TTD module is tested on a Newport 8-axis precision automated alignment station, which has a 10nm horizontal alignment accuracy and 5nm vertical alignment accuracy. In order to measure the output characteristics of the fabricated device, light from a broadband laser source is TE polarized and coupled to the TTD module through a polarization maintaining lensed fiber. The output signal from the TTD module is collected using single mode lensed fibers. The output power uniformity of the 1x4 MMI splitter is characterized first. The infrared (IR) image of the 1x4 MMI output at 1550nm taken using a top down IR camera is shown in Figure 6 - 2 (b). According to the measurement data, the power fluctuation of the 1*4 MMI is within 8%, which is reasonable given the fabrication tolerance.

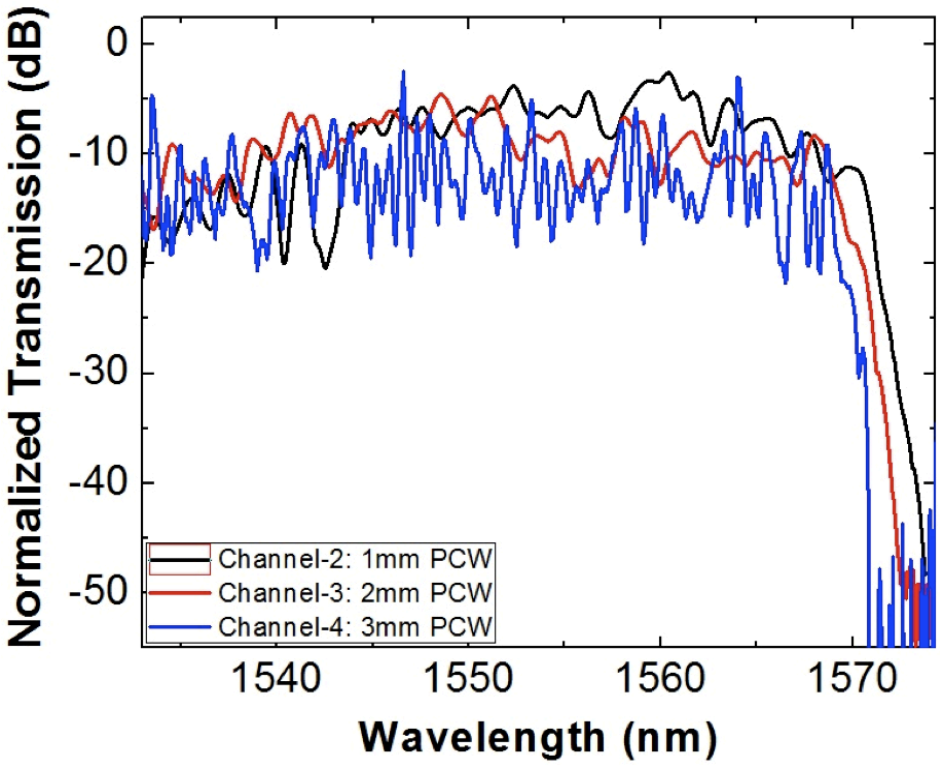

Figure 6 - 3. Transmission spectra of the channels containing 1~3mm PCWs.

Transmission spectra of the channels containing PCWs were also characterized to identify the transmission bands of the PCWs experimentally. Note that the measurement data were taken from integrated devices, i.e. the transmission through MMI and PCWs. Transmission spectra for channel-2~4 are shown in Figure 6 - 3, which clearly show overlapping transmission bands from 1533nm to 1573nm. Each set of data is composed of 1200 data points to ensure good accuracy, and the results for each of the channels from 2~4 were normalized to the transmission of the strip waveguide channel. The coupling loss of PCWs is significantly reduced due to the implementation of PCW tapers. The highest transmission point is -2.68dB for channel-2, which contains 1mm long PCW. The increasingly large fluctuation in the transmission spectra for longer PCWs channels are

mainly due to the propagation loss from the fabrication related imperfections in the PCWs.

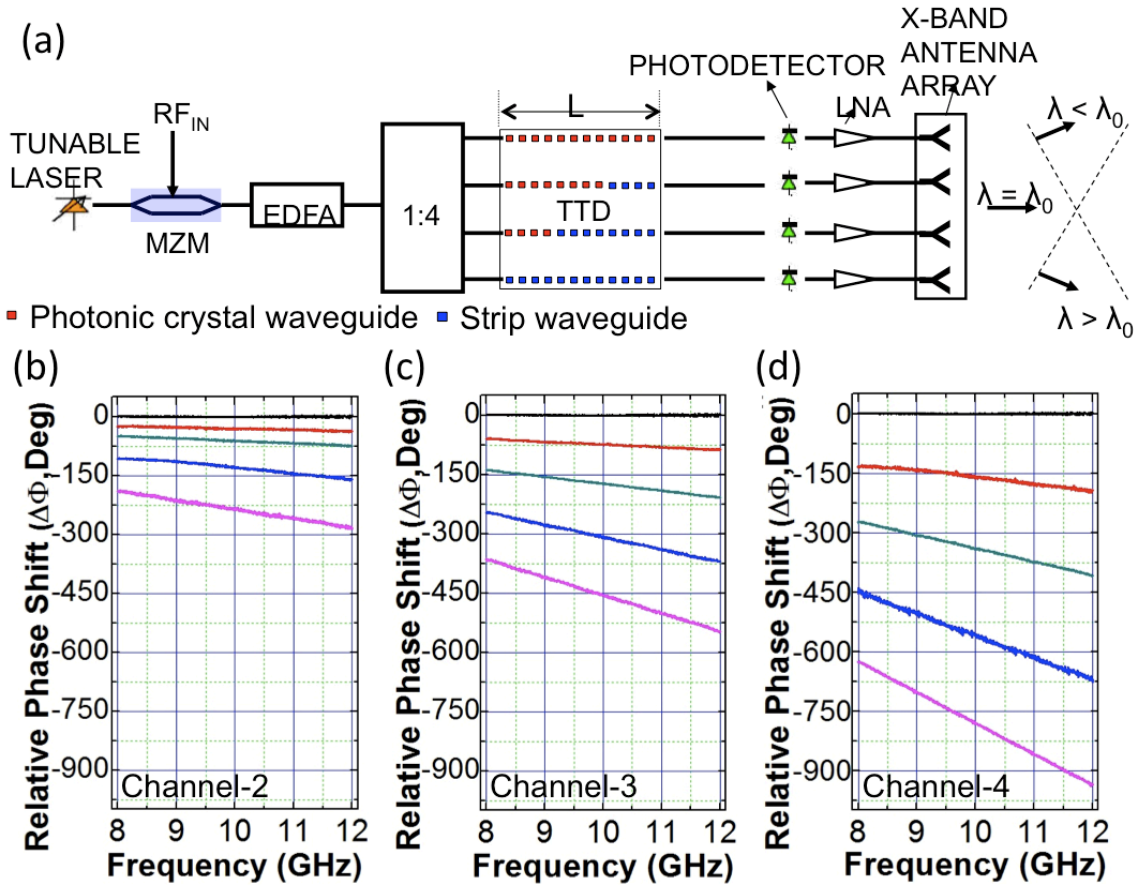

Figure 6 - 4. (a) A schematic of the measurement setup of a PCW-based TTD module. Measurement results of phase vs. frequency relation for (b) channel-2, (c) channel-3, and (d) channel-4. Measurement results were normalized to the strip waveguide (channel-1). The horizontal line (black) in (b), (c), and (d) represents the normalized phase shift of channel-1.

The schematic of the measurement setup is shown in Figure 6 - 4 (a). In order to measure the time delay from the TTD lines, a X-band (8-12GHz) RF signal from an HP8510C vector network analyzer (VNA) is modulated onto an optical carrier from a tunable

continuous wave laser by a $LiNbO_3$ modulator. The output of the modulator is coupled to the on-chip TTD module using the same method used to characterize the transmission spectra of TTD channels. A photodetector (PD) covering the X-band frequency range is used to convert the modulated optical signal to an electrical signal, which is then amplified using an X-band RF amplifier and fed back to the network analyzer. The phase vs frequency relationship of all the channels is measured on the network analyzer. Due to the strong fluctuation in transmission spectra below 1545nm and above 1572nm, time delay measurements were only performed between 1545nm and 1572nm to avoid strong optical loss. The measurement results are shown in Figure 6 - 4 (b)~(d). The phase-frequency results are normalized to the strip waveguide channel (channel-1) using VNA to show the relative phase change. Highly linear phase-frequency relation is seen in all the channels, which clearly shows the signature of true time delay. This characteristic is critical to have a wide band phased array antenna without beam squint effect covering the whole X-band (8 to 12.5 GHz)[34]. The time delay (τ) in the PCWs is derived from a linear regression fit following the relation $\tau = \Delta\Phi/\Delta\omega$, where $\Delta\Phi$ represents the changes of phase in the measurement frequency range $\Delta\omega$. Accordingly, the maximum time delays obtained are 64.96ps, 126.31ps, and 216.66ps for channels-2, 3, and 4, respectively. The wavelength-tunable time delay results are summarized in Figure 6 - 5. When external tunable delay lines are used to offset the time delay difference between adjacent delay lines, this TTD module can provide a steering angle from -44.34 degree to 44.34 degree if wavelength is tuned from a central wavelength λ_0=1558.5nm for an X-Band PAA with inter-element spacing of 1.25cm. Further system demonstration

containing a real X-band phased array antenna is under investigation and further results will be presented in the near future.

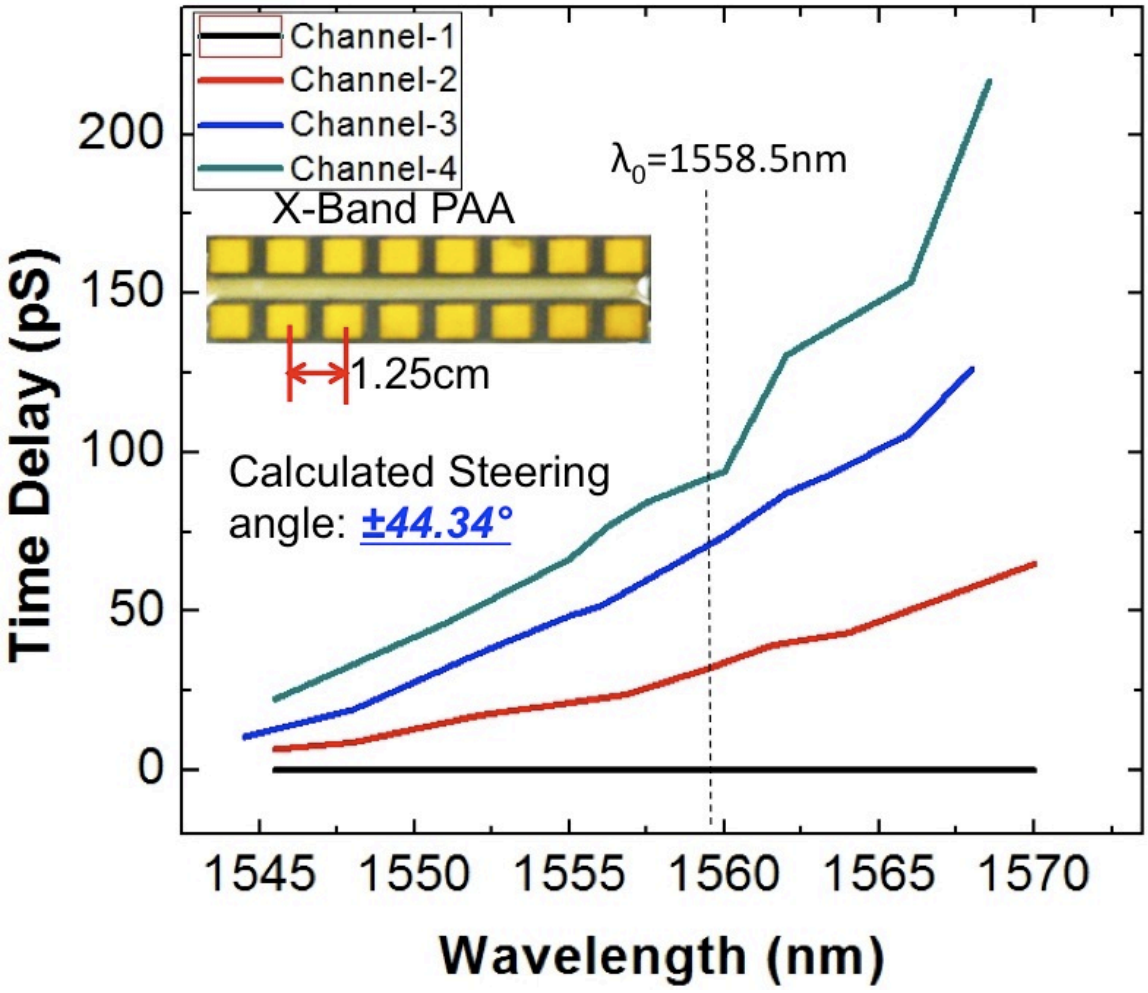

Figure 6 - 5. Wavelength-Tunable Time Delay for all four channels

6.6 **Conclusion**

In conclusion, we experimentally demonstrate a chip-scale four-channel TTD module based on slow light photonic crystal waveguides. The implementation of photonic crystal waveguide tapers enables device operation in the high group index region near the band

edge, thus allowing access to much larger time delays. The integrated TTD module offers continuous wavelength tunable time delays up to 216.7ps for a PCW with a length of 3mm. Further optimization of the interfaces between MMI and PCWs can lead to lower optical loss, and better signal quality. The utilization of even longer PCW channels can cover time delays up to 1ns, which can accommodate more delay line channels and give better directivity. Such a compact device can be implemented in a broadband PAA system in order to achieve large steering angles within the whole X-band.

6.7 **Acknowledgement**

The authors would like to acknowledge the Air Force Office of Scientific Research (AFOSR) for supporting this work under the Multi-disciplinary University Research Initiative (MURI) program (Grant No. FA 9550-08-1-039) and Small Business Technology Transfer (Contract No. FA9550-11-C-0014), monitored by Dr. Gernot Pomrenke.

6.8 **References**

[1] Xiaolong Wang, **Che-Yun Lin**, Swapnajit Chakravarty, Jingdong Luo, Alex K. Y. Jen, and Ray T. Chen, "*Effective in-device r33 of 735pm/V on electro-optic polymer infiltrated silicon photonic crystal slot waveguides*," Opt. Lett. **36** (6), 882-884 (2011).

[2] **Che-Yun Lin**, Xiaolong Wang, Swapnajit Chakravarty, Beom Suk Lee, Weicheng Lai, Jingdong Luo, Alex K.-Y. Jen, and Ray T. Chen, "*Electro-optic polymer infiltrated silicon photonic crystal slot waveguide modulator with 23 dB slow light enhancement*," Appl. Phys. Lett. **97** (9), 093304 (2010).

[3] Jan-Michael Brosi, Christian Koos, Lucio C. Andreani, Michael Waldow, Juerg Leuthold, and Wolfgang Freude, "*High-speed low-voltage electro-optic modulator with a polymer-infiltrated silicon photonic crystal waveguide*," Optics Express **16** (6), 4177-4191 (2008).

[4] Jan H. Wulbern, Alexander Petrov, and Manfred Eich, "*Electro-optical modulator in a polymer-infiltrated silicon slotted photonic crystal waveguide heterostructure resonator*," Opt. Express **17** (1), 304-313 (2009).

[5] Jan Hendrik Wulbern, Jan Hampe, Alexander Petrov, Manfred Eich, Jingdong Luo, Alex K. Y. Jen, Andrea Di Falco, Thomas F. Krauss, and Jurgen Bruns, "*Electro-optic modulation in slotted resonant photonic crystal heterostructures*," Appl. Phys. Lett. **94** (24), 241107-241103 (2009).

[6] Alan X. Wang, **Che-Yun Lin**, Swapnajit Chakravarty, Jingdong Luo, Alex K. Y. Jen, and Ray T. Chen, "*Slow Light Enhanced E-O Polymer Nano-Photonic Modulator with Ultra-High Effective In-Device r33*", presented at the CLEO, (2011).

[7] **Che-Yun Lin**, Beomsuk Lee, Alan X. Wang, Wei-Cheng Lai, Swapnajit Chakravarty, Yazhao Liu, David Kwong, Ray T. Chen, Jingdong Luo, and Alex K. Y. Jen, "*Ultra-compact silicon nanophotonic modulator based on electro-optic polymer infiltrated slot photonic crystal waveguide*", presented at the Proc. SPIE, San Francisco, (2010).

[8] Xiaolong Wang, Chakravarty Swapnajit, Boem Suk Lee, **Che-Yun Lin**, and Chen R. T., "*Electro-optic polymer based nanophotonic modulator with ultra high efficiency*", presented at the Avionics, Fiber-Optics and Phototonics and Photonics Technology Conference, 2009. AVFOP '09. IEEE, San Antonio, TX, (2009).

[9] Xiaolong Wang, Swapnajit Chakravarty, Boem Suk Lee, **Che-Yun Lin**, Jingdong Luo, Alex K. Y. Jen, and Ray T. Chen, "*Nano-Photonic Electro-Optic Polymer Modulator Based on Photonic Band Gap Engineering*", presented at the Integrated Photonics and Nanophotonics Research and Applications, (2009).

[10] Richard A. Soref and Brian R. Bennett, "*Electrooptical effects in silicon*," IEEE J. Quantum Electron. **23** (1), 123-129 (1987).

[11] Hong C. Nguyen, Yuya Sakai, Mizuki Shinkawa, Norihiro Ishikura, and Toshihiko Baba, "*10 Gb/s operation of photonic crystal silicon optical modulators*," Opt. Express **19** (14), 13000-13007 (2011).

[12] Takasumi Tanabe, Katsuhiko Nishiguchi, Eiichi Kuramochi, and Masaya Notomi, "*Low power and fast electro-optic silicon modulator with lateral p-i-n embedded photonic crystal nanocavity*," Opt. Express **17** (25), 22505-22513 (2009).

[13] Xiaonan Chen, Alan X. Wang, Swapnajit Chakravarty, and Ray T. Chen, "*Electrooptically-Active Slow-Light-Enhanced Silicon Slot Photonic Crystal*

Waveguides," IEEE J. Sel. Top. Quantum Electron. **15** (5), 1506-1509 (2009).

[14] Xiaonan Chen, Yun-Sheng Chen, Yang Zhao, Wei Jiang, and Ray T. Chen, "*Capacitor-embedded 0.54 pJ/bit silicon-slot photonic crystal waveguide modulator*," Opt. Lett. **34** (5), 602-604 (2009).

[15] Gu Lanlan, Jiang Wei, Chen Xiaonan, and R. T. Chen, "*Physical Mechanism of p-i-n-Diode-Based Photonic Crystal Silicon Electrooptic Modulators for Gigahertz Operation*," Selected Topics in Quantum Electronics, IEEE Journal of **14** (4), 1132-1139 (2008).

[16] Lanlan Gu, Wei Jiang, Xiaonan Chen, Li Wang, and Ray T. Chen, "*High speed silicon photonic crystal waveguide modulator for low voltage operation*," Appl. Phys. Lett. **90** (7), 071105 (2007).

[17] Yongqiang Jiang, Wei Jiang, Lanlan Gu, Xiaonan Chen, and Ray T. Chen, "*80-micron interaction length silicon photonic crystal waveguide modulator*," Appl. Phys. Lett. **87** (22), 221105-221103 (2005).

[18] Xiaolong Wang, Swapnajit Chakravarty, Boem Suk Lee, **Che-Yun Lin**, and Ray T. Chen, "*Ultraefficient control of light transmission through photonic potential barrier modulation*," Opt. Lett. **34** (20), 3202-3204 (2009).

[19] Yonghao Cui, Ke Liu, Duncan L. MacFarlane, and Jeong-Bong Lee, "*Thermo-optically tunable silicon photonic crystal light modulator*," Opt. Lett. **35** (21), 3613-3615 (2010).

[20] Lanlan Gu, Wei Jiang, Xiaonan Chen, and Ray T. Chen, "*Thermooptically Tuned Photonic Crystal Waveguide Silicon-on-Insulator Mach-Zehnder Interferometers*,"

Photonics Technology Letters, IEEE **19** (5), 342-344 (2007).

[21] Yurii A. Vlasov, Martin O'Boyle, Hendrik F. Hamann, and Sharee J. McNab, "*Active control of slow light on a chip with photonic crystal waveguides*," Nature (London) **438** (7064), 65-69 (2005).

[22] Daryl M. Beggs, Thomas P. White, Liam O'Faolain, and Thomas F. Krauss, "*Ultracompact and low-power optical switch based on silicon photonic crystals*," Opt. Lett. **33** (2), 147-149 (2008).

[23] Wei-Cheng Lai, Swapnajit Chakravarty, Xiaolong Wang, Cheyun Lin, and Ray T. Chen, "*Photonic crystal slot waveguide absorption spectrometer for on-chip near-infrared spectroscopy of xylene in water*," Appl. Phys. Lett. **98** (2), 023304 (2011).

[24] Wei-Cheng Lai, Swapnajit Chakravarty, Xiaolong Wang, Cheyun Lin, and Ray T. Chen, "*On-chip methane sensing by near-IR absorption signatures in a photonic crystal slot waveguide*," Opt. Lett. **36** (6), 984-986 (2011).

[25] Yi Zou, Swapnajit Chakravarty, Wei-Cheng Lai, **Che-Yun Lin**, and Ray T. Chen, "*Methods to Array Photonic Crystal Microcavities for High Throughput High Sensitivity Bio-Sensing on a Silicon-Chip Based Platform (Accepted)*," LChip (2012).

[26] Masaya Notomi, K Yamada, A Shinya, J Takahashi, C Takahashi, and I Yokohama, "*Extremely Large Group-Velocity Dispersion of Line-Defect Waveguides in Photonic Crystal Slabs*," Phys. Rev. Lett. **87** (25), 253902 (2001).

[27] H. Subbaraman, M. Y. Chen, and R. T. Chen, "*Photonic Crystal Fiber-Based True-Time-Delay Beamformer for Multiple RF Beam Transmission and Reception of an X-Band Phased-Array Antenna*," Lightwave Technology, Journal of **26** (15), 2803-2809

(2008).

[28] I. Frigyes and A. J. Seeds, "*Optically generated true-time delay in phased-array antennas*," Microwave Theory and Techniques, IEEE Transactions on **43** (9), 2378-2386 (1995).

[29] L. Ofaolain, X. Yuan, D. McIntyre, S. Thoms, H. Chong, R. M. De La Rue, and T. F. Krauss, "*Low-loss propagation in photonic crystal waveguides*," Electron. Lett. **42** (25), 1454-1455 (2006).

[30] Yurii A. Vlasov and Sharee J. McNab, "*Coupling into the slow light mode in slab-type photonic crystal waveguides*," Opt. Lett. **31** (1), 50-52 (2006).

[31] Che-Yun Lin, Xiaolong Wang, Swapnajit Chakravarty, Beom Suk Lee, Wei-Cheng Lai, and Ray T. Chen, "*Wideband group velocity independent coupling into slow light silicon photonic crystal waveguide*," Appl. Phys. Lett. **97** (18), 183302 (2010).

[32] A. Melloni, A. Canciamilla, C. Ferrari, F. Morichetti, L. O'Faolain, T. F. Krauss, R. De La Rue, A. Samarelli, and M. Sorel, "*Tunable Delay Lines in Silicon Photonics: Coupled Resonators and Photonic Crystals, a Comparison*," Photonics Journal, IEEE **2** (2), 181-194 (2010).

[33] Amir Hosseini, Harish Subbaraman, David Kwong, Yang Zhang, and Ray T. Chen, "*Optimum access waveguide width for 1 x N multimode interference couplers on silicon nanomembrane*," Opt. Lett. **35** (17), 2864-2866 (2010).

[34] Harish Subbaraman, Maggie Yihong Chen, and Ray T. Chen, "*Photonic dual RF beam reception of an X band phased array antenna using a photonic crystal fiber-based true-time-delay beamformer*," Appl. Opt. **47** (34), 6448-6452 (2008).

Chapter 7 High dynamic range electric field sensor for electromagnetic pulse detection

7.1 Abstract

We design a high dynamic range electric field sensor based on domain inverted electro-optic (E-O) polymer Y-fed directional coupler for electromagnetic wave detection. This electrode-less, all optical, wideband electrical field sensor is fabricated using standard processing for E-O polymer photonic devices. Experimental results demonstrate effective detection of electric field from 16.7V/m to 750KV/m at a frequency of 1GHz, and spurious free measurement range of 70dB.

7.2 Introduction: Electromagnetic Wave Sensors

There has been rapidly increasing interest in electric field (E-field) sensors during last decades [1-4]. Electro-magnetic (EM) wave measurement has played a crucial role in various scientific and technical areas, including process control, E-field monitoring in medical apparatuses, ballistic control, electromagnetic compatibility measurements, microwave-integrated circuit testing, and detection of directional energy weapon attack. Conventional EM wave measurement systems use active metallic probes, which can disturb the EM waves to be measured and make the sensor very sensitive to electromagnetic noises. Photonic E-field sensors exhibit significant advantages with respect to the electronic ones due to their smaller size, lighter weight, higher sensitivity,

and extremely broad bandwidth. Because of these exclusive merits, photonic E-field sensors based on integrated optical devices and optical fibers have emerged in the last ten years [2,3,5,6]. These photonic E-field sensors using Mach-Zehnder (MZ) interferometer or ring resonator, however, are facing a significant challenge in its spurious free dynamic range (SFDR) for high fidelity measurement of the EM waves. For example, the inherent nonlinear distortion resulted from the sinusoidal transfer curve make the linearity of a conventional MZ interferometer only to be about 70% [7], which is too small for the EM wave measurement with large dynamic range. A more important feature is that MZ interferometer designs are bias sensitive. The sinusoidal transfer function between the optical output power versus the drive voltage requires the bias point setting at the half power point, where maximum linear dynamic range can be provided. The optimum bias point could drift slowly due to charging effects [8], ambient changes such as the variation of temperature, optical power, and wavelength shifts [9].

7.3 **Design of Polymer Y-Fed Directional Coupler Waveguides**

In this paper, we present the design and experimental results of a photonic E-field sensor based on domain inverted E-O polymer Y-fed directional coupler for electromagnetic wave detection. The Y-fed directional coupler was originally proposed as a linear E-O modulator for RF photonic communication system to achieve a large SFDR [10]. In the following years, more in-depth theoretical investigation was published on how the linearity of a Y-fed directional coupler can be improved by optimizing the lengths and number of the domain inverted sections [11], and experimental results with significantly

suppressed inter-modulation distortion signals and enhanced SFDR were successfully demonstrated [12,13]. We follow the same token of the design principle as our previous work on E-O polymer linear modulator in this paper, but with the removal of the bottom and top electrode to sense the electric field in the free space.

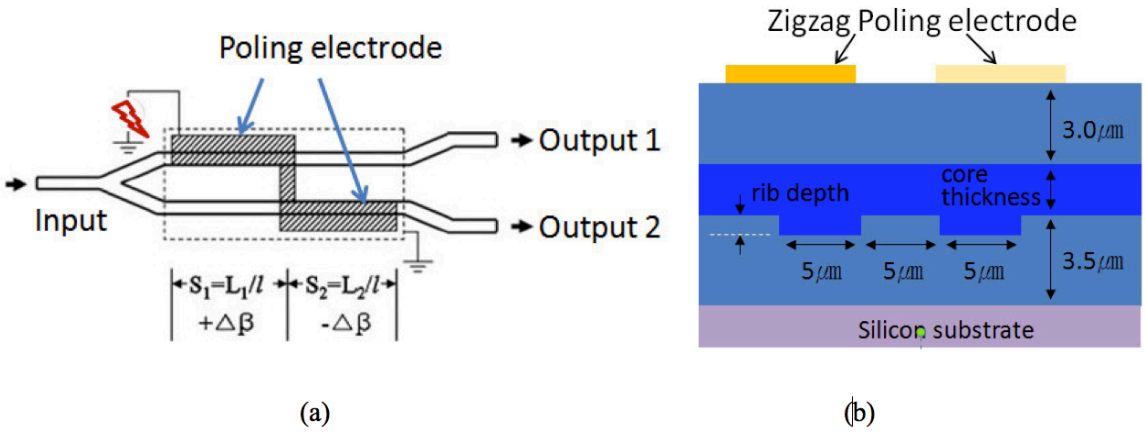

Figure 7 - 1. (a) Schematic of the photonic electric field sensor based on domain inverted E-O polymer Y-fed directional coupler (b) Cross sectional view of the directional coupler waveguide with equivalent domain inversion

The schematic of the photonic E-field sensor is shown in Figure 7 - 1 (a). One input waveguide branches into a pair of symmetric waveguides that are optically coupled with each other. Because of the symmetry, equal optical power with the same phase is launched into the coupled waveguides and, hence, the operating point is automatically set at the 3 dB point without any bias voltage. Phase modulation (Δβ) reversal can be realized by poling the E-O polymer waveguide using a lumped electrode that alternately zigzags from one waveguide to the opposite waveguide in the two domains, with cross sectional view shown in Figure 7 - 1 (b). This configuration creates an equivalent Δβ

reversal without domain-inverted poling of the E-O polymer waveguide. After removing the poling electrode, the uniform electric field from free space (far field pattern with wavelength much longer than the E-field sensor dimension) will induce equal phase modulation with reversed polarity. The key design parameters such as the E-O polymer waveguide dimension and the length of the inverted domains exactly follow those in [12,13].

7.4 **Fabrication of Electric Field Sensors**

The photonic E-field sensors are fabricated on silicon wafer carrier. The bottom cladding polymer (UV-15LV) is spin coated and cured to obtain a 3.5μm film. Ridge waveguide structures are formed by etching 0.42μm × 5μm trench using reactive ion etching (RIE), and then followed by spin-coating a 1.8μm-thick EO polymer layer (excluding the ridge depth). The E-O polymer core layer is made by doping AJ-CKL1 chromophore into amorphous polycarbonate (APC) with 25% weight percentage and then dissolved in cyclopentanone. The solution phase E-O polymer can be spun-on to any substrate and has demonstrated excellent capability to fill narrow trenches [14,15], which offers great processing simplicity. In the next step, another polymer layer (UFC-170A) is coated on top of the E-O polymer layer and cured to serve as the top cladding. Electrodes for poling are patterned by photolithography, metal deposition, image reversal and lift off. During the poling process, the sample is heated up to the glass transition temperature (Tg) of E-O polymer (Tg=135°C) under a strong DC poling electric field (100V/μm) between the poling electrode and the bottom silicon substrate to align the dipole moment of the E-O polymer molecules. Upon reaching the glass transition temperature, the heater is switched

off and the sample is naturally cooled down to room temperature under the same DC electric field. This process freezes the aligned E-O polymer molecules, which preserves electro-optic response of the E-O polymer film without the presence of poling electric field. After poling, the poling electrode is removed by metal etchant. Finally, the photonic E-field sensor devices are diced and polished to for characterization.

7.5 **Measurements of The Electric Field Sensor**

The fabricated photonic E-field sensors are tested under a microstrip transmission line that can generate electric field at RF frequency in a direction that is perpendicular to the directional coupler waveguides. The characteristic impedance of the microstrip line is experimentally measured to be 55.6-j5.4 without the insertion of the EM wave sensor and 55-j4.9 with the insertion of the EM wave sensor at 1GHz. The testing setup is shown in Figure 7 - 2. The input optical signal coming from a tunable laser source with TM polarization is butt-coupled to the directional waveguide using a polarization maintaining single mode fiber. The output optical signal is collected using a single mode fiber at one branch of the directional waveguide. The measured insertion loss is around 21dB, which corresponds to 6dB propagation loss and 7.5dB/facet coupling loss, respectively. When the RF electrical signal is guided on the microstrip line, it generates electrical field that oscillates in the vertical direction that can modulate the refractive index of the E-O polymer. Similar to an electro-optic modulator for optical communication application, this modulation in refractive index induces the modulation of the output optical signal, which can be detected with a high-speed avalanche photodiode and analyzed with a

microwave spectrum analyzer. It is worth noting that the insertion of the EM wave sensor can slightly enhance the electric field by ~9%. The uniformity of the electric field under the microstrip line is almost unaffected. Also, due to the difference of the dielectric constant between polymer (ε_r~3.2) and air (ε_r=1), the electric field in the polymer layers is ~31% of that in the air.

In our experiment, we use 1GHz RF wave as the simulant electric field. The photonic E-field sensors are expected to sense EM waves with much higher frequency in free space (limited by the silicon substrate absorption); however, the microstrip line that we use in our testing setup has significant limited bandwidth due to the skin effect and dielectric absorption. The response from the photonic E-field sensor is shown in Figure 7 - 3 with 20dBm RF input power. The photonic E-field sensor shows optical response at the same frequency with 35dB signal to noise ratio (SNR).

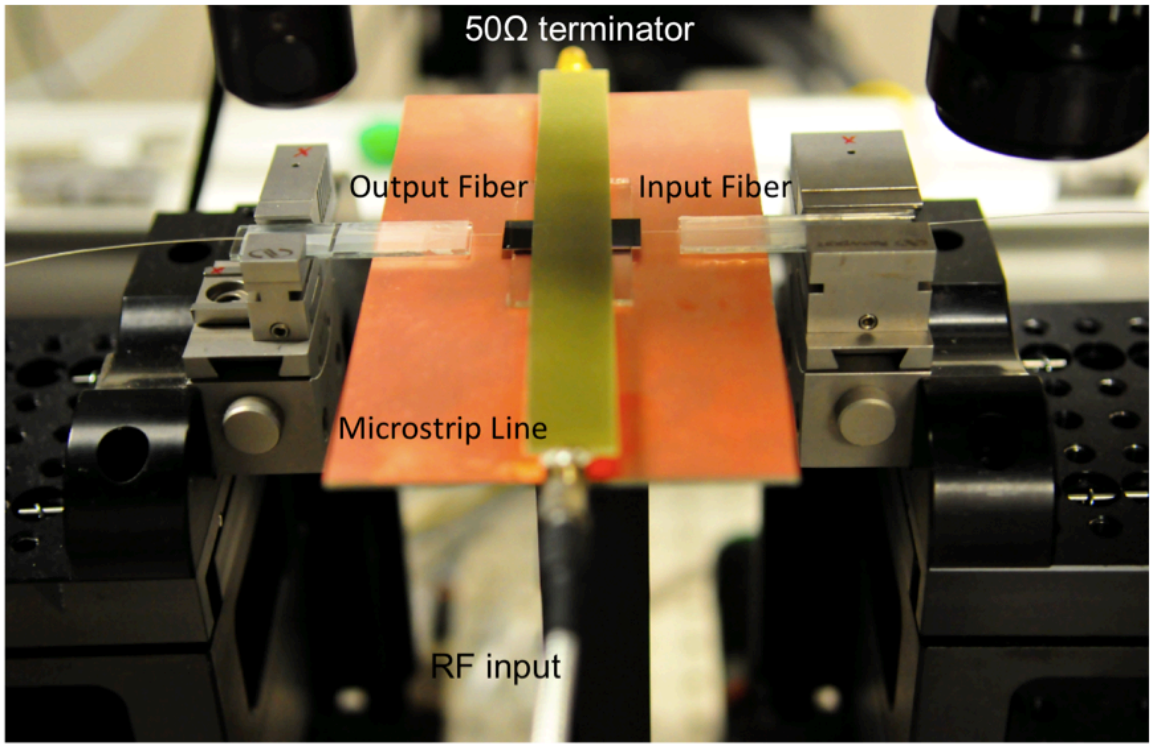

Figure 7 - 2. Testing setup for the photonic E-field sensor with the microstrip line that generate vertical electric field, polarization maintaining single mode fiber for input coupling, and single mode fiber for output coupling. The microstrip line is connected to a RF source with an SMA cable on one end and terminated with a 50ohm terminator on the other end to avoid reflection

To test the sensitivity of the photonic E-field sensor, the input RF power is gradually decreased until the sensing signal from the sensor is buried under the noise level. The signal intensity of the photonic E-field sensor is plotted against the input electric field intensity as shown in Figure 7 - 4. The electric field E inside the microstrip line can be calculated from the input RF power (P_{in}) [16]:

$\vec{E} = \sqrt{2 \cdot P_{in} \cdot Z_0}$, where Z_0 is the characteristic impedance of the microstrip line.

The measurement shows that the minimum detectable electric field is found to be 16.7V/m. In our experiment, we measured the electric field up to 550V/m. This is NOT the upper sensing limit of sensor, but simply due to the fact that our RF power source has a maximum output of 20dBm. The variation of the measured curve in Figure 7 - 4 is attributed to the instability of optical coupling and laser power fluctuation.

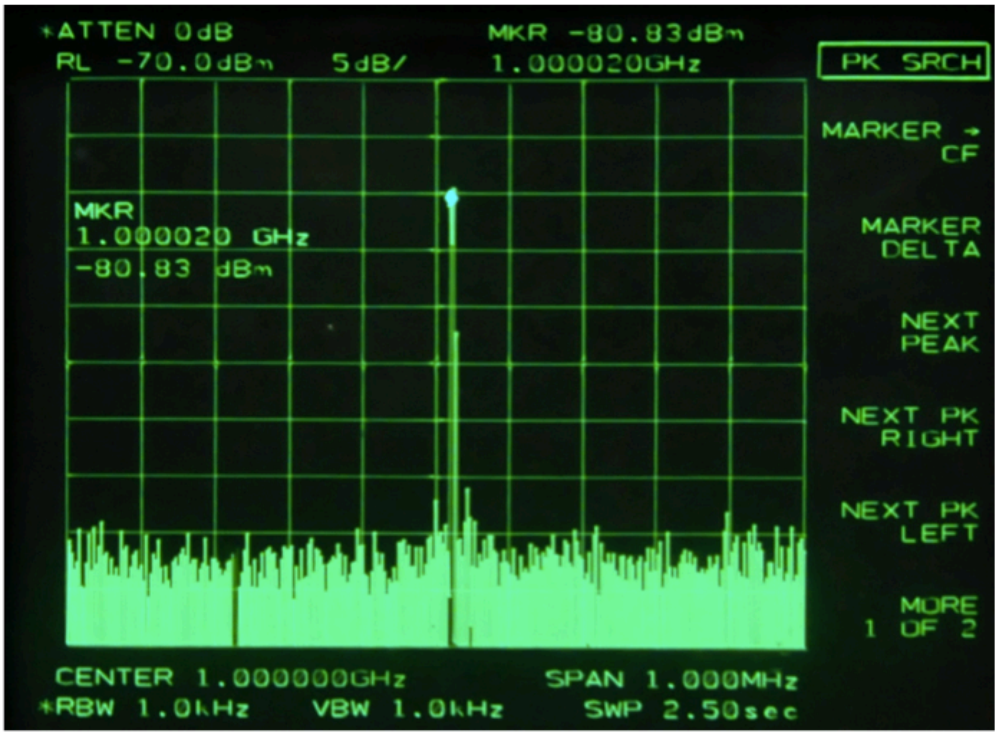

Figure 7 - 3. The response of the photonic E-field sensor with 20dBm RF input power at 1GHz.

In order to determine the maximum electric field the device can sense, we measured another photonic E-field on the same chip without removing the poling electrode on top. By this means, we can apply the driving voltage across a very narrow gap (~8μm) to generate a much stronger electric field. The photonic E-field sensor shows over modulation at 6V, which corresponding to an electric field intensity of 750KV/m. Taking

consideration of the sensible electric field E from 16.7V/m to 750KV/m, and the Poynting vector of the EM wave is given by $\langle S \rangle = \frac{1}{2}\varepsilon_0 \varepsilon_r c E^2$, this corresponds to a power range from 1.04W/m^2 to 2.09×109W/m^2, which is as large as 93dB dynamic range. To measure the noise free dynamic range of the photonic E-field sensor, we use two tone RF signals (100KHz and 105KHz) to drive the sensor with top electrode. It shows the maximum noise free dynamic range of 70dB, which is shown in Figure 7 - 5. This result would be of high significance for high fidelity measurement of the EM waves.

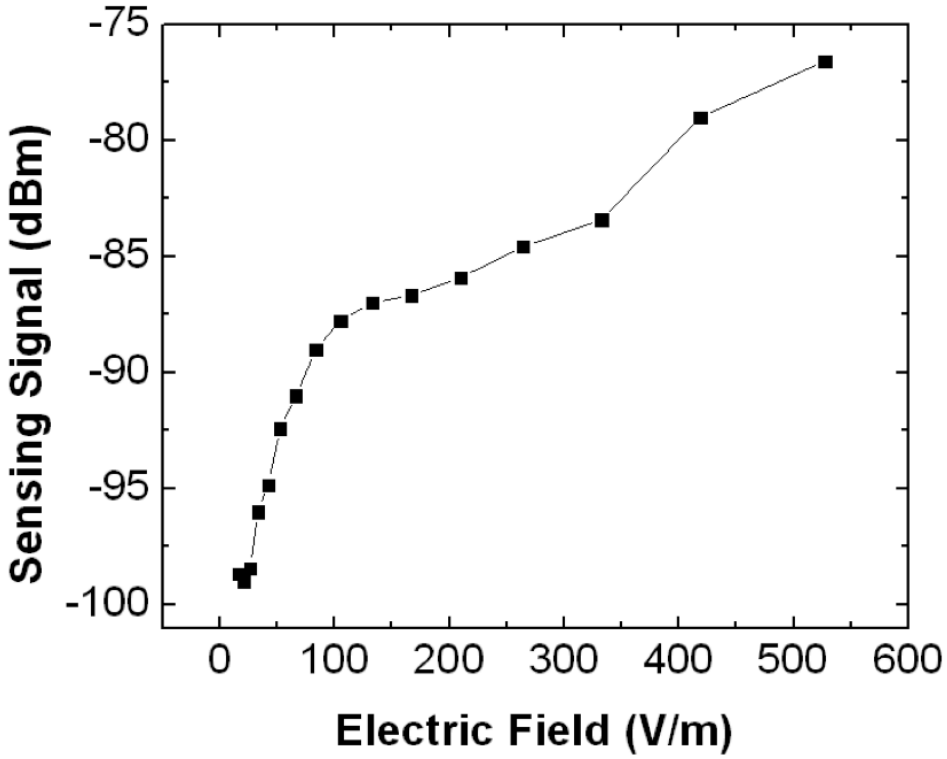

Figure 7 - 4. Response from the photonic E-field sensor as a function of the electric field.

7.6 **Conclusion**

In conclusion, we have successfully demonstrated electric field sensor based on domain inverted electro-optic (E-O) polymer Y-fed directional coupler for electromagnetic wave detection. The sensor can detect electric field from 16.7V/m to 750KV/m, corresponding to EM waves with large dynamic range of power from 1.04W/m2 to 2.09×109W/m2 . The fabricated photonic E-field sensor also achieves a noise free dynamic range of 70dB. Further optimization of E-field sensor through fine tuning the fabrication processes, improving the poling efficiency, and reducing the optical waveguide loss should allow better performance in sensitivity.

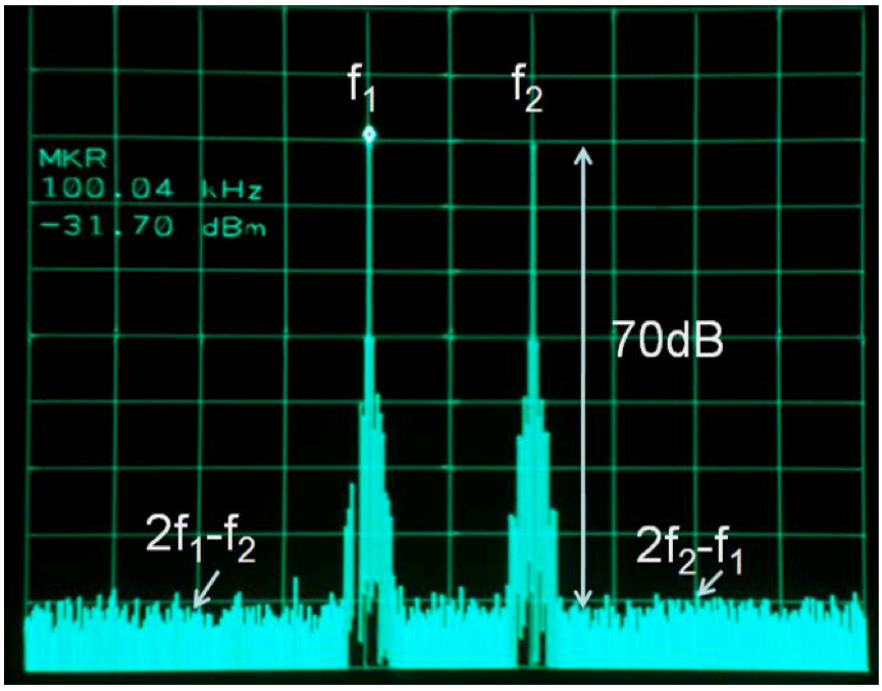

Figure 7 - 5. The photonic E-field sensor shows a noise free dynamic range of 70dB.

7.7 **Acknowledgement**

The authors would like to acknowledge the U.S. ARMY Space & Missile Defense Command/Army Forces Strategic Command (USASMDC/ARSTRAT) for supporting this work under the SBIR grant W9113M-10-P-0076 that is monitored by Dr. Mark Rader.

7.8 **References**

[1] P. Drexler and P. Fiala, "*Methods for High-Power EM Pulse Measurement*," IEEE Sensors Journal **7** (7), 1006-1011 (2007).

[2] N. Kuwabara, K. Tajima, R. Kobayashi, and F. Amemiya, "*Development and analysis of electric field sensor using LiNbO3 optical modulator*," IEEE Transactions on Electromagnetic Compatibility **34** (4), 391-396 (1992).

[3] S. C. Rashleigh, "*Magnetic-field sensing with a single-mode fiber*," Opt. Lett. **6** (1), 19-21 (1981).

[4] J. Kanwisher and K. Lawson, "*Electromagnetic flow sensors*," Limnology and Oceanography **20** (2), 174-182 (1975).

[5] Sriram S. Sriram and Stuart A. Kingsley, "*Sensitivity enhancements to photonic electric field sensor***"**, presented at the Proc. SPIE, (2004).

[6] K. Tajima, R. Kobayashi, N. Kuwabara, and M. Tokuda, "*Optical Fibers and Devices. Development of Optical Isotropic E-Field Sensor Operating More than 10GHz Using Mach-Zehnder Interferometers*," IEICE Trans Electron **85** (4), 961-968 (2002).

[7] E.M. Zolotov and RF Tavlykaev, "*Integrated optical Mach-Zehnder modulator with a*

linearized modulation characteristic," Quantum Electronics **18** (3), 401-402 (1988).

[8] R.L. Jungerman, C. Johnsen, D.J. McQuate, K. Salomaa, M.P. Zurakowski, R.C. Bray, G. Conrad, D. Cropper, and P. Hernday, "*High-speed optical modulator for application in instrumentation*," J. Lightwave Technol. **8** (9), 1363-1370 (1990).

[9] R.A. Becker, "*Circuit effect in LiNbO3 channel-waveguide modulators*," Opt. Lett. **10** (8), 417-419 (1985).

[10] R.F. Tavlykaev and R.V. Ramaswamy, "*Highly linear Y-fed directional coupler modulator with low intermodulation distortion*," J. Lightwave Technol. **17** (2), 282-291 (1999).

[11] Xiaolong Wang, Beom-Suk Lee, **Che-Yun Lin**, Dechang An, and Ray T. Chen, "*Electroptic Polymer Linear Modulators Based on Multiple-Domain Y-Fed Directional Coupler*," Lightwave Technology, Journal of **28** (11), 1670-1676 (2010).

[12] B. Lee, C.Y. Lin, A.X. Wang, R. Dinu, and R.T. Chen, "*Linearized electro-optic modulators based on a two-section Y-fed directional coupler*," Appl. Optics **49** (33), 6485-6488 (2010).

[13] B. Lee, C. Lin, X. Wang, R.T. Chen, J. Luo, and A.K.Y. Jen, "*Bias-free electro-optic polymer-based two-section Y-branch waveguide modulator with 22 dB linearity enhancement*," Opt. Lett. **34** (21), 3277-3279 (2009).

[14] Xiaolong Wang, Che-Yun Lin, Swapnajit Chakravarty, Jingdong Luo, Alex K. Y. Jen, and Ray T. Chen, "*Effective in-device r33 of 735pm/V on electro-optic polymer infiltrated silicon photonic crystal slot waveguides*," Opt. Lett. **36** (6), 882-884 (2011).

[15] Che-Yun Lin, Xiaolong Wang, Swapnajit Chakravarty, Beom Suk Lee, Weicheng Lai,

Jingdong Luo, Alex K.-Y. Jen, and Ray T. Chen, "*Electro-optic polymer infiltrated silicon photonic crystal slot waveguide modulator with 23 dB slow light enhancement*," Appl. Phys. Lett. **97** (9), 093304 (2010).

[16] K.C. Gupta and I.J. Bahl, "*Microstrip lines and slotlines*," Microstrip lines and slotlines (1996).

Chapter 8 On-chip spot size converter for fiber to chip coupling

8.1 Introduction

In many photonic devices, interface problems are normally the most difficult ones to address. A good example of this issue is the strip waveguide-photonic crystal waveguide interface. Without a properly designed interface, large mode profile mismatch and group index mismatch will cause strong back reflection and scattering, resulting in a very high coupling loss. In order for a silicon photonic integrated circuit to be implemented in any commercial optical communication or sensor systems, it is necessary to have good coupling efficiency to a fiber. However, there exists a strong optical mode profile mismatch between a silicon waveguide and an optical fiber. Because of the high index contrast in a silicon waveguide, the cross section for such a waveguide is only 230nm by 500nm. By contrast, a single mode optical fiber has a diameter around 9 microns. As a result, this geometrical mismatch causes strong optical mode mismatch, which are shown in Figure 8 - 1. At a fiber-silicon waveguide interface, the small mode overlap between the guided modes makes the optical coupling from an optical fiber to a silicon waveguide very inefficient.

To address this issue, many approaches was proposed and implemented. These include grating couplers[1-4] and on-ship spot size converters based on inverted tapers[5-10]. It has been reported that 31% coupling efficiency is achieved using grating coupler[1]. Adding a

gold bottom mirror to the SOI substrate has improved the coupling efficiency to 69%[3]. Non-uniform grating fabricated using the lag effect in a etch process also shows 64% efficiency[4]. To increase the tolerance of etch process control, a photonic crystal grating using fully etched grating was also demonstrated with 42% peak coupling efficiency.

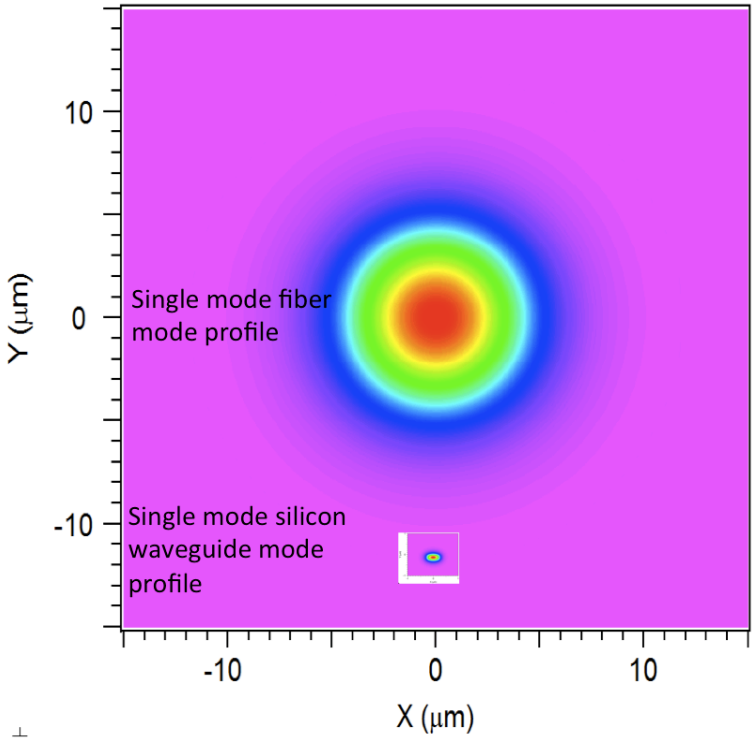

Figure 8 - 1. Optical mode profiles for a single mode fiber and a single mode silicon waveguide with 230nm

Although optical coupling are much more efficient with grating couplers, good coupling efficiency is polarization and wavelength dependent. By contrast, an on-chip spot size converter does not suffer from these restrictions. A schematic of an on-chip spot size converter is shown in Figure 8 - 2. Such structure utilizes an inversely tapered silicon waveguide and a low index waveguide on top of silicon waveguide to significantly

reduce the confinement and increase the mode size[6,7,9,10] when the width of the silicon waveguide is reduced. This results in a loosely confined mode with a mode size that matches that of a optical fiber. In our study, we choose SU-8 photoresist to form the low index waveguide due to several reasons. First, SU-8 can be pattern easily with photolithography or electron-beam lithography. Second, SU-8 is highly transparent near 1550nm. Third, SU-8 is mechanically and chemically stable under room temperature after it is cross-linked. Finally, the refractive index (n) of SU-8 is 1.575 at 1550nm, which can form a waveguide with air cladding (n=1). It can also serves as cladding material for silicon waveguide (n=3.47). These characteristics make SU-8 a very good material for a proof of concept experiment.

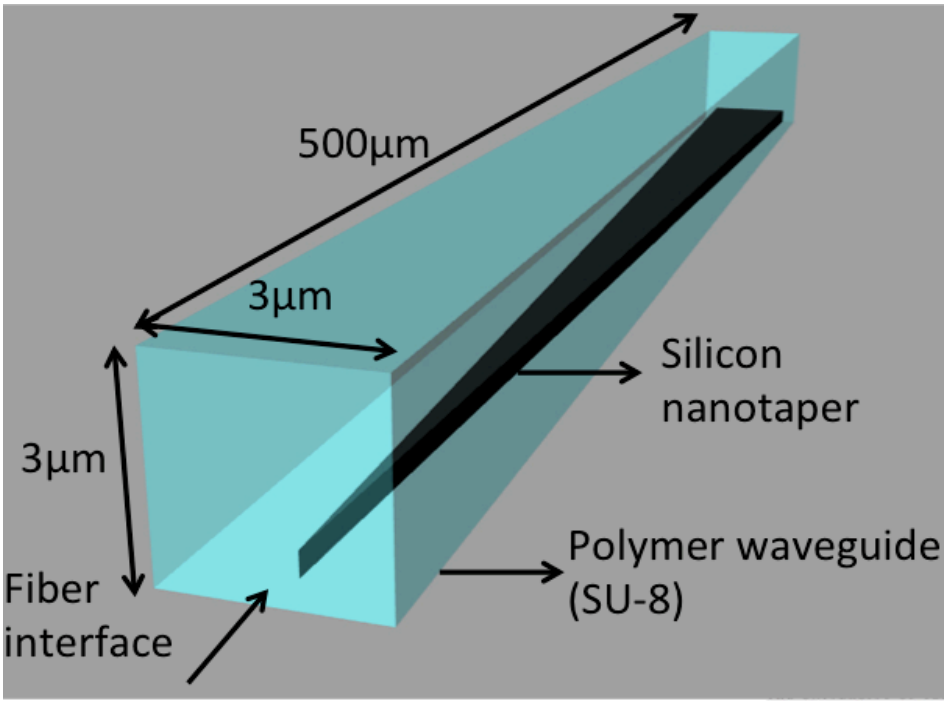

Figure 8 - 2. Schematic of the on-chip spot size converter made of a silicon nanotaper (n=3.47) and a polymer waveguide (n=1.575)

8.2 **Design of on-chip spot size converter**

A mode conversion process in the spot size converter is illustrated in Figure 8 - 3. At the end of a silicon nanotaper with 50nm silicon width, the TE guided mode is mostly confined in SU-8 waveguide region as shown in Figure 8 - 3 (a). The dimension of the SU-8 waveguide is chosen to be 3μm by 3μm to mode match with a lensed fiber. At the fiber interface, input light from a fiber will excite a waveguide mode in the SU-8 waveguide with small optical loss. Moving away from the fiber interface, the width of the silicon nanotaper increases gradually from 50nm to 500nm within 500μm distance. As the width of the silicon nanotaper increases, the guided mode will gradually couple to the high index silicon at the bottom of the SU-8 waveguide. When the width of the silicon taper reaches 500nm, light becomes mostly confined in the silicon waveguide. As a result, the SU-8 structure no longer works as a waveguide; instead, it becomes a cladding layer for the single mode silicon waveguide. This phenomenon is shown in a series of pictures from Figure 8 - 3 (a) to (f).

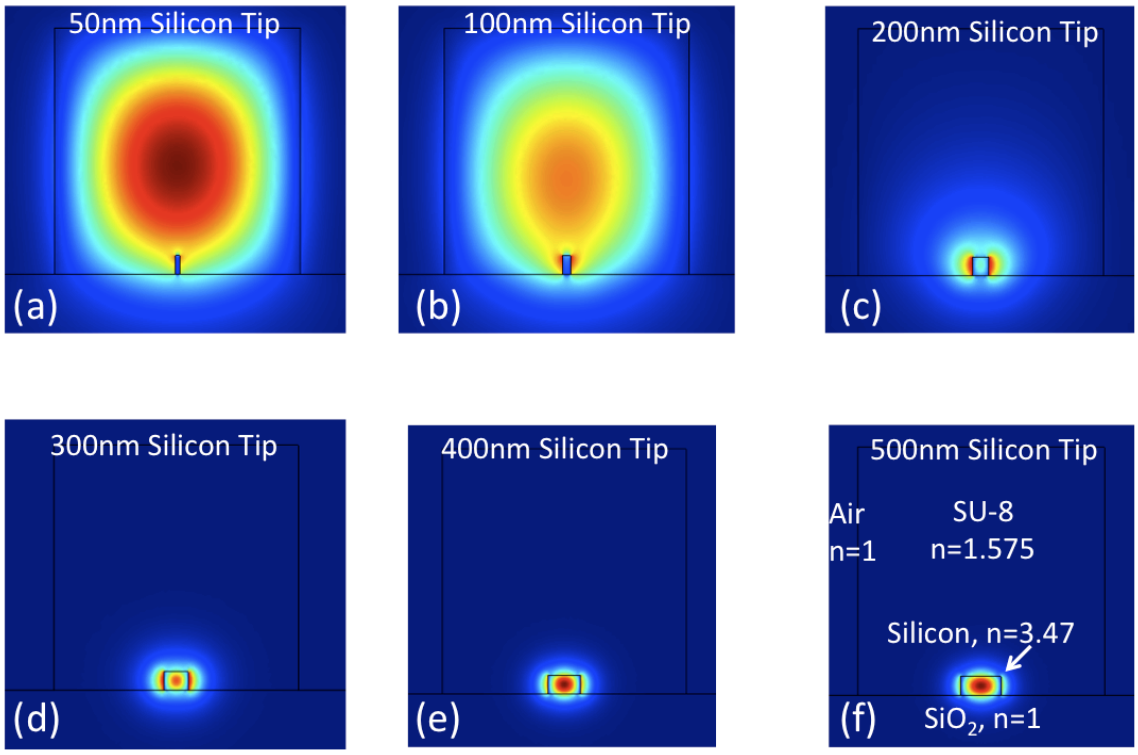

Figure 8 - 3. Transverse electric (TE) optical mode profiles for silicon nanotapers at 1550nm wavelength with (a) 50nm to (f) 500nm width. The height of the silicon nanotaper is determined by the thickness of the silicon slab (230nm).

8.3 **Fabrication of the on-chip spot size converter**

The fabrication of the silicon nanotaper shares identical processing steps with slotted photonic crystal waveguide modulators as described in Chapter 5. The SU-8 polymer waveguide can be made with a standard photolithography using EVG620 mask aligner in microelectronic research center cleanroom.

The first step is to spin SU-8 2005 on SOI chip with 8000rpm for one minute, followed by a soft bake at 95 degree C on a hotplate for 2minutes. This creates a SU-8 film with

~4.7μm thickness. The second step is to UV expose the SU-8 film for 6.5 seconds on the EVG620 mask aligner, followed by a post exposure bake on a hotplate at 95 degree C for three minutes. The exposed SU-8 will start to cross-link after 30~40 sec of baking and the pattern will show up accordingly. After the chip is cooled down to room temperature, it should be developed for one minute in SU-8 developer followed by one-minute IPA rinse. Finally, the chip is hard baked at 160 degree C for 10 minutes for the SU-8 resist to cross-link. After the SU-8 is cross-linked, it becomes a permanent structure that works as an optical waveguide.

8.4 **Measurement and discussion**

Measurements were first performed on SU-8 waveguides fabricated on SOI chip with top silicon layer removed. The testing procedure and equipment are identical to Chapter 3. The same SU-8 waveguide before and after baking are both tested for comparison. Measurement results and the microscope pictures are shown in Figure 8 - 4.

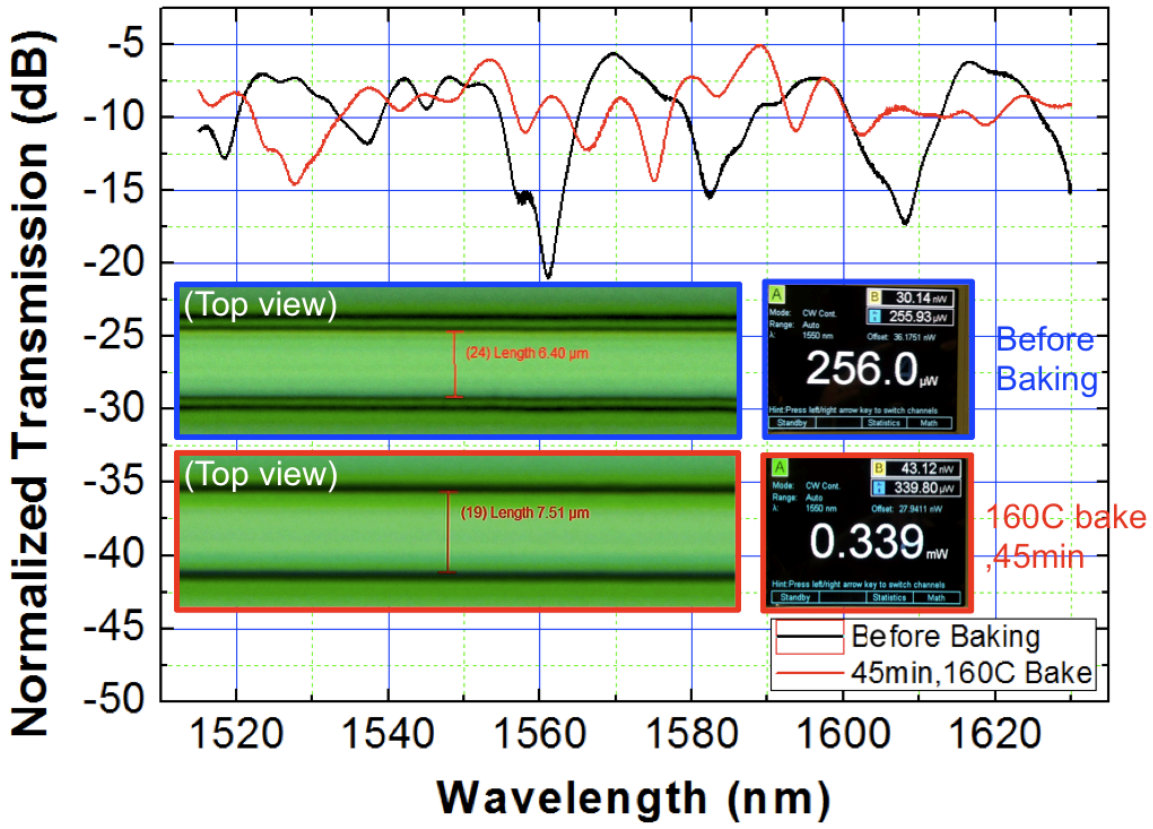

Figure 8 - 4. Measurement result of the transmission spectra for the same SU-8 waveguide before and after baking. The insets show the top view of SU-8 waveguides before and after baking. The insets on the right shows the screen shots of the power meter that display the total power collected at the output fiber.

The measurement results show that it is possible to achieve a broadband coupling with moderate insertion loss. The lowest insertion loss is around 5dB at 1590nm. The fluctuations in the transmission spectrum are mainly due to Fabry-Perot effect at a fiber and chip facet interface. Note that the SU-8 waveguide geometry is not yet optimized, and it is 7.5μm wide and 4.3μm high. This non-optimized geometry causes optical mode mismatch at the SU-8 and fiber interface and increases insertion loss. With further process optimization, it is expected to get lower insertion loss performance.

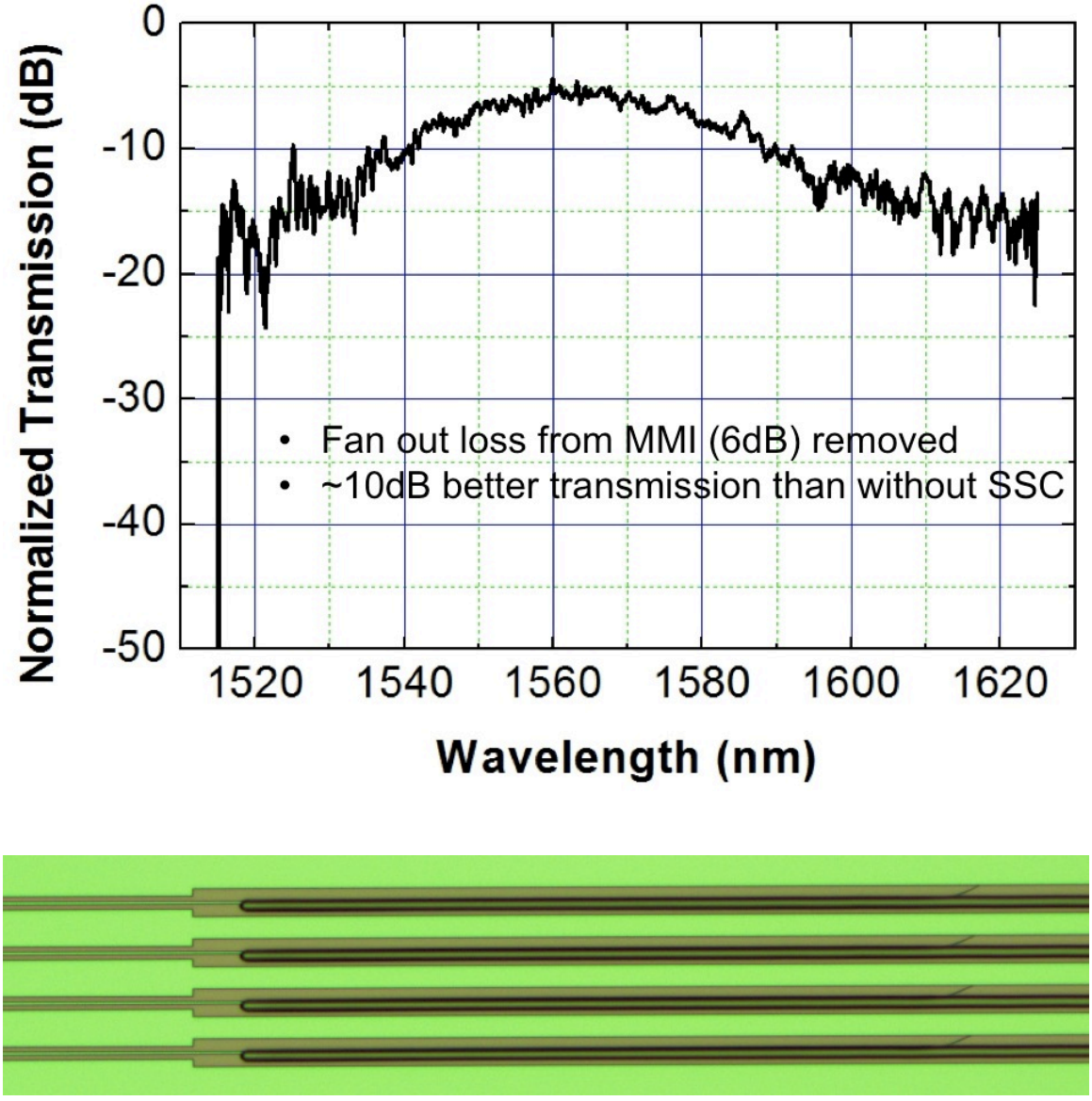

Figure 8 - 5. Transmission spectrum of a silicon strip waveguide from one of the four channels of a 1x4 MMI. Spot size converters are included in both input and output.

The testing result of using spot size converters on all four channels of the TTD module is shown in Figure 8 - 5, and the microscope picture of the output is shown in the bottom panel. The result shows a minimum insertion loss around 5dB, which includes the

coupling loss between fiber and SU-8 waveguide and propagation loss in 8mm long silicon waveguide. Compare to the best result in the literature, which has 1dB/facet coupling loss, our result shows higher insertion loss. This is mainly due to the misalignment of SU-8 waveguide on top of silicon nanotaper and the bending of silicon nanotaper tip that make the mode conversion process in the silicon nanotaper region less efficient. The bending of silicon nanotaper tip issue is caused by the bending of e-beam resist pattern during development process, and it is transferred to the silicon layer during subsequent etching processes. The silicon nanotaper tip has 100nm tip width and the resist thickness is around 300nm. During development process, the tip structure with high aspect ratio formed on e-beam resist tends to collapse. Therefore, it is often necessary to reduce the pattern aspect ratio at the tip region of silicon nanotaper. This problem can be solved by using diluted ZEP520A, which can give 131nm-thick resist layer and significantly reduce the aspect ratio at the silicon nanotaper tip. With further process optimization to eliminate the bending of silicon nanotaper, we expect further reduction of insertion loss using the spot size converter we designed.

8.5 **Conclusion**

In conclusion, we have shown the design and experimental results as a proof of concept for a low loss and broadband on-chip spot size converter that can significantly reduce the insertion loss between a optical fiber and a silicon photonic chip. This structure will create a better interface between a fiber and a silicon photonic chip, and help drive the

implementation of silicon photonics technology in areas such as optical communications and sensors.

8.6 References

[1] D. Taillaert, F. Van Laere, M. Ayre, W. Bogaerts, D. Van Thourhout, P. Bienstman, and R. Baets, "*Grating couplers for coupling between optical fibers and nanophotonic waveguides*," Jpn. J. Appl. Phys., Part 1 **45** (2006).

[2] Liu Liu (刘柳), Minhao Pu (蒲敏皓), Kresten Yvind, and Jørn M. Hvam, "*High-efficiency, large-bandwidth silicon-on-insulator grating coupler based on a fully-etched photonic crystal structure*," Appl. Phys. Lett. **96** (051126) (2010).

[3] Frederik Van Laere, G¸nther Roelkens, Melanie Ayre, Jonathan Schrauwen, Dirk Taillaert, Dries Van Thourhout, Thomas F. Krauss, and Roel Baets, "*Compact and Highly Efficient Grating Couplers Between Optical Fiber and Nanophotonic Waveguides*," J. Lightwave Technol. **25** (1), 151-156 (2007).

[4] Yongbo Tang, Zhechao Wang, Lech Wosinski, Urban Westergren, and Sailing He, "*Highly efficient nonuniform grating coupler for silicon-on-insulator nanophotonic circuits*," Opt. Lett. **35** (8), 1290-1292 (2010).

[5] Minhao Pu, Liu Liu, Haiyan Ou, Kresten Yvind, and J√∏rn M. Hvam, "*Ultra-low-loss inverted taper coupler for silicon-on-insulator ridge waveguide*," OptCo **283** (19), 3678-3682 (2010).

[6] G. Roelkens, P. Dumon, W. Bogaerts, D. Van Thourhout, and R. Baets, "*Efficient silicon-on-insulator fiber coupler fabricated using 248-nm-deep UV lithography*," Photonics Technology Letters, IEEE **17** (12), 2613-2615 (2005).

[7] Sharee McNab, Nikolaj Moll, and Yurii Vlasov, "*Ultra-low loss photonic integrated circuit with membrane-type photonic crystal waveguides*," Opt. Express **11** (22), 2927-2939 (2003).

[8] Vilson R. Almeida, Roberto R. Panepucci, and Michal Lipson, "*Nanotaper for compact mode conversion*," Opt. Lett. **28** (15), 1302-1304 (2003).

[9] T. Shoji, T. Tsuchizawa, T. Watanabe, K. Yamada, and H. Morita, "*Low loss mode size converter from 0.3 μm square Si wire waveguides to singlemode fibres*," Electron. Lett. **38** (25), 1669-1670 (2002).

[10] Y. Shani, C. H. Henry, R. C. Kistler, K. J. Orlowsky, and D. A. Ackerman, "*Efficient coupling of a semiconductor laser to an optical fiber by means of a tapered waveguide on silicon*," Appl. Phys. Lett. **55** (23), 2389-2391 (1989).

Chapter 9 Suggested Future Work

9.1 Ultra-compact electro-optic modulator based on active control of photonic band edge

In the previous chapters, we have demonstrated group velocity independent coupling to both photonic crystal waveguide and photonic crystal slot waveguide. Utilizing these highly efficient coupling approaches, we demonstrate record-low $V_\pi \cdot L$ figure of merit for EO polymer modulator. Our modulators devices with ~300μm interaction length shows significant reduction of device footprints as compared to conventional waveguide devices that have centimeter scale interaction length. However, for on-chip optical interconnect, further reduction of device footprint is necessary.

For future work, instead of using interferometer-based modulator, which operates based on phase change in the individual arm, we propose using a modulation mechanism based on active control of photonic band gap[1]. This modulation scheme is illustrated in Figure 9 - 1. Since a mode represents a resonance condition of a waveguide, the resonance moves when refractive index of the waveguide material is perturbed. In photonic crystal waveguides, when the material index is modified, it induces a shift in the defect-guided mode. For photonic crystal waveguides with very sharp band edge cut-off, while operating at the edge of guided mode, this shift in guided mode drives the device into photonic band gap region under the same operation wavelength. This effect is simulated by FDTD as shown in Figure 9 - 2 (b). Since this mechanism operates based on shifting

at the edge of defect-guided mode instead of phase change, it does not require a long active region to switch on/off the incident light. During the coupling study, we have demonstrated that it only requires 10μm long of photonic crystal waveguide to achieve 35dB of on/off operation. When an index changing mechanism is introduced in such a photonic crystal waveguide, it is possible to demonstrate ultra-compact electro-optic modulator. In addition, it is worth to note that the index change mechanism is very generic. Same modulation effect can be achieved through various index-changing mechanism such as free carrier effect[2,3], thermo-heating[4], or applying voltage on EO polymer[5,6]. Therefore, one can design modulators based on the speed requirement of different applications.

Lastly for high speed electro-optic modulator, EO polymer with electro-optic response up to THz range[7] is the best candidate. Our plan is to use the EO polymer-infiltrated silicon photonic crystal waveguide for this demonstration. Examples of the fabricated devices are shown in Figure 9 - 2 and Figure 9 - 3.

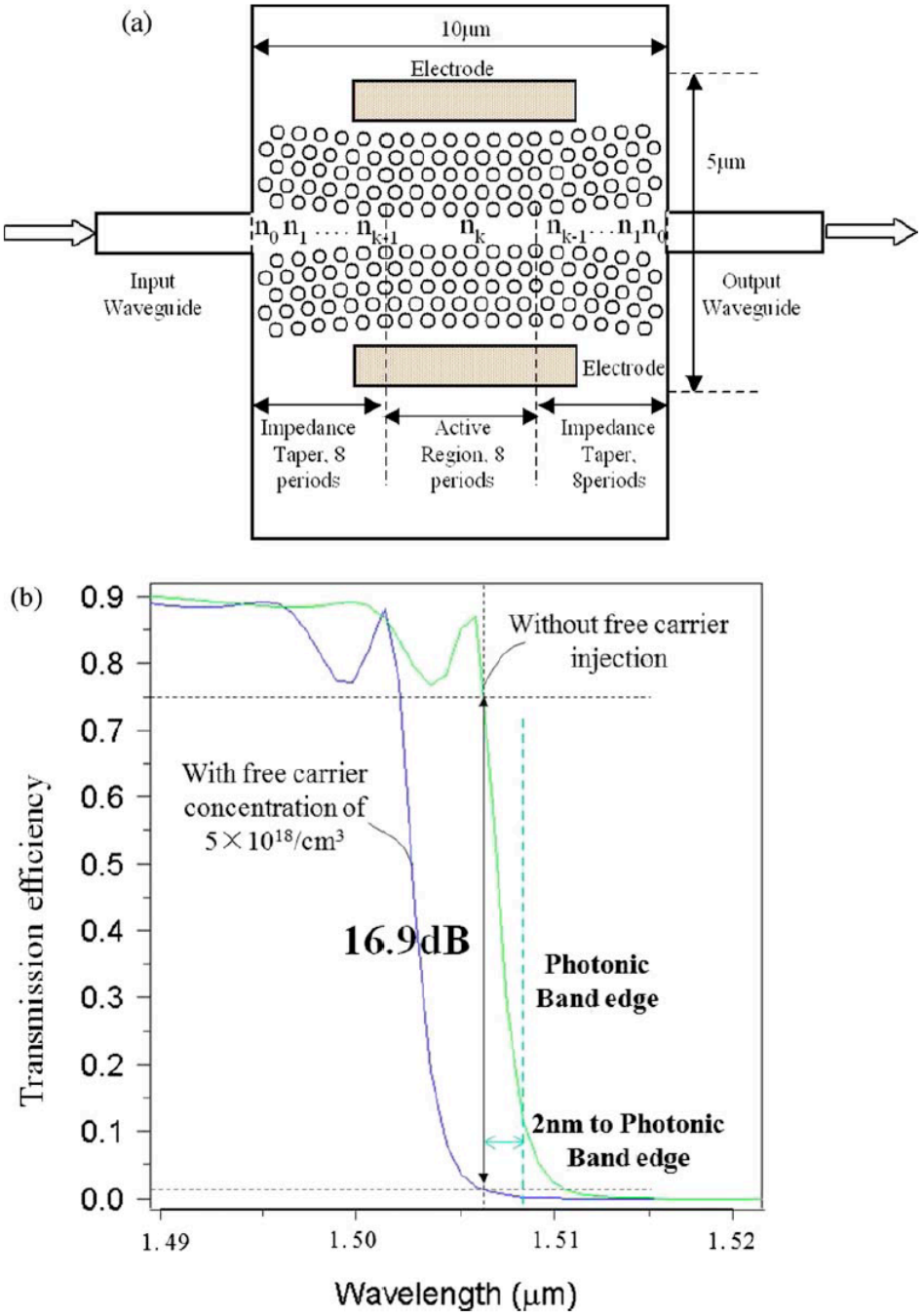

Figure 9 - 1 (a) Schematic of the photonic band modulation device with 10μm by 5μm footprint (Media 5). (b) Simulated transmission spectrum by 2-D FDTD method.

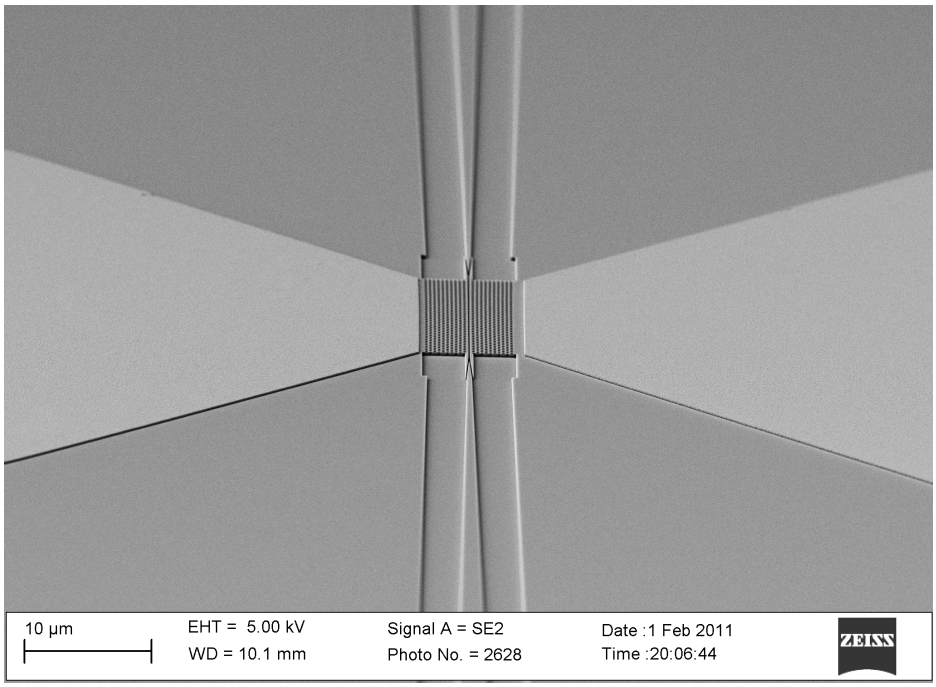

Figure 9 - 2. Scanning electron micrograph of electro-optic band-shift modulator using EO polymer as an active material

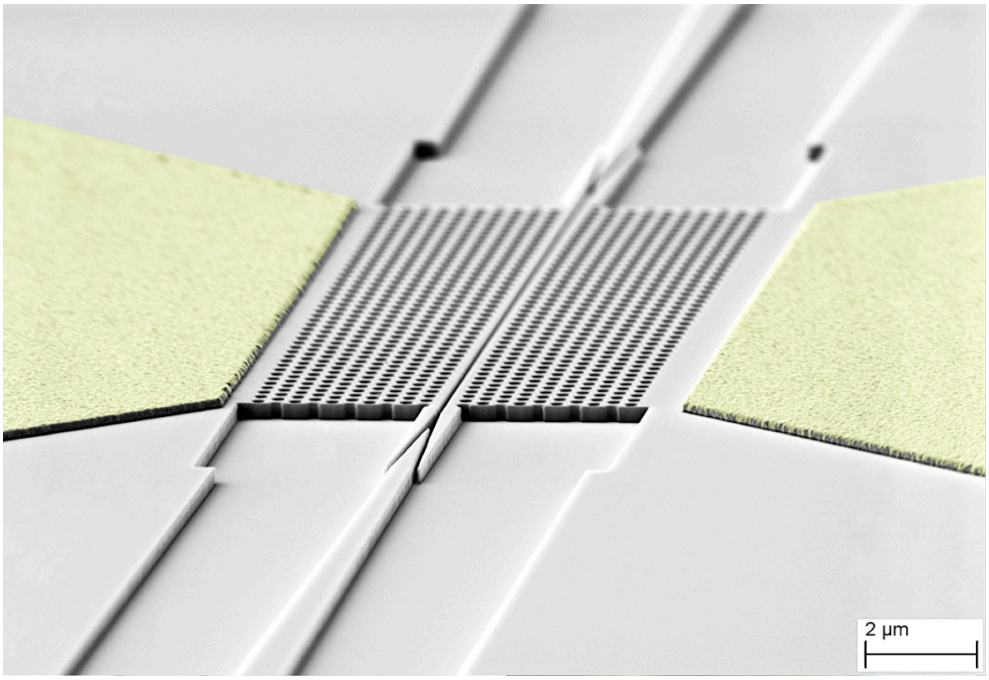

Figure 9 - 3. Zoom-in view of the electro-optic bandshift modulator

9.2 References

[1] Xiaolong Wang, Swapnajit Chakravarty, Boem Suk Lee, Che-Yun Lin, and Ray T. Chen, "*Ultraefficient control of light transmission through photonic potential barrier modulation*," Opt. Lett. **34** (20), 3202-3204 (2009).

[2] Xiaonan Chen, Alan X. Wang, Swapnajit Chakravarty, and Ray T. Chen, "*Electrooptically-Active Slow-Light-Enhanced Silicon Slot Photonic Crystal Waveguides*," IEEE J. Sel. Top. Quantum Electron. **15** (5), 1506-1509 (2009).

[3] Richard A. Soref and Brian R. Bennett, "*Electrooptical effects in silicon*," IEEE J. Quantum Electron. **23** (1), 123-129 (1987).

[4] Lanlan Gu, Wei Jiang, Xiaonan Chen, and Ray T. Chen, "*Thermooptically Tuned Photonic Crystal Waveguide Silicon-on-Insulator Mach-Zehnder Interferometers*," Photonics Technology Letters, IEEE **19** (5), 342-344 (2007).

[5] Che-Yun Lin, Xiaolong Wang, Swapnajit Chakravarty, Jingdong Luo, Alex K. Y. Jen, and Ray T. Chen, "*735pm/V Effective In-Device r_{33} on Electro-Optic Polymer Infiltrated Silicon Photonic Crystal Slot Waveguide*," Optics Letters (Accepted) (2011).

[6] Che-Yun Lin, Xiaolong Wang, Swapnajit Chakravarty, Beom Suk Lee, Weicheng Lai, Jingdong Luo, Alex K.-Y. Jen, and Ray T. Chen, "*Electro-optic polymer infiltrated silicon photonic crystal slot waveguide modulator with 23 dB slow light enhancement*," Appl. Phys. Lett. **97** (9), 093304 (2010).

[7] Michael Hochberg, Tom Baehr-Jones, Guangxi Wang, Michael Shearn, Katherine Harvard, Jingdong Luo, Baoquan Chen, Zhengwei Shi, Rhys Lawson, Phil Sullivan,

Alex K. Y. Jen, Larry Dalton, and Axel Scherer, "*Terahertz all-optical modulation in a silicon-polymer hybrid system*," Nature Materials **5** (9), 703-709 (2006).

APPENDIX A: JOURNAL PUBLICATIONS

[1] Yi Zou, Swapnajit Chakravarty, Wei-Cheng Lai, **Che-Yun Lin**, and Ray T. Chen, "Methods to Array Photonic Crystal Microcavities for High Throughput High Sensitivity Bio-Sensing on a Silicon-Chip Based Platform (Accepted)," LChip (2012).

[2] Xiaochuan Xu, Harish Subbaraman, Amir Hosseini, **Che-Yun Lin**, David Kwong, and Ray T. Chen, "Stamp Printing of Silicon Nanomembrane Based Photonic Devices onto Flexible Substrates with a Suspended Configuration," Optics Letters (Accepted) (2012).

[3] **Che-Yun Lin**, Alan X. Wang, Wei-Cheng Lai, John L. Covey, Swapnajit Chakravarty, and Ray T. Chen, "Coupling loss minimization of slow light slotted photonic crystal waveguides using mode matching with continuous group index perturbation," Opt. Lett. **37** (2), 232-234 (2012).

[4] Xiaolong Wang, **Che-Yun Lin**, Swapnajit Chakravarty, Jingdong Luo, Alex K. Y. Jen, and Ray T. Chen, "Effective in-device r33 of 735pm/V on electro-optic polymer infiltrated silicon photonic crystal slot waveguides," Opt. Lett. **36** (6), 882-884 (2011).

[5] **Che-Yun Lin**, Alan X. Wang, Beom Suk Lee, Xingyu Zhang, and Ray T. Chen, "High dynamic range electric field sensor for electromagnetic pulse detection," Opt. Express **19** (18), 17372-17377 (2011).

[6] Beom Suk Lee, **Che-Yun Lin**, Alan X. Wang, and Ray T. Chen, "Demonstration of a Linearized Traveling Wave Y-Fed Directional Coupler Modulator Based on Electro-

Optic Polymer," Lightwave Technology, Journal of **29** (13), 1931-1936 (2011).

[7] Wei-Cheng Lai, Swapnajit Chakravarty, Xiaolong Wang, **Che-Yun Lin**, and Ray T. Chen, "Photonic crystal slot waveguide absorption spectrometer for on-chip near-infrared spectroscopy of xylene in water," Appl. Phys. Lett. **98** (2), 023304-023303 (2011).

[8] Wei-Cheng Lai, Swapnajit Chakravarty, Xiaolong Wang, **Che-Yun Lin**, and Ray T. Chen, "On-chip methane sensing by near-IR absorption signatures in a photonic crystal slot waveguide," Opt. Lett. **36** (6), 984-986 (2011).

[9] Ray T. Chen and **Che-Yun Lin**, "Broadband, Group Index Independent, and Ultra-Low Loss Coupling into Slow Light Slotted Photonic Crystal Waveguides", US Patent (Pending) (2011).

[10] Xiaolong Wang, Beom-Suk Lee, **Che-Yun Lin**, Dechang An, and Ray T. Chen, "Electroptic Polymer Linear Modulators Based on Multiple-Domain Y-Fed Directional Coupler," Lightwave Technology, Journal of **28** (11), 1670-1676 (2010).

[11] **Che-Yun Lin**, Xiaolong Wang, Swapnajit Chakravarty, Beom Suk Lee, Weicheng Lai, Jingdong Luo, Alex K.-Y. Jen, and Ray T. Chen, "Electro-optic polymer infiltrated silicon photonic crystal slot waveguide modulator with 23 dB slow light enhancement," Appl. Phys. Lett. **97** (9), 093304 (2010).

[12] **Che-Yun Lin**, Xiaolong Wang, Swapnajit Chakravarty, Beom Suk Lee, Weicheng Lai, and Ray T. Chen, "Wideband Group Velocity Independent Coupling into

Slow Light Silicon Photonic Crystal Waveguide," Appl. Phys. Lett. **97** (19) (2010).

[13] Beomsuk Lee, **Che-Yun Lin**, Alan X. Wang, Raluca Dinu, and Ray T. Chen, "Linearized electro-optic modulators based on a two-section Y-fed directional coupler," Appl. Opt. **49** (33), 6485-6488 (2010).

[14] Amir Hosseini, David Kwong, **Che-Yun Lin**, Beomsuk Lee, and Ray T. Chen, "Output Formulation for Symmetrically Excited One-to-N Multimode Interference Coupler," Selected Topics in Quantum Electronics, IEEE Journal of **16** (1), 61 - 69 (2010).

[15] Xiaolong Wang, Swapnajit Chakravarty, Boem Suk Lee, **Che-Yun Lin**, and Ray T. Chen, "Ultraefficient control of light transmission through photonic potential barrier modulation," Opt. Lett. **34** (20), 3202-3204 (2009).

[16] Beomsuk Lee, **Che-Yun Lin**, Xiaolong Wang, Ray T. Chen, Jingdong Luo, and Alex K. Y. Jen, "Bias-free electro-optic polymer-based two-section Y-branch waveguide modulator with 22 dB linearity enhancement," Opt. Lett. **34** (21), 3277-3279 (2009).

[17] Ray T. Chen, Xiaonan Chen, and **Che-Yun Lin**, "Methods for Compact Strip/Slot Waveguide Coupling with 20dB Efficiency Enhancement", US Patent (Pending) (2009).

APPENDIX B: CONFERENCE PUBLICATIONS

[1] **Che-Yun Lin**, Alan X. Wang, Beom Suk Lee, Xingyun Zhang, and Ray T. Chen, "*EO-Polymer Waveguide Based High Dynamic Range EM Wave Sensors* " SPIE Photonics West (Invited Talk) (2012).

[2] **Che-Yun Lin**, Amir Hosseini, Harish Subbaraman, Zheng Xue, Alan X. Wang, and Ray T. Chen, "*Wavelength-Tunable on-Chip True Time Delay Lines Based on Photonic Crystal Waveguides for X-Band Phased Array Antenna Applications*," CLEO (Accepted) (2012).

[3] Alan X. Wang, **Che-Yun Lin**, Swapnajit Chakravarty, Jingdong Luo, Alex K. Y. Jen, and Ray T. Chen, "*Slow Light Enhanced E-O Polymer Nano-Photonic Modulator with Ultra-High Effective In-Device r33***"**, presented at the CLEO, (2011).

[4] **Che-Yun Lin**, Alan X. Wang, Beomsuk Lee, Wei-Cheng Lai, Swapnajit Chakravarty, and Ray T. Chen, "*Group velocity independent coupling into slow light photonic crystal waveguide on Silicon Nanophotonic Integrated Circuits*," Proc. SPIE (2011).

[5] **Che-Yun Lin**, Alan X. Wang, Swapnajit Chakravarty, Wei-Cheng Lai, Beom Suk Lee, and Ray T. Chen, "*Experimental Demonstration of Ultra-Low Loss Coupling into Slow Light Slotted Photonic Crystal Waveguide on Silicon Nanomembrane*," Integrated Photonic Research Conference (2011).

[6] Wei-Cheng Lai, Katy Moncivais, Swapnajit Chakravarty, Alan X. Wang, **Che-Yun Lin**, Johnathan Zhang, and Ray T. Chen, "*High density ink jet printing of biomolecules for photonic crystal-based microarray applications*," Optical Sensors Topical Meeting, Toronto, Canada (2011).

[7] Wei-Cheng Lai, Katy Moncivais, Swapnajit Chakravarty, Alan X. Wang, **Che-Yun Lin**, Johnathan Zhang, and Ray T. Chen, "*Photonic crystal microarray nano-platform for high-throughput detection of biomolecules for diagnostic assays*," SPIE Defense, Security and Sensing (Oral Presentation) (2011).

[8] Swapnajit Chakravarty, Wei-Cheng Lai, Xiaolong Wang, **Che-Yun Lin**, and Ray T. Chen, "*Photonic crystal slot waveguide spectrometer for the detection of methane (Proceedings Paper)*," Proc. SPIE (2011).

[9] Swapnajit Chakravarty, Wei-Cheng Lai, Xiaolong Wang, **Che-Yun Lin**, and Ray T. Chen, "*Photonic crystal slot waveguide for high sensitivity on-chip near-infrared optical absorption spectroscopy of xylene in water (Proceedings Paper)*," Proc. SPIE (2011).

[10] Swapnajit Chakravarty, Wei-Cheng Lai, Alan X. Wang, **Che-Yun Lin**, and Ray T. Chen, "*Photonic crystal slot waveguide optical absorption spectrometer for high-sensitivity near-infrared detection of xylene in water*," SPIE Defense, Security and Sensing (Oral Presentation) (2011).

[11] Swapnajit Chakravarty, Wei-Cheng Lai, Kathryn Moncivais, Xiaolong Wang, **Che-Yun Lin**, Zhiwen J. Zhang, and Ray T. Chen, "*Photonic crystal microarray nanoplatform for high throughput detection of biomolecules (Proceedings Paper)*," SPIE Defese and Sensing (2011).

[12] **Che-Yun Lin**, Beomsuk Lee, Alan X. Wang, Wei-Cheng Lai, Swapnajit Chakravarty, Yazhao Liu, David Kwong, Ray T. Chen, Jingdong Luo, and Alex K. Y. Jen, "*Ultra-*

compact silicon nanophotonic modulator based on electro-optic polymer infiltrated slot photonic crystal waveguide", presented at the Proc. SPIE, San Francisco, (2010).

[13] Beomsuk Lee, **Che-Yun Lin**, Alan X. Wang, Raluca Dinu, and Ray T. Chen, "*Bias-free Y-branch waveguide modulator based on domain-inversed modulation of electro-optic polymer*," Proc. SPIE (2010).

[14] David Kwong, YaZhao Liu, Amir Hosseini, Yang Zhang, Beomsuk Lee, **Che-Yun Lin**, and Ray T. Chen, "*Silicon-integrated photonic circuit for a single-stage large-angle beam steering optical phased array*", presented at the Proc. SPIE, San Francisco, California, USA, (2010).

[15] Xiaolong Wang, Chakravarty Swapnajit, Boem Suk Lee, **Che-Yun Lin**, and Chen R. T., "*Electro-optic polymer based nanophotonic modulator with ultra high efficiency*", presented at the Avionics, Fiber-Optics and Phototonics and Photonics Technology Conference, 2009. AVFOP '09. IEEE, San Antonio, TX, (2009).

[16] Xiaolong Wang, Swapnajit Chakravarty, Boem Suk Lee, **Che-Yun Lin**, Jingdong Luo, Alex K. Y. Jen, and Ray T. Chen, "*Nano-Photonic Electro-Optic Polymer Modulator Based on Photonic Band Gap Engineering*", presented at the Integrated Photonics and Nanophotonics Research and Applications, (2009).

[17] Beomsuk Lee, **Che-Yun Lin**, Xiaolong Wang, Ray. T. Chen, Jingdong Luo, and Alex. K. Y. Jen, "*Domain-inversion-equivalent EO polymer based Y-fed directional coupler modulator with high linearity*", presented at the IEEE/LEOS Winter Topicals Meeting Series, (2009).

REFERENCES

[1] Thomas F. Krauss, "*Slow light in photonic crystal waveguides*," J. Phys. D: Appl. Phys. **40**, 2666-2670 (2007).

[2] Marin Soljačić and John. D. Joannopoulos, "*Enhancement of nonlinear effects using photonic crystals*," Nat Mater **3** (4), 211-219 (2004).

[3] Masaya Notomi, K Yamada, A Shinya, J Takahashi, C Takahashi, and I Yokohama, "*Extremely Large Group-Velocity Dispersion of Line-Defect Waveguides in Photonic Crystal Slabs*," Phys. Rev. Lett. **87** (25), 253902 (2001).

[4] Eli Yablonovitch, "*Inhibited Spontaneous Emission in Solid-State Physics and Electronics*," Phys. Rev. Lett. **58** (20), 2059 (1987).

[5] Sajeev John, "*Strong localization of photons in certain disordered dielectric superlattices*," Phys. Rev. Lett. **58** (23), 2486 (1987).

[6] **Che-Yun Lin**, Xiaolong Wang, Swapnajit Chakravarty, Beom Suk Lee, Weicheng Lai, Jingdong Luo, Alex K.-Y. Jen, and Ray T. Chen, "*Electro-optic polymer infiltrated silicon photonic crystal slot waveguide modulator with 23 dB slow light enhancement*," Appl. Phys. Lett. **97** (9), 093304 (2010).

[7] Xiaolong Wang, Swapnajit Chakravarty, Boem Suk Lee, Che-Yun Lin, and Ray T. Chen, "*Ultraefficient control of light transmission through photonic potential barrier modulation*," Opt. Lett. **34** (20), 3202-3204 (2009).

[8] B. Corcoran, C. Monat, C. Grillet, D. J. Moss, B. J. Eggleton, T. P. White, O'FaolainL, and T. F. Krauss, "*Green light emission in silicon through slow-light enhanced third-*

harmonic generation in photonic-crystal waveguides," Nat Photon **3** (4), 206-210 (2009).

[9] Jan-Michael Brosi, Christian Koos, Lucio C. Andreani, Michael Waldow, Juerg Leuthold, and Wolfgang Freude, "*High-speed low-voltage electro-optic modulator with a polymer-infiltrated silicon photonic crystal waveguide*," Optics Express **16** (6), 4177-4191 (2008).

[10] Daryl M. Beggs, Thomas P. White, Liam O'Faolain, and Thomas F. Krauss, "*Ultracompact and low-power optical switch based on silicon photonic crystals*," Opt. Lett. **33** (2), 147-149 (2008).

[11] Toshihiko Baba, "*Slow light in photonic crystals*," Nature Photonics **2** (8), 465-473 (2008).

[12] Nobuhiko Ozaki, Yoshinori Kitagawa, Yoshiaki Takata, Naoki Ikeda, Yoshinori Watanabe, Akio Mizutani, Yoshimasa Sugimoto, and Kiyoshi Asakawa, "*High transmission recovery of slow light in a photonic crystal waveguide using a hetero groupvelocity waveguide*," Opt. Express **15** (13), 7974-7983 (2007).

[13] J. P. Hugonin, P. Lalanne, T. P. White, and Thomas. F. Krauss, "*Coupling into slow-mode photonic crystal waveguides*," Opt. Lett. **32** (18), 2638-2640 (2007).

[14] Lanlan Gu, Wei Jiang, Xiaonan Chen, Li Wang, and Ray T. Chen, "*High speed silicon photonic crystal waveguide modulator for low voltage operation*," Appl. Phys. Lett. **90** (7), 071105 (2007).

[15] Lanlan Gu, Wei Jiang, Xiaonan Chen, and Ray T. Chen, "*Thermooptically Tuned Photonic Crystal Waveguide Silicon-on-Insulator Mach-Zehnder Interferometers*," Photonics Technology Letters, IEEE **19** (5), 342-344 (2007).

[16] C. Martijn de Sterke, J. Walker, Kokou B. Dossou, and Lindsay C. Botten, "*Efficient slow light coupling into photonic crystals*," Opt. Express **15** (17), 10984-10990 (2007).

[17] Yurii A. Vlasov and Sharee J. McNab, "*Coupling into the slow light mode in slab-type photonic crystal waveguides*," Opt. Lett. **31** (1), 50-52 (2006).

[18] Yurii A. Vlasov, Martin O'Boyle, Hendrik F. Hamann, and Sharee J. McNab, "*Active control of slow light on a chip with photonic crystal waveguides*," Nature (London) **438** (7064), 65-69 (2005).

[19] M. Povinelli, Steven Johnson, and J. Joannopoulos, "*Slow-light, band-edge waveguides for tunable time delays*," Opt. Express **13** (18), 7145-7159 (2005).

[20] Yongqiang Jiang, Wei Jiang, Lanlan Gu, Xiaonan Chen, and Ray T. Chen, "*80-micron interaction length silicon photonic crystal waveguide modulator*," Appl. Phys. Lett. **87** (22), 221105-221103 (2005).

[21] Solomon Assefa, Peter T. Rakich, Peter Bienstman, Steven G. Johnson, Gale S. Petrich, John D. Joannopoulos, Leslie A. Kolodziejski, Erich P. Ippen, and Henry I. Smith, "*Guiding 1.5 mu m light in photonic crystals based on dielectric rods*," Appl. Phys. Lett. **85** (25), 6110-6112 (2004).

[22] Steven G. Johnson, Peter Bienstman, M. A. Skorobogatiy, Mihai Ibanescu, Elefterios Lidorikis, and J. D. Joannopoulos, "*Adiabatic theorem and continuous*

coupled-mode theory for efficient taper transitions in photonic crystals," Phys. Rev. E **66** (6), 066608 (2002).

[23] Xiaolong Wang, **Che-Yun Lin**, Swapnajit Chakravarty, Jingdong Luo, Alex K. Y. Jen, and Ray T. Chen, "*Effective in-device r33 of 735pm/V on electro-optic polymer infiltrated silicon photonic crystal slot waveguides*," Opt. Lett. **36** (6), 882-884 (2011).

[24] M. G. Scullion, T. F. Krauss, and A. Di Falco, "*High Efficiency Interface for Coupling Into Slotted Photonic Crystal Waveguides*," Photonics Journal, IEEE **3** (2), 203-208 (2011).

[25] Hong C. Nguyen, Yuya Sakai, Mizuki Shinkawa, Norihiro Ishikura, and Toshihiko Baba, "*10 Gb/s operation of photonic crystal silicon optical modulators*," Opt. Express **19** (14), 13000-13007 (2011).

[26] Wei-Cheng Lai, Swapnajit Chakravarty, Xiaolong Wang, Cheyun Lin, and Ray T. Chen, "*On-chip methane sensing by near-IR absorption signatures in a photonic crystal slot waveguide*," Opt. Lett. **36** (6), 984-986 (2011).

[27] Wei-Cheng Lai, Swapnajit Chakravarty, Xiaolong Wang, Cheyun Lin, and Ray T. Chen, "*Photonic crystal slot waveguide absorption spectrometer for on-chip near-infrared spectroscopy of xylene in water*," Appl. Phys. Lett. **98** (2), 023304 (2011).

[28] Che-Yun Lin, Xiaolong Wang, Swapnajit Chakravarty, Beom Suk Lee, Wei-Cheng Lai, and Ray T. Chen, "*Wideband group velocity independent coupling into slow light silicon photonic crystal waveguide*," Appl. Phys. Lett. **97** (18), 183302 (2010).

[29] Zhechao Wang, Ning Zhu, Yongbo Tang, Lech Wosinski, Daoxin Dai, and Sailing He, "*Ultracompact low-loss coupler between strip and slot waveguides*," Opt. Lett. **34** (10), 1498-1500 (2009).

[30] M. R. Patterson, S. Hughes, S. Schulz, D. M. Beggs, T. P. White, L. O'Faolain, and Thomas. F. Krauss, "*Disorder-induced incoherent scattering losses in photonic crystal waveguides: Bloch mode reshaping, multiple scattering, and breakdown of the Beer-Lambert law*," Phys. Rev. B **80** (19), 195305 (2009).

[31] Xiaonan Chen, Alan X. Wang, Swapnajit Chakravarty, and Ray T. Chen, "*Electrooptically-Active Slow-Light-Enhanced Silicon Slot Photonic Crystal Waveguides*," IEEE J. Sel. Top. Quantum Electron. **15** (5), 1506-1509 (2009).

[32] Xiaonan Chen, Yun-Sheng Chen, Yang Zhao, Wei Jiang, and Ray T. Chen, "*Capacitor-embedded 0.54 pJ/bit silicon-slot photonic crystal waveguide modulator*," Opt. Lett. **34** (5), 602-604 (2009).

[33] Gu Lanlan, Jiang Wei, Chen Xiaonan, and R. T. Chen, "*Physical Mechanism of p-i-n-Diode-Based Photonic Crystal Silicon Electrooptic Modulators for Gigahertz Operation*," Selected Topics in Quantum Electronics, IEEE Journal of **14** (4), 1132-1139 (2008).

[34] Thomas F. Krauss, "*Why do we need slow light?*," Nat Photon **2** (8), 448-450 (2008).

[35] Andrea Di Falco, L OíFaolain, and Thomas F. Krauss, "*Dispersion control and slow light in slotted photonic crystal waveguides*," Appl. Phys. Lett. **92**, 083501 (2008).

[36] Pierre Pottier, Marco Gnan, and Richard M. De La Rue, "*Efficient coupling into slow-light photonic crystal channel guides using photonic crystal tapers*," Opt. Express **15** (11), 6569-6575 (2007).

[37] Xiaonan Chen, Wei Jiang, Jiaqi Chen, Lanlan Gu, and Ray T. Chen, "*20 dB-enhanced coupling to slot photonic crystal waveguide using multimode interference coupler*," Appl. Phys. Lett. **91** (9), 091111 (2007).

[38] P. Andrew Anderson, Bradley S. Schmidt, and Michal Lipson, "*High confinement in silicon slot waveguides with sharp bends*," Opt. Express **14** (20), 9197-9202 (2006).

[39] Qianfan Xu, Vilson R. Almeida, Roberto R. Panepucci, and Michal Lipson, "*Experimental demonstration of guiding and confining light in nanometer-sizelow-refractive-index material*," Opt. Lett. **29** (14), 1626-1628 (2004).

[40] Xu Qianfan, R. Almeida Vilson, A. Barrios Carlos, R. Panepucci Roberto, and Lipson Michal, "*Silicon void nano-waveguides for guiding and confining light***"**, presented at the Conference on Lasers and Electro-Optics/International Quantum Electronics Conference and Photonic Applications Systems Technologies, (2004).

[41] Vilson R. Almeida, Qianfan Xu, Carlos A. Barrios, and Michal Lipson, "*Guiding and confining light in void nanostructure*," Opt. Lett. **29** (11), 1209-1211 (2004).

[42] Ding Ran, T. Baehr-Jones, Kim Woo-Joong, A. Spott, M. Fournier, J. M. Fedeli, Huang Su, Luo Jingdong, A. K. Y. Jen, L. Dalton, and M. Hochberg, "*Sub-Volt Silicon-Organic Electro-optic Modulator With 500 MHz Bandwidth*," Lightwave Technology, Journal of **29** (8), 1112-1117 (2011).

[43] **Che-Yun Lin**, Beomsuk Lee, Alan X. Wang, Wei-Cheng Lai, Swapnajit Chakravarty, Yazhao Liu, David Kwong, Ray T. Chen, Jingdong Luo, and Alex K. Y. Jen, "*Ultra-compact silicon nanophotonic modulator based on electro-optic polymer infiltrated slot photonic crystal waveguide***"**, presented at the Proc. SPIE, San Francisco, (2010).

[44] Jan Hendrik Wulbern, Jan Hampe, Alexander Petrov, Manfred Eich, Jingdong Luo, Alex K. Y. Jen, Andrea Di Falco, Thomas F. Krauss, and Jurgen Bruns, "*Electro-optic modulation in slotted resonant photonic crystal heterostructures*," Appl. Phys. Lett. **94** (24), 241107-241103 (2009).

[45] C Koos, P Vorreau, T Vallaitis, P Dumon, W Bogaerts, R Baets, B Esembeson, I Biaggio, T Michinobu, and F Diederich, "*All-optical high-speed signal processing with silicon/organic hybrid slot waveguides*," Nature Photonics (2009).

[46] Tomoko Gray, Tae-Dong Kim, Daniel B. Knorr, Jingdong Luo, Alex K. Y. Jen, and Rene M. Overney, "*Mesoscale Dynamics and Cooperativity of Networking Dendronized Nonlinear Optical Molecular Glasses*," Nano Lett. **8** (2), 754-759 (2008).

[47] H. Chen, B. Chen, D. Huang, D. Jin, Jingdong Luo, Alex. K. Y. Jen, and Raluca. Dinu, "*Broadband electro-optic polymer modulators with high electro-optic activity and low poling induced optical loss*," Appl. Phys. Lett. **93** (4), 043507-043503 (2008).

[48] Tom Baehr-Jones, Boyan Penkov, Jingqing Huang, Phil Sullivan, Joshua Davies, Jocelyn Takayesu, Jingdong Luo, Tae-Dong Kim, Larry Dalton, Alex Jen, Michael Hochberg, and Axel Scherer, "*Nonlinear polymer-clad silicon slot waveguide*

modulator with a half wave voltage of 0.25 V," Appl. Phys. Lett. **92** (16), 163303 (2008).

[49] Y. Enami, D. Mathine, C. T. DeRose, R. A. Norwood, J. Luo, A. K. Y. Jen, and N. Peyghambarian, "*Hybrid cross-linkable polymer/sol-gel waveguide modulators with 0.65 V half wave voltage at 1550 nm*," Appl. Phys. Lett. **91** (9), 093505-093503 (2007).

[50] Yasufumi Enami, C. T. Derose, D. Mathine, C. Loychik, C. Greenlee, R. A. Norwood, T. D. Kim, Jingdong Luo, Y. Tian, Alex. K. Y. Jen, and Naser Peyghambarian, "*Hybrid polymer/sol-gel waveguide modulators with exceptionally large electro-optic coefficients*," Nature Photonics **1** (3), 180-185 (2007).

[51] Michael Hochberg, Tom Baehr-Jones, Guangxi Wang, Michael Shearn, Katherine Harvard, Jingdong Luo, Baoquan Chen, Zhengwei Shi, Rhys Lawson, Phil Sullivan, Alex K. Y. Jen, Larry Dalton, and Axel Scherer, "*Terahertz all-optical modulation in a silicon-polymer hybrid system*," Nature Materials **5** (9), 703-709 (2006).

[52] Qianfan Xu, Bradley Schmidt, Sameer Pradhan, and Michal Lipson, "*Micrometre-scale silicon electro-optic modulator*," Nature (London) **435** (7040), 325-327 (2005).

[53] T. Baehr-Jones, M. Hochberg, Guangxi Wang, R. Lawson, Y. Liao, P. Sullivan, L. Dalton, A. Jen, and A. Scherer, "*Optical modulation and detection in slotted Silicon waveguides*," Opt. Express **13** (14), 5216-5226 (2005).

[54] Ansheng Liu, Richard Jones, Ling Liao, Dean Samara-Rubio, Doron Rubin, Oded Cohen, Remus Nicolaescu, and Mario Paniccia, "*A high-speed silicon optical modulator based on a metal-oxide-semiconductor capacitor*," Nature (London) **427** (6975), 615-618 (2004).

[55] Marin Soljačić, Steven G. Johnson, Shanhui Fan, Mihai Ibanescu, Erich Ippen, and J. D. Joannopoulos, "*Photonic-crystal slow-light enhancement of nonlinear phase sensitivity*," J. Opt. Soc. Am. B **19** (9), 2052-2059 (2002).

[56] Mark Lee, Howard E. Katz, Christoph Erben, Douglas M. Gill, Padma Gopalan, Joerg D. Heber, and David J. McGee, "*Broadband Modulation of Light by Using an Electro-Optic Polymer*," Science **298** (5597), 1401-1403 (2002).

[57] Datong Chen, Harold R. Fetterman, Antao Chen, William H. Steier, Larry R. Dalton, Wenshen Wang, and Yongqiang Shi, "*Demonstration of 110 GHz electro-optic polymer modulators*," Appl. Phys. Lett. **70** (25), 3335-3337 (1997).

[58] Su Huang, Tae-Dong Kim, Jingdong Luo, Steven K. Hau, Zhengwei Shi, Xing-Hua Zhou, Hin-Lap Yip, and Alex K.-Y. Jen, "*Highly efficient electro-optic polymers through improved poling using a thin TiO_2-modified transparent electrode*," Appl. Phys. Lett. **96** (24), 243311 (2010).

[59] Charles Greenlee, Anael Guilmo, Ayodeji Opadeyi, Roland Himmelhuber, Robert A. Norwood, Mahmoud Fallahi, Jingdong Luo, Su Huang, Xing-Hua Zhou, Alex K.-Y. Jen, and Nasser Peyghambarian, "*Mach--Zehnder interferometry method for decoupling electro-optic and piezoelectric effects in poled polymer films*," Appl. Phys. Lett. **97** (4), 041109 (2010).

[60] R. Ding, T. Baehr-Jones, Y. Liu, R. Bojko, J. Witzens, S. Huang, J. Luo, S. Benight, P. Sullivan, J. M. Fedeli, M. Fournier, L. Dalton, A. Jen, and M. Hochberg, "*Demonstration of a low VπL modulator with GHz bandwidth based on electro-optic polymer-clad silicon slot waveguides*," Opt. Express **18** (15), 15618-15623 (2010).

[61] Jan H. Wulbern, Alexander Petrov, and Manfred Eich, "*Electro-optical modulator in a polymer-infiltrated silicon slotted photonic crystal waveguide heterostructure resonator*," Opt. Express **17** (1), 304-313 (2009).

[62] D. M. Beggs, T. P. White, L. Cairns, L. O'Faolain, and T. F. Krauss, "*Ultrashort Photonic Crystal Optical Switch Actuated by a Microheater*," Photonics Technology Letters, IEEE **21** (1), 24-26 (2009).

[63] Yongqiang Shi, Cheng Zhang, Hua Zhang, James H. Bechtel, Larry R. Dalton, Bruce H. Robinson, and William H. Steier, "*Low (Sub-1-Volt) Halfwave Voltage Polymeric Electro-optic Modulators Achieved by Controlling Chromophore Shape*," Science **288** (5463), 119-122 (2000).

[64] Yi Zou, Swapnajit Chakravarty, Wei-Cheng Lai, **Che-Yun Lin**, and Ray T. Chen, "*Methods to Array Photonic Crystal Microcavities for High Throughput High Sensitivity Bio-Sensing on a Silicon-Chip Based Platform (Accepted)*," LChip (2012).

[65] Alan X. Wang, **Che-Yun Lin**, Swapnajit Chakravarty, Jingdong Luo, Alex K. Y. Jen, and Ray T. Chen, "*Slow Light Enhanced E-O Polymer Nano-Photonic Modulator with Ultra-High Effective In-Device r33***"**, presented at the CLEO, (2011).

[66] A. Melloni, A. Canciamilla, C. Ferrari, F. Morichetti, L. O'Faolain, T. F. Krauss, R. De La Rue, A. Samarelli, and M. Sorel, "*Tunable Delay Lines in Silicon Photonics: Coupled Resonators and Photonic Crystals, a Comparison*," Photonics Journal, IEEE **2** (2), 181-194 (2010).

[67] Amir Hosseini, Harish Subbaraman, David Kwong, Yang Zhang, and Ray T. Chen, "*Optimum access waveguide width for 1 x N multimode interference couplers on silicon nanomembrane*," Opt. Lett. **35** (17), 2864-2866 (2010).

[68] Yonghao Cui, Ke Liu, Duncan L. MacFarlane, and Jeong-Bong Lee, "*Thermo-optically tunable silicon photonic crystal light modulator*," Opt. Lett. **35** (21), 3613-3615 (2010).

[69] Xiaolong Wang, Chakravarty Swapnajit, Boem Suk Lee, **Che-Yun Lin**, and Chen R. T., "*Electro-optic polymer based nanophotonic modulator with ultra high efficiency***"**, presented at the Avionics, Fiber-Optics and Phototonics and Photonics Technology Conference, 2009. AVFOP '09. IEEE, San Antonio, TX, (2009).

[70] Xiaolong Wang, Swapnajit Chakravarty, Boem Suk Lee, **Che-Yun Lin**, Jingdong Luo, Alex K. Y. Jen, and Ray T. Chen, "*Nano-Photonic Electro-Optic Polymer Modulator Based on Photonic Band Gap Engineering***"**, presented at the Integrated Photonics and Nanophotonics Research and Applications, (2009).

[71] Takasumi Tanabe, Katsuhiko Nishiguchi, Eiichi Kuramochi, and Masaya Notomi, "*Low power and fast electro-optic silicon modulator with lateral p-i-n embedded photonic crystal nanocavity*," Opt. Express **17** (25), 22505-22513 (2009).

[72] Harish Subbaraman, Maggie Yihong Chen, and Ray T. Chen, "*Photonic dual RF beam reception of an X band phased array antenna using a photonic crystal fiber-based true-time-delay beamformer*," Appl. Opt. **47** (34), 6448-6452 (2008).

[73] H. Subbaraman, M. Y. Chen, and R. T. Chen, "*Photonic Crystal Fiber-Based True-Time-Delay Beamformer for Multiple RF Beam Transmission and Reception of an*

X-Band Phased-Array Antenna," Lightwave Technology, Journal of **26** (15), 2803-2809 (2008).

[74] L. Ofaolain, X. Yuan, D. McIntyre, S. Thoms, H. Chong, R. M. De La Rue, and T. F. Krauss, "*Low-loss propagation in photonic crystal waveguides*," Electron. Lett. **42** (25), 1454-1455 (2006).

[75] I. Frigyes and A. J. Seeds, "*Optically generated true-time delay in phased-array antennas*," Microwave Theory and Techniques, IEEE Transactions on **43** (9), 2378-2386 (1995).

[76] Richard A. Soref and Brian R. Bennett, "*Electrooptical effects in silicon*," IEEE J. Quantum Electron. **23** (1), 123-129 (1987).

[77] Xiaolong Wang, Beom-Suk Lee, **Che-Yun Lin**, Dechang An, and Ray T. Chen, "*Electroptic Polymer Linear Modulators Based on Multiple-Domain Y-Fed Directional Coupler*," Lightwave Technology, Journal of **28** (11), 1670-1676 (2010).

[78] B. Lee, C.Y. Lin, A.X. Wang, R. Dinu, and R.T. Chen, "*Linearized electro-optic modulators based on a two-section Y-fed directional coupler*," Appl. Optics **49** (33), 6485-6488 (2010).

[79] B. Lee, C. Lin, X. Wang, R.T. Chen, J. Luo, and A.K.Y. Jen, "*Bias-free electro-optic polymer-based two-section Y-branch waveguide modulator with 22 dB linearity enhancement*," Opt. Lett. **34** (21), 3277-3279 (2009).

[80] P. Drexler and P. Fiala, "*Methods for High-Power EM Pulse Measurement*," IEEE Sensors Journal **7** (7), 1006-1011 (2007).

[81] Sriram S. Sriram and Stuart A. Kingsley, "*Sensitivity enhancements to photonic electric field sensor*", presented at the Proc. SPIE, (2004).

[82] K. Tajima, R. Kobayashi, N. Kuwabara, and M. Tokuda, "*Optical Fibers and Devices. Development of Optical Isotropic E-Field Sensor Operating More than 10GHz Using Mach-Zehnder Interferometers*," IEICE Trans Electron **85** (4), 961-968 (2002).

[83] R.F. Tavlykaev and R.V. Ramaswamy, "*Highly linear Y-fed directional coupler modulator with low intermodulation distortion*," J. Lightwave Technol. **17** (2), 282-291 (1999).

[84] K.C. Gupta and I.J. Bahl, "*Microstrip lines and slotlines*," Microstrip lines and slotlines (1996).

[85] N. Kuwabara, K. Tajima, R. Kobayashi, and F. Amemiya, "*Development and analysis of electric field sensor using LiNbO3 optical modulator*," IEEE Transactions on Electromagnetic Compatibility **34** (4), 391-396 (1992).

[86] R.L. Jungerman, C. Johnsen, D.J. McQuate, K. Salomaa, M.P. Zurakowski, R.C. Bray, G. Conrad, D. Cropper, and P. Hernday, "*High-speed optical modulator for application in instrumentation*," J. Lightwave Technol. **8** (9), 1363-1370 (1990).

[87] E.M. Zolotov and RF Tavlykaev, "*Integrated optical Mach-Zehnder modulator with a linearized modulation characteristic*," Quantum Electronics **18** (3), 401-402 (1988).

[88] R.A. Becker, "*Circuit effect in LiNbO3 channel-waveguide modulators*," Opt. Lett. **10** (8), 417-419 (1985).

[89] S. C. Rashleigh, "*Magnetic-field sensing with a single-mode fiber*," Opt. Lett. **6** (1), 19-21 (1981).

[90] J. Kanwisher and K. Lawson, "*Electromagnetic flow sensors*," Limnology and Oceanography **20** (2), 174-182 (1975).

[91] Yongbo Tang, Zhechao Wang, Lech Wosinski, Urban Westergren, and Sailing He, "*Highly efficient nonuniform grating coupler for silicon-on-insulator nanophotonic circuits*," Opt. Lett. **35** (8), 1290-1292 (2010).

[92] Minhao Pu, Liu Liu, Haiyan Ou, Kresten Yvind, and J√∏rn M. Hvam, "*Ultra-low-loss inverted taper coupler for silicon-on-insulator ridge waveguide*," OptCo **283** (19), 3678-3682 (2010).

[93] Liu Liu (刘柳), Minhao Pu (蒲敏皓), Kresten Yvind, and Jørn M. Hvam, "*High-efficiency, large-bandwidth silicon-on-insulator grating coupler based on a fully-etched photonic crystal structure*," Appl. Phys. Lett. **96** (051126) (2010).

[94] Frederik Van Laere, G¸nther Roelkens, Melanie Ayre, Jonathan Schrauwen, Dirk Taillaert, Dries Van Thourhout, Thomas F. Krauss, and Roel Baets, "*Compact and Highly Efficient Grating Couplers Between Optical Fiber and Nanophotonic Waveguides*," J. Lightwave Technol. **25** (1), 151-156 (2007).

[95] D. Taillaert, F. Van Laere, M. Ayre, W. Bogaerts, D. Van Thourhout, P. Bienstman, and R. Baets, "*Grating couplers for coupling between optical fibers and nanophotonic waveguides*," Jpn. J. Appl. Phys., Part 1 **45** (2006).

[96] G. Roelkens, P. Dumon, W. Bogaerts, D. Van Thourhout, and R. Baets, "*Efficient silicon-on-insulator fiber coupler fabricated using 248-nm-deep UV lithography*," Photonics Technology Letters, IEEE **17** (12), 2613-2615 (2005).

[97] Sharee McNab, Nikolaj Moll, and Yurii Vlasov, "*Ultra-low loss photonic integrated circuit with membrane-type photonic crystal waveguides*," Opt. Express **11** (22), 2927-2939 (2003).

[98] Vilson R. Almeida, Roberto R. Panepucci, and Michal Lipson, "*Nanotaper for compact mode conversion*," Opt. Lett. **28** (15), 1302-1304 (2003).

[99] T. Shoji, T. Tsuchizawa, T. Watanabe, K. Yamada, and H. Morita, "*Low loss mode size converter from 0.3 μm square Si wire waveguides to singlemode fibres*," Electron. Lett. **38** (25), 1669-1670 (2002).

[100] Y. Shani, C. H. Henry, R. C. Kistler, K. J. Orlowsky, and D. A. Ackerman, "*Efficient coupling of a semiconductor laser to an optical fiber by means of a tapered waveguide on silicon*," Appl. Phys. Lett. **55** (23), 2389-2391 (1989).